Dynamic Term Structure Modeling and the LIBOR Transition

Jacob Bjerre Skov

Department of Mathematical Sciences
Faculty of Science
University of Copenhagen

This thesis has been submitted to the PhD School of The Faculty of Science, University of Copenhagen.

PhD Thesis by:

Jacob Bjerre Skov
Birkegade 8, 3. th.
DK-2200 Copenhagen N
jacob.bjerre.skov@gmail.com

Assessment committee:

Jesper Lund Pedersen (chairperson)
Associate Professor, University of Copenhagen

Anders Bjerre Trolle
Professor, Copenhagen Business School

Jens Henrik Eggert Christensen
Research Advisor, Federal Reserve Bank of San Francisco

Supervisor:

David Glavind Skovmand
Associate Professor, University of Copenhagen

This thesis has been submitted to the PhD School of The Faculty of Science, University of Copenhagen on April 29, 2023.

ISBN: 978-87-7125-215-6.

Abstract

This thesis deals with the topic of term structure modeling with a focus on the current LIBOR transition. We begin by studying the SOFR futures market in the context of Gaussian dynamic term structure models. We show that, despite jumps and spikes in the overnight benchmark, a continuous Gaussian arbitrage-free Nelson-Siegel model is able to fit the term structure of SOFR futures rates. Furthermore, using a shadow rate extension, we find that accounting for the zero lower bound has significant impact on volatility. Next, we develop a multi-curve model, which endogenously generates the spreads between different tenors of secured and unsecured rates. We show that the model is able to simultaneously fit the term structure of SOFR, Federal Funds, and Eurodollar futures rates as well as spot USD LIBOR and term repo rates. The framework models the spreads as roll-over risk, which we further separate into a credit and funding-liquidity component allowing us to decompose the LIBOR-OIS spread. The last paper considers the task of accurately modeling both overnight and term rates based the SOFR benchmark. We show that a continuous model is unable to simultaneously reflect the near piecewise constant dynamics of overnight SOFR and the diffusive dynamics of SOFR futures rates. Instead, we construct a model of scheduled and unscheduled jumps in the short-rate reflecting jumps in the central bank policy rate following scheduled and unscheduled FOMC meetings. Accounting for jumps in the short-rate, the jump model is able to reconcile the overnight and futures rate dynamics.

Resumé

Denne afhandling omhandler rentemodellering med fokus på den igangværende LIBOR transition. Vi starter med at studere markedet for SOFR futures kontrakter ved brug af Gaussiske dynamiske rentemodeller. Her viser vi, at en kontinuert Gaussisk arbitrage-fri Nelson-Siegel model er i stand til at beskrive rentestrukturen af SOFR futures renter på trods af permanente og kortvarige spring i den underliggende dag-til-dag reference rente. Derudover viser vi, at en skygge-rente udvidelse, som tager højde for den nedre grænse for nominelle renter, har en signifikant indvirkning på volatilitet. I den næste artikel udvikler vi en multikurve model, der endogent genererer spændet mellem forskellige løbetider for sikrede og usikrede renter. Modellen kan beskrive rentestrukturen for SOFR, Federal Funds og Eurodollar futures renter samt USD LIBOR og repo renter. Modellen forklarer spændene ved hjælp af 'roll-over' risiko, som vi yderligere opdeler i en kredit og funding-likviditets komponent, hvilket gør det muligt at dekomponere LIBOR-OIS spændet. Den sidste artikel undersøger, hvordan man korrekt kan modellere både dag-til-dag og futures renter baseret på SOFR. Vi viser, at en kontinuert model ikke er i stand til samtidig at beskrive den næsten stykvis konstante dynamik af dag-til-dag SOFR og den diffusionslignende dynamik for SOFR futures renter. I stedet konstruerer vi en model med planlagte og uplanlagte spring i den korte rente, der afspejler spring i styringsrenten som følge af planlagte og uplanlagte FOMC møder. Ved at tage højde for spring i den korte rente er modellen i stand til at forene dag-til-dag og futures rente dynamikkerne.

Preface

This thesis has been prepared in fulfillment of the requirements for the PhD degree at the Department of Mathematical Sciences, Faculty of Science, University of Copenhagen.

The work was carried out under the supervision of Associate Professor David Glavind Skovmand during the period from May 2020 to April 2023 at the University of Copenhagen.

The thesis consists of an introduction and three separate manuscripts. Each of the manuscripts are self-contained scientific papers and can be read independently. The introduction provides a brief summary of the historical and theoretical background of the thesis as well as an overview of the papers and their contributions.

Acknowledgments

First and foremost, I would like to thank David Glavind Skovmand for encouraging me to pursue a PhD in financial mathematics and subsequently supervising my PhD. Thank you for always taking the time to discuss whatever problem I was struggling with. I have always felt more positive after one of our meetings.

From November 2022 to March 2023 I was lucky to get to visit Professor Erik Schlögl at the University of Technology in Sydney. I am thankful for our discussions and the opportunity to escape the Danish winter.

Thanks to the Department of Mathematics at the University of Copenhagen for awarding me with a PhD stipend. Thanks to my office mates and colleagues at the university. I have enjoyed our many tea and lunch breaks during my three years at the department. A special thanks to Christian Furrer for sharing the LaTeX-template used to compile this thesis.

Thanks to my family and friends for showing or at least faking interest in my research. Finally, I would like to thank my girlfriend, Eva, for always supporting me and making me smile.

Jacob Bjerre Skov
Copenhagen, April 2023

List of papers

Chapter 2: Skov, J.B. and Skovmand, D. (2021). Dynamic Term Structure Models for SOFR Futures. *Journal of Futures Markets*, 41(10), 1520-1544.
DOI: 10.1002/fut.22246

Chapter 3: Skov, J.B. and Skovmand, D. (2022). Decomposing LIBOR in Transition: Evidence from the Futures Markets. *Quantitative Finance*, 23(6), 959-978.
DOI: 10.1080/14697688.2023.2205438

Chapter 4: Schlögl, E., Skov, J.B. and Skovmand, D. (2023). Term Structure Modeling of SOFR: Evaluating the Importance of Scheduled Jumps. *Submitted for publication.*

Contents

Chapter 1

Introduction

Arguably the most important change to the fixed income markets in recent years is the ongoing benchmark transition from London Interbank Offered Rates (LIBORs) to Risk-Free Rates (RFRs). The purpose of this introduction is to provide the historical background on the benchmark transition. We also give a brief description of the theoretical framework that is the basis of the thesis. The last section motivates some of the resulting challenges within the field of dynamic term structure modeling and contains an overview of the main contributions in each of the remaining chapters.

1.1 The LIBOR Transition

This section covers the timeline of the LIBOR transition and the events that sparked transition away from LIBOR as the main interest rate benchmark. Furthermore, we describe the new RFR benchmarks and some of the basic properties in which LIBORs differ from RFRs.

1.1.1 The London Interbank Offered Rate

LIBORs are a set of benchmark rates, which have long played a key role as the main benchmark rate in fixed income contracts. The LIBOR benchmarks exist in multiple different currencies (USD, CHF, GBP, Euro, and JPY) and tenors (O/N, 1W, 1M, 3M, 6M, and 12M). As of mid 2018, LIBORs were the reference rates in $400 trillion notional of derivatives, loans, and other financial products.[1]

In each currency, LIBOR is calculated as a trimmed average of submitted quotes from a set of LIBOR panel banks. The quotes are obtained from each panel bank as the answer to the question:

"At what rate could you borrow funds, were you to do so by asking for and then accepting interbank offers in a reasonable market size just prior to 11 a.m. London

[1] See Schrimpf and Sushko, 2019.

time?"

As such LIBOR is meant to reflect the marginal unsecured interbank funding costs of the LIBOR panel banks. Since financial intermediaries are at the center of providing funding this feature was one of the main reasons that LIBOR gained its popularity as a benchmark rate. However, the method also implies that the LIBOR fixings are based on quotes from a fairly small set of panel banks and not necessarily based on actual transactions.

The lack of actual transactions underpinning the submitted LIBOR quotes has indeed largely been the case since the Great Financial Crisis (GFC). Multiple reasons have caused the interbank market for unsecured lending at term to largely disappear following the GFC. First, the events of the GFC brought attention to the risks associated with this type of funding, which were previously assumed to be mostly negligible. Second, post GFC central bank policies and regulation greatly increased the amount of reserves held by financial institutions while reducing the attractiveness of interbank funding.

The quote based construction and lack of underlying transactions made LIBOR increasingly susceptible to manipulation. This became evident following the LIBOR scandal during the 2010s in which several major LIBOR panel banks were fined billions of dollars for submitting misleading quotes. During the scandal, panel banks were accused of manipulating LIBOR in multiple ways such as banks colluding on submitting quotes that would be favourable to their own derivatives positions as well as LIBOR systematically rising on the first day of each month when adjustable-rate mortgages were set to reset.

The lack of an underlying market and manipulation scandal ultimately led to the announcement of the discontinuation of LIBOR by the Financial Conduct Authority in the UK. This was officially done in the speech by Andrew Bailey, 2017 in which he noted:

"The absence of active underlying markets raises a serious question about the sustainability of the LIBOR benchmarks that are based upon these markets."

Initially, the LIBOR discontinuation date was scheduled at the end of 2021. However, due to the COVID-19 crisis, the cessation of USD LIBOR was delayed to June 2023 for all USD LIBOR fixings except the one-week and two-month tenors. Following the announcement of the LIBOR discontinuation a set of alternative benchmarks have been proposed by regulators. These new benchmarks are collectively referred to as Risk-Free Rates or simply RFRs.

1.1.2 RFRs and the Secured Overnight Financing Rate

The following RFRs have been chosen to replace LIBOR in each of the LIBOR currencies: SOFR (USD), €STR (EUR), TONAR (JPY), SARON (CHF), and SONIA (GBP). Unlike the quote-based construction of LIBOR, the new benchmarks are calculated based on actual transactions in an underlying market, which is sufficiently large to make manipulation of the benchmark implausible. Furthermore, while LIBOR is published for multiple different tenors, RFRs are overnight rates.

Since the main focus of this thesis is on the USD LIBOR transition we will focus on the USD RFR. In 2017, the Secured Overnight Financing Rate (SOFR) was recommended by the Alternative Reference Rates Committee (ARRC) as the USD LIBOR replacement. SOFR is a secured overnight rate, which also includes transactions with wholesale non-bank counterparties.

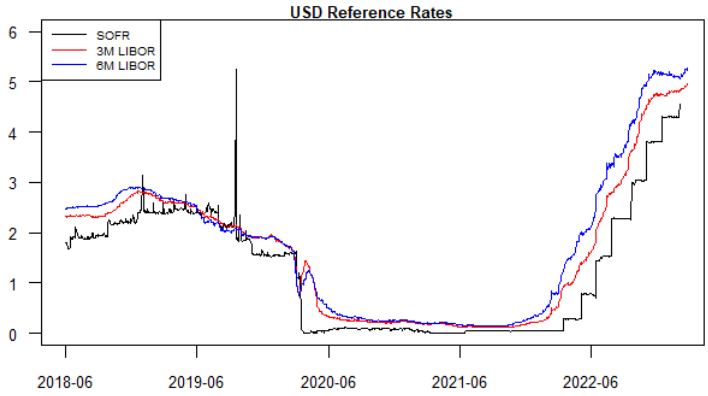

Figure 1.1: *Historical SOFR and three- and six-month USD LIBOR fixings.*

Figure 1.1 plots the historical time series of SOFR as well as the commonly used three- and six-month USD LIBOR. There are several reasons as to why SOFR differs from LIBOR. First, LIBOR is a term rate, it therefore reflects expectations about future interest rate levels during its term, whereas SOFR only reflect interest rates on an overnight basis. Second, since LIBOR reflects unsecured funding at term it contains a credit or term funding risk component. SOFR, on the other hand, being a secured overnight rate, does not contain such risks. Finally, disruptions in the Treasury repo markets as well as the regulatory end of month reports on dealers' balance sheet exposures have at times caused short-lived upward spikes in SOFR.

Financial contracts referencing SOFR are usually not written on the individual SOFR fixings, but rather compounded averages of the overnight rate. The compounded averages reflect a backward-looking rate only known by the end of the compounding period and at the time of payment. The setting in arrears of the compounded SOFR averages is distinctly different from LIBOR, which is a forward-

looking rate and thus fixes in advance and pays in arrears. A forward-looking rate is still preferred in some markets. The ARRC therefore expressed the need for a forward-looking term SOFR and later recommended CME Term SOFR to be used as the forward-looking SOFR term rate. CME Term SOFR is based on SOFR futures contract quotes and does not represent actual lending at term. It therefore does not contain the credit or term funding risk present in LIBOR. The lack of these components has sparked the creation of multiple credit sensitive benchmarks such as the ICE Bank Yield Index (IBYI), Bloomberg Short-Term Bank Yield Index (BSBY) and AMERIBOR.

1.2 Dynamic Term Structure Models

Dynamic term structure models are used in numerous fixed income tasks such as forecasting, determining risk-premiums, risk-management, and hedging. Since bonds and other fixed income derivatives are highly traded assets arbitrage opportunities are usually short-lived. The absence of arbitrage is thus a common assumption in these markets. This puts restrictions on how the cross-section of yields can move. Arbitrage-free dynamic term structure models naturally impose such restrictions on the cross-section of bond yields. The models also enable the separation of risk premiums from actual expectations.

Perhaps the most widely used class of term structure models are Affine Term Structure Models (ATSMs). As indicated by the name, ATSMs are based on affine processes. In the next section, we briefly summarize affine processes and their use in ATSMs.

1.2.1 Affine Procesesses and Term Structure Models

Affine processes are ubiquitous in financial mathematics and have been the main workhorse in dynamic term structure models for decades. In this section, we review the basic theory of affine processes in relation to term structure modeling.

We begin by fixing a standard filtered probability space $(\Omega, \mathcal{F}, (\mathcal{F}_t)_{t\geq 0}, P)$. Our objective is to model a stochastic process in continuous time, X_t. The purpose of this process could be to capture the dynamics of interest rates, volatility, default intensity, etc. In general, we refer to a process as being affine if the conditional characteristic function is exponentially affine in the current state

$$\mathbb{E}\left[e^{iz'X_T}|\mathcal{F}_t\right] = e^{\alpha(t,T,z)+\beta(t,T,z)'X_t}. \tag{1.2.1}$$

The majority of ATSMs studied in the literature are based on the continuous time-homogeneous affine term structure models formalized in Duffie and Kan, 1996. These assume that X_t is a d-dimensional process, which solves

$$dX_t = \mu(X_t)dt + \sigma(X_t)dW_t. \tag{1.2.2}$$

Where W_t is a P Wiener process with independent components and

$$\mu(x) = K_0 + K_1 x, \quad K_0 \in \mathbb{R}^d, \quad K_1 \in \mathbb{R}^{d\times d}$$
$$(\sigma(x)\sigma(x)')_{ij} = H_{0ij} + H_{1ij} \cdot x, \quad H_{0ij} \in \mathbb{R}, \quad H_{1ij} \in \mathbb{R}^d.$$

That is, both the drift and instantaneous variance are affine in the state, X_t. Assuming that the discount rate is also an affine function of X_t defined as $r_t = \rho_0 + \rho_1' X_t$, the discounted transform admits an exponentially affine solution

$$\mathbb{E}\left[e^{-\int_t^T r_s ds + z' X_T} | X_t\right] = e^{\alpha(T-t)+\beta(T-t)' X_t}. \tag{1.2.3}$$

Furthermore, the coefficients $\alpha(\tau)$ and $\beta(\tau)$ can be found as a solution to the Riccati equations

$$\frac{\partial \beta(\tau)}{\partial \tau} = -\rho_1 + K_1' \beta(\tau) + \frac{1}{2}\beta(\tau)' H_1 \beta(\tau),$$
$$\frac{\partial \alpha(\tau)}{\partial \tau} = -\rho_0 + K_0' \beta(\tau) + \frac{1}{2}\beta(\tau)' H_0 \beta(\tau)$$

with initial conditions $\alpha(0) = 0$ and $\beta(0) = z$. In special cases these admit analytical solutions, otherwise they can be efficiently evaluated using numerical methods for ordinary differential equations such as Runge-Kutta.

Zero Coupon Bonds (ZCBs) are essential in the construction of the term structure of interest rates. Assuming the dynamics are specified under a suitable risk-neutral measure, Q, the price of the continuously compounded ZCB can be calculated as

$$p(t,T) = \mathbb{E}^Q\left[e^{-\int_t^T r_s ds} \cdot 1 | \mathcal{F}_t\right]. \tag{1.2.4}$$

The price of the ZCB can therefore be computed using the transform in Equation 1.2.3 with $z = 0$.

The literature on ATSMs is vast and various extensions to the stochastic differential equation in 1.2.2 have been considered. Likewise, the transform in Equation 1.2.3 has also been extended to more general payoffs allowing for the pricing of increasingly complicated contracts such as interest rate options.

1.2.2 Multi-curve Models

Before the GFC, interest rates could be reasonably explained by the term structure of a single risk-free rate. Thus, the same interest rate curve was used for both discounting and determining future cash flows from the reference rate fixings. The GFC resulted in a significant repricing of the risks associated with unsecured and term funding such as LIBOR. This led to large increases in the spread between LIBOR or Interest Rate Swaps (IRSs) referencing LIBOR and the maturity-matched Overnight Index Swap (OIS) referencing the overnight Effective Federal Funds Rate

(EFFR). It also resulted in notable basis spreads between IRSs referencing different tenors of LIBOR making longer tenors of LIBOR more valuable.

Post-GFC market reforms to reduce interbank counterparty risk in over-the-counter derivatives have further caused a shift to central clearing of standardized contracts and an increased focus on collateralization of these products. Cleared contracts are usually collateralized using cash remunerated at the OIS rate. Assuming full cash collateralization on a continuous mark-to-market basis remunerated at the collateral rate r_t^c, the present value of a contract $V(t)$ with a time $T > t$ payoff X can be shown to satisfy

$$V(t) = \mathbb{E}^Q \left[e^{-\int_t^T r_s^c ds} X | \mathcal{F}_t \right]. \tag{1.2.5}$$

Where Q denotes a risk-neutral measure. That is, the payoff should be discounted at the collateral rate. This implies that a single-curve framework cannot be used to accurately value a collateralized derivative with payments dependent on a benchmark rate significantly different from the collateral rate used for discounting. Multi-curve models solve this issue by allowing for separate curves for discounting and generating future cash flows.

On October 16, 2020, as a part of the USD LIBOR transition, the main clearing houses moved from EFFR to SOFR as the primary collateral rate in what was referred to as the discounting "big bang". This has effectively caused a large part of the market to transition back to the traditional single-curve setup in which SOFR is used both for discounting and determining the cash flows. Multi-curve models are however still likely to remain relevant as multiple alternative benchmarks to overnight SOFR may become popular with the cessation of LIBOR while other reference rates such as EFFR continue to exist.

1.3 Overview and Contributions

In light of the historical background presented in the previous section, we now proceed to motivate each of the three remaining chapters contained in the thesis. The chapters represent independent research papers and the use of slightly different notation as well as the repetition of certain key concepts should be expected. While written as independent papers, all of the chapters share the same main objective of developing and estimating dynamic term structure models used to analyze various aspects of the USD LIBOR transition.

1.3.1 Dynamic Term Structure Models for SOFR Futures

In May of 2018, following the announcement of SOFR as the new USD benchmark rate, the Chicago Mercantile Exchange (CME) introduced one- and three-month futures contracts referencing SOFR. In Chapter 2, we study the use of dynamic term structure models for the SOFR futures market. Specifically, we study a special

Gaussian case of the dynamics in Equation (1.2.2) referred to as the class of Arbitrage-free Nelson-Siegel Gaussian models.

The models are estimated to the historical record of SOFR futures contracts using maximum-likelihood in conjunction with the Kalman filter. While Figure 1.1 shows the presence of jumps and, in the beginning of the sample, spikes in overnight SOFR, we find that a three-factor Gaussian model is able to capture the cross-section of SOFR futures rates during our sample period. As a robustness check, we also estimate our model to Federal Funds futures and compare the SOFR futures market to the well-established Federal Funds futures market.

Following the COVID-19 crisis, the Federal Reserve lowered the Federal Funds target range to its post-GFC 0-25 basis point level. The drop in rates revived the importance of interest rate modeling at the zero lower bound. In the chapter, we therefore also consider a non-affine shadow-rate extension of the Gaussian model, which respects the zero lower bound of nominal rates. We find that the shadow-rate extension has a substantial impact on volatility during the low-rate regime affecting futures convexity adjustments and option pricing.

1.3.2 Decomposing LIBOR in Transition: Evidence from the Futures Markets

In Chapter 3 we study the differences in risk between term and overnight as well as secured and unsecured funding. To quantify these risks, we develop an affine multi-curve model, which is able to consistently model contracts based on secured and unsecured overnight and term rates. The spreads between rates at different tenors are explained as roll-over risk. The concept of roll-over risk captures the idea that a financial entity may not be able to roll-over future short-term borrowing at the prevailing reference rate. We divide roll-over risk into two separate components. The first component is a credit-downgrade component, which arises from the risk of a future increase in funding costs as a result of a deterioration in credit quality of the entity. We refer to the second component as a funding-liquidity component, which captures the risk of the entity not being able to roll-over its debt due to a non-credit related reason such as a freeze in lending liquidity.

The paper builds on a vast literature studying the LIBOR-OIS spread following the repricing of the risks associated with LIBOR during the GFC. The majority of these papers focus on the period around the GFC when the spread first became significant. However, the recent transition period from LIBOR to SOFR defines a distinct period in which futures contracts referencing fixings of both SOFR and LIBOR have traded simultaneously. In the empirical section of the paper we use the coexistence of both benchmarks in order to estimate the outlined multi-curve model to a joint data set of SOFR, Federal Funds, and Eurodollar futures rates as well as

spot USD LIBOR and term repo rates. We therefore focus on a more recent data period including the onset of the COVID-19 crisis in which the LIBOR-OIS spread also temporarily spiked. We find that on average credit and liquidity risks contribute equally to the LIBOR-OIS spread, however, the spike during COVID-19 was driven by a large increase in credit risk. Furthermore, the model also provides an insight to the effect of interventions in the repo market by the Federal Reserve after the repo squeeze in September, 2019.

Understanding the risks related to term lending has gained an increased importance in the context of the LIBOR transition in which markets transition from a term to an overnight interest rate benchmark. Our model highlights that a forward-looking term SOFR based on SOFR derivatives does not reflect actual term lending. In particular, it does not reflect secured term lending such as a term repo due to the lack of a funding-liquidity premium while it is missing both a credit and funding-liquidity premium when compared to LIBOR.

1.3.3 Term Structure Modeling of SOFR: Evaluating the Importance of Scheduled Jumps

The transition to RFRs has made the overnight rate the main building block in fixed income products. However, the vast majority of papers on interest rate modeling do not attempt to accurately model overnight rates or include overnight rates in the estimation sample. Studying the historical SOFR fixings in Figure 1.1, we note that, unlike LIBOR, SOFR is highly discontinuous with both lasting jumps and, particularly during the start of the sample, also short-lived spikes. With exception of two unscheduled rate cuts during March 2020 in response to the COVID-19 crisis, all of the observed jumps in SOFR follow scheduled FOMC meeting dates. This suggests that in order to accurately capture the dynamics of SOFR it is necessary to account for the FOMC meeting calendar.

In Chapter 4 we first argue that while the Federal Reserve publishes a 25 basis points Target Range for the Federal Funds rate, the main policy rate determining changes in SOFR is the Interest On Reserve Balances (IORB). Based on this we develop a model of scheduled and unscheduled jumps in the short-rate. We show that by including scheduled jumps in the policy rate following FOMC meeting dates, the model is able to simultaneously generate the near piecewise constant dynamics of overnight SOFR and the diffusive dynamics of SOFR futures rates. Furthermore, we also estimate a continuous model with dynamics similar to those in Equation 1.2.2 and thus ignores the impact of the scheduled FOMC meeting dates on the short-rate. We find evidence that the continuous model is misspecified, especially around FOMC meeting dates with changes in the policy rate. In contrast, our model, which incorporates the FOMC meeting calendar, does not reflect the same misspecifications. Our analysis suggests that accounting for the scheduled jumps is

increasingly important for shorter-term rates or near the end of the accumulation period in backward-looking rates when only few fixings of the overnight benchmark remain. Similarly, the importance decreases as the term of the considered rate increases. In partiuclar, when only three-month futures contracts are considered, as is the case in Eurodollar futures referencing LIBOR, the continuous model is able to capture the futures rate dynamics.

Chapter 2

Dynamic Term Structure Models for SOFR Futures

This chapter contains the manuscript *Skov and Skovmand (2021)*.

Abstract

LIBOR is scheduled for discontinuation, and the replacement advocated by US regulators is the Secured Overnight Financing Rate (SOFR). The only SOFR linked derivative with significant liquidity and trading history is the SOFR futures contract, traded at the CME. We use the historical record of futures prices to construct dynamic arbitrage-free models for the SOFR term structure. We find that a Gaussian arbitrage-free Nelson-Siegel model describes term structure well without accounting for jumps and seasonal effects observed in SOFR. However, a shadow-rate extension is needed to describe volatility near the zero-boundary impacting the futures convexity adjustment and option pricing.

Keywords: SOFR, LIBOR, Futures, Arbitrage-Free Nelson-Siegel, Term Structure Models.

2.1 Introduction

In 2017 it was announced by the Financial Conduct Authority in the UK that their intention was to phase out LIBOR by the end of 2021. The same year the Alternative Reference Rates Committee (ARRC) announced that the recommended replacement in the US, would be the Secured Overnight Financing Rate (SOFR). Due to this forthcoming disruption of the sizeable LIBOR derivatives market, studying the dynamics and proper model specification of SOFR is imperative for pricing and risk managing the transition from LIBOR to SOFR.

In this paper we develop arbitrage-free models for SOFR with a view towards describing the dynamics of the SOFR term structure implied from futures prices. The SOFR futures market being the only one with any significant liquidity and trading history. More precisely we construct models that are arbitrage-free and able to generate realistic SOFR term structures. Our work is to the authors knowledge the first to estimate dynamic arbitrage-free models for the SOFR term structure. Other dynamic models for SOFR have been put forward for example Lyashenko and Mercurio (2019), Macrina and Skovmand (2020), Andersen and Bang (2020). But the existing approaches have mainly focused on pricing derivatives on the compounded SOFR average, and have not taken their models to actual data. An exception is Gellert and Schlögl (2021), who perform a multi-date calibration under the risk-neutral measure with a view towards analyzing the impact of SOFR spikes.
Our research focuses on models that can be easily estimated to futures data, using standard statistical methods. With this view, we limit our analysis to Gaussian affine term structure models in particular the arbitrage-free Nelson-Siegel framework of Christensen, Diebold, and Rudebusch (2011), and its shadow-rate extension in Christensen and Rudebusch (2016). The models are estimated using the maximum-likelihood Kalman filtering method. This is straightforward in the purely Gaussian models, but for the Shadow-rate model it is complicated by a lack of closed form expressions for the futures prices. We develop an approximation formula and verify its accuracy using simulation methods.

Our work draws heavy inspiration from Heitfield and Park (2019), who have put forward a model free approach to translating SOFR futures prices into a forward looking term rate. In particular their approach is currently used by the Federal Reserve to publish an indicative term SOFR rate derived from futures prices. We use their indicative rates as a robustness check on our model and find that our model aligns with those rates to a very high degree. We furthermore find that the jumps and seasonal effects observed in SOFR do not need to be specifically accounted for when the goal is to describe the futures curve.
Since Heitfield and Park (2019) do not use a dynamic arbitrage-free term structure model, they as a result ignore the nonlinear nature of futures contracts measured by the so-called convexity adjustment. Convexity has been studied for SOFR futures in Henrard (2018) and in more detail in Rosen (2019), but not to the authors knowledge in a model estimated to the historical record. Having an estimated dynamic model allows us to gauge the practical relevance of convexity. We find evidence that the convexity adjustment, shows significant model dependence at the lower bound, but is only relevant if futures prices are used to build a term structure beyond 2-3 years in the future. In particular the convexity adjustment is not significant when translating futures prices into term rates with a tenor less than one year, which aligns with the methods of Heitfield and Park (2019). Finally we study how the spike in SOFR of September 2019 as well as the March 2020 drop in overall interest rates has

impacted the SOFR and the related rates. We find that the Gaussian models and the shadow-rate models yield similar results up until March 2020 rate drop. But we find that Gaussian models are unable to capture the volatility compression that occurs after this rate drop.

The paper is structured in the following way. We begin with a brief background on the LIBOR transition followed by a general description of our empirical setup including a general description of for forward looking term rates. We describe the models the pricing formulas, the data and estimation method relegating most of the mathematical detail to the Appendix. In section 4 we present our results and in section 5 we investigate the size and dynamics of the the convexity adjustment for SOFR futures.

2.2 Background on SOFR

The SOFR is an overnight rate based on repo transactions for US treasury securities. The rate was chosen to replace LIBOR, due to the sizeable volume of the repo market, but also because it was not a direct policy rate, unlike the EFFR, which is the rate the Fed refers to in the published targets of the Federal Open Market Comittee (FOMC). SOFR has already been partially implemented, replacing the EFFR as the the main rate used for discounting.[1] This is part of a global trend as regulators throughout the world have pushed towards moving away from LIBOR or its equivalents to overnight transactions based rates generically referred to as a Risk-Free Rates (RFR).[2]

The transition from LIBOR to SOFR is not frictionless as SOFR is fundamentally different from LIBOR. The key difference is that LIBOR is reported across multiple tenors covering unsecured term lending up to 12 months. SOFR, being an overnight rate, by construction has no in-built view of the future beyond the 24 hour term, and is furthermore secured in the sense that credit risk is mitigated in a repo transaction (see also Lou (2021) for a discussion of credit risk in SOFR). Furthermore, SOFR has shown itself to be extremely volatile at times. This was exemplified by the September 17, 2019 so called "SOFR Surge" where the rate jumped 282 basis points compared to the previous day. The ARRC has recommended (see for example Alternative Reference Rate Committee (2019)) that LIBOR is replaced by a running three month compounded daily average of SOFR, and this will naturally decrease the volatility. The recommendation for existing contracts is that the LIBOR fixing should be replaced by this backward-looking average rate plus a spread that reflects the historical median spread to LIBOR.

Changing the fixing rate from LIBOR to some transformation of SOFR in an existing contract can in principle be easily done if both parties of the loan or derivative

[1] The switch from EFFR to SOFR as the primary discounting rate at the LCH and CME clearing houses took place on October 16 2020.

[2] In the UK SONIA, the Eurozone has chosen ESTER, SARON in Switzerland, and so on.

agree to make the switch̊footnoteIn practicality there are multiple complications and potential for legal battles see for example Henrard (2019) for a quant perspective on this part of the transition. But moving from EFFR discounting to SOFR discounting requires, not only the value of the benchmark itself, but a liquid market of forward-looking instruments underlying SOFR. The previous practice of discounting using EFFR relied heavily on a liquid OIS market to derive the EFFR discounting curve. A similar market for SOFR OIS' does not yet exist. The ISDA counted just 389 trades in all SOFR related swaps (including basis swaps) the week ending February 19, 2021. This compared to 14,321 trades in swaps referencing USD LIBOR.

Having a liquid derivatives market underlying SOFR is desirable not just for deriving a discounting curve, but also for implying the "term SOFR" i.e. a discrete forward rate referencing the markets expectation of SOFR over the term period. Market participants (see Risk.net (2020)) have called for such a benchmark, preferring the forward-looking nature of LIBOR over the backward-looking SOFR average. As a result, it is written in the transition plan of the ARRC (See Alternative Reference Rate Committee (2020)) that a term SOFR benchmark rate should be published by the end of 2021. Various methods for constructing such a benchmark have been suggested by the ARRC in Alternative Reference Rate Committee (2018). They express some doubts that the SOFR swap market will be robust enough in the near future to underlie an index due to its lack of liquidity. This leaves SOFR futures as the only realistic underlying asset class for a term SOFR benchmark. The average daily trading volume of SOFR futures has been increasing steadily since their introduction at the CME in 2018 and for the month of January 2021 it was 1,8 mio. contracts up 117% from January 2020. Translating futures prices into a term structure is inherently a model dependent task due to the so called convexity adjustment measured as the difference between the forward and futures rate. Model-free attempts to calculate the convexity generally requires volatility inputs derived from non-linear derivatives, but such a market with a SOFR underlying is not likely to materialize until LIBOR is fully discontinued.[3] This effectively means that using a model is the only way to consistently construct the SOFR term structure. And of course also the only way to price and hedge SOFR derivatives. If the wishes of the regulators come to fruition and SOFR becomes the main benchmark replacing LIBOR it would be natural to expect a liquid market to spawn of SOFR equivalents to the massively popular LIBOR derivatives such as swaptions, caps, floors and other non-linear derivatives. A model for the dynamics of the SOFR term structure based on futures data would therefore be particularly important to price and hedge these products in the early stages of the transition, when futures are arguably the only credible source for market expectations of SOFR. However, the future dominance of SOFR is by no means guaranteed. As of 2021 it seems likely that SOFR will exist

[3]Since Jan 2020 the CME also offers options on SOFR futures. But by January 2021, there has been little to no trading in these instruments.

along side a variety of other interest rate benchmarks reflecting the funding costs in different types of markets and at different levels of risk (see for example Risk.net (2021) for an overview of many of the alternative indices).

2.3 Empirical Setup

2.3.1 Defining SOFR term rates

Define the filtered probability space $(\Omega, \mathcal{F}, \{\mathcal{F}_t\}_{t\geq 0}, Q)$, with Q being the risk neutral measure defined the by the continuous savings account numeraire given by $B_t = e^{\int_0^t r_s ds}$. $\{r_t\}_{t\geq 0}$ is the risk free short rate. We can then define the zero coupon bond as

$$p(t,T) = B_t \mathbb{E}^Q \left[B_T^{-1} | \mathcal{F}_t \right]. \tag{2.3.1}$$

This allows to construct the discrete overnight SOFR is defined as,

$$R_{d_i}(t_i) = \frac{1}{d_i} \left(\frac{1}{p(t_i, t_i + d_i)} - 1 \right) \tag{2.3.2}$$

with d_i denoting the day count fraction multiplied by the amount of days to which the overnight rate applies. E.g. $d_i = 3/360$ on Fridays and $d_i = 1/360$ on business days that are not followed by a holiday.
A critical part of the LIBOR transition has been to define a replacement benchmark for LIBOR based on the new RFRs. The regulatory agencies and the ARRC has decided LIBOR is to be replaced by a backward-looking compounded average calculated as

$$R^B(S,T) = \frac{1}{T-S} \left(\prod_{i=1}^{N} (1 + d_i R_{d_i}(t_i)) - 1 \right). \tag{2.3.3}$$

Unlike LIBOR rates, which are fixed in advance, the RFR based backward-looking rates are only known at the end of the term and thus $\mathcal{F}_T$-measurable, hence they can hardly be considered as proper term rates. Figure 2.1 plots the three month compounded term SOFR term rate against the overnight SOFR and EFFR. The SOFR is closely related to the federal funds rate, however it displays clear rate spikes on certain month, quarter or year ends known from the repo market it is based on. The figure shows that the backward-looking running average is significantly volatility reducing to the point that even the September 2019 spike in SOFR reduces to a minor uptick in the backward-looking benchmark. While it cannot be said that the backward-looking rate has been excessively volatile, it has nevertheless been highlighted by the Alternative Reference Rate Committee (2018) that a forward-looking term rate is preferable by market participants, since it would incorporate market expectations about the future rates, but also because of the so called 'measurability

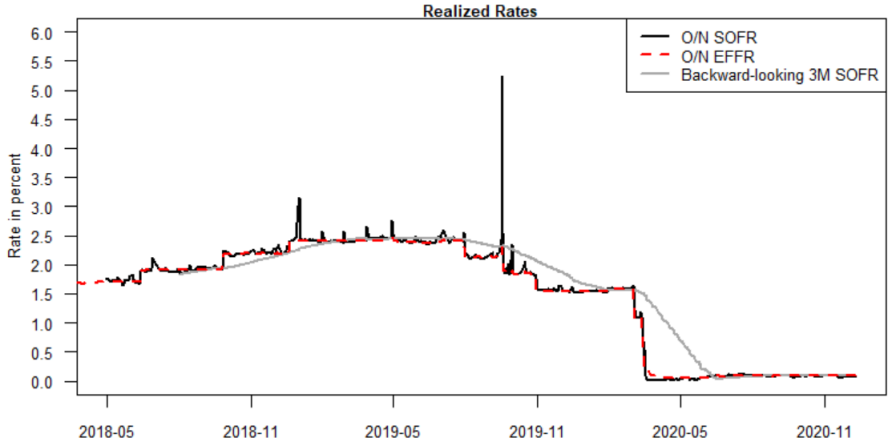

Figure 2.1: *Overnight SOFR and EFFR as well as the backward-looking discretely compounded three-month SOFR term rate.*

problem' (see Henrard (2019)) that arises from having a rate that is measurable at the end as opposed to the beginning of the term. However, assuming that a synthetic zero-coupon bond term structure can be implied from market prices such a proper forward looking term rate is simply calculated as the discrete spot rate,

$$R^F(S,T) = \frac{1}{T-S}\left(\frac{1}{p(S,T)} - 1\right). \tag{2.3.4}$$

The backward and the forward-looking rates are easily seen, by repeated application of the tower property, to be related through discounted expectation as

$$B_t\mathbb{E}^Q\left[B_T^{-1}R^F(S,T)|\mathcal{F}_t\right] = B_t\mathbb{E}^Q\left[B_T^{-1}R^B(S,T)|\mathcal{F}_t\right], \quad t \leq S \leq T. \tag{2.3.5}$$

Which means that the price of any forward starting linear derivative will be the same at any point before the accrual date regardless of whether a backward or forward-looking benchmark is used to determine the cash-flows. In particular setting $t = S$, and changing to the T-forward measure we get

$$R^F(S,T) = \frac{B_S}{p(S,T)}\mathbb{E}^Q\left[B_T^{-1}R^B(S,T)|\mathcal{F}_S\right] = \mathbb{E}^T[R^B(S,T)|\mathcal{F}_S], \tag{2.3.6}$$

from which we can see that the forward looking term rate is a prediction of the backward-looking rate under the T-forward measure.

An Overnight-Index-Swap (OIS) is a fixed for floating swap with floating payments equal that of the backward looking rates in (2.3.3). From (2.3.5) and (2.3.6) it therefore follows that OIS prices would determine forward looking term rate in a model free manner. But as stated above the OIS market with a SOFR underlying is not yet sufficiently liquid. The current market for OIS is still very much dominated by EFFR as the underlying overnight rate. We are thus left with the SOFR futures

as the main source of data for inferring forward looking SOFR term rates. Since this is an inherently model dependent task we will consider the ability of a model to construct correct forward looking SOFR term rates from futures data as one of the main criteria to assess the performance of the models specified in the next section.

2.3.2 Constructing the short rate models

When modeling the term structure of futures rates we consider one-, two-, and three-factor versions of Gaussian arbitrage-free short-rate models. Since unrestricted affine multi-factor models often suffer from over-parametrization resulting in multiple maxima of the likelihood function, we consider the parameter restrictions of the arbitrage-free Nelson-Siegel (AFNS) model presented in Christensen, Diebold, and Rudebusch (2011) belonging to the class of Gaussian affine term structure models. The AFNS model is a three-factor model effectively replicating the yield factor loadings of the popular Dynamic Nelson-Siegel model in Diebold and Li (2006). Furthermore, we consider a two-factor version of the AFNS model omitting the final (curvature) factor as well as the standard Gaussian single-factor model by Vasicek (1977). Finally, we consider a shadow-rate extension of the AFNS model where the short rate satisfies the zero lower bound as in Black (1995). We briefly outline the general setup of the models used in this paper, while model specific parameter restrictions and results are given in Appendix 2.A. As before we define the filtered probability space $(\Omega, \mathcal{F}, \{\mathcal{F}_t\}_{t\geq 0}, Q)$ and assume that the state variable, $\{X_t\}_{t\geq 0}$, is a Markov process, which solves the stochastic differential equation

$$dX_t = K^Q[\theta^Q - X_t]dt + \Sigma dW_t^Q, \tag{2.3.7}$$

where K^Q and Σ are $N \times N$ matrices, $\theta^Q \in \mathbb{R}^N$ and $\{W^Q\}_{t\geq 0}$ is an $\mathcal{F}$-adapted Brownian motion on $\mathbb{R}^N$. In the Gaussian models the short rate is given by

$$r_t = \rho_0 + \rho_1' X_t, \tag{2.3.8}$$

with ρ_0 a scalar and $\rho_1 \in \mathbb{R}^N$. While in the shadow-rate model we let $s_t = \rho_0 + \rho_1' X_t$ denote the shadow short rate and define

$$r_t = \max(s_t, 0) \tag{2.3.9}$$

as the actual short rate. As in the previous section we set $B_t = e^{\int_0^t r_s ds}$ and $p(t,T) = B_t \mathbb{E}^Q \left[B_T^{-1} | \mathcal{F}_t\right]$.
The real world dynamics are connected to the risk neutral dynamics by specifying a market price of risk, Λ_t,

$$dW_t^Q = \Lambda_t dt + dW_t^P. \tag{2.3.10}$$

We consider an essentially affine market price of risk as in Duffee (2002), which under Gaussian state variable dynamics reduces to

$$\Lambda_t = \lambda_1 + \lambda_2 X_t. \tag{2.3.11}$$

The resulting P-dynamics share the same form as the Q-dynamics and are thus also Gaussian

$$dX_t = K^P[\theta^P - X_t]dt + \Sigma dW_t^P. \tag{2.3.12}$$

Throughout we will assume independent dynamics of the state variables under the physical measure and thus restrict K^P and Σ to be diagonal matrices.

2.3.3 Pricing SOFR futures

The settlement price of the futures contract is quoted as $100(1 - R(S,T))$ where $R(S,T)$ denotes the futures rate and is a function of the discrete overnight reference rates during the contract period and thus $\mathcal{F}_T$-measurable. $R(S,T)$ is defined differently for One-Month and the Three-Month SOFR futures. In both cases we can use the well known result (see for example Hunt and Kennedy (2004)) that the value of a futures contract with a random payoff equals the risk neutral expectation of the non-discounted payoff. The time t futures rate between time S and T can therefore be computed as

$$f(t;S,T) = \mathbb{E}^Q\left[R(S,T)|\mathcal{F}_t\right]. \tag{2.3.13}$$

We present general futures rates formulas for both one- and three-month futures contracts. Specific solutions to the AFNS model are provided in Appendix 2.A, and the development of the approximation formulas for the shadow-rate model can be found in Appendix 2.B

One-month SOFR futures

The one-month futures rate is based on the arithmetic average of the daily reference rate during the contract month

$$R^{1m}(S,T) = \frac{1}{N}\sum_{i=1}^{N} R_{d_i}(t_i). \tag{2.3.14}$$

Where N denotes the total number of days in the month and $R_{d_i}(t_i)$ for $i \in 1,...,N$ with $S \leq t_1,...,t_N \leq T$ the published SOFR rates given in (2.3.1). For any date for which the rate is not published the last preceding rate is used, as specified in the futures contract. As in Mercurio (2018) we approximate the discrete average by an integral of the instantaneous short rate

$$R^{1m}(S,T) \approx \frac{1}{T-S}\int_S^T r_s ds. \tag{2.3.15}$$

As we show in Appendix 2.D, this approximation is strictly not necessary as an exact solution does exist in the affine case. We compute the exact one-month rate in Appendix 2.D, which shows that the approximation error is similar across all contracts

and only a fraction of a basis point. We nevertheless apply the approximation for ease of computation.
Denote the time t rate of the one-month futures starting to accrue at time S and with settlement on time T by $f^{1m}(t;S,T)$ then

$$f^{1m}(t;S,T) = \frac{1}{T-S}\mathbb{E}^Q\left[\int_S^T r_s ds|\mathcal{F}_t\right]. \tag{2.3.16}$$

When pricing a futures contract settling at the end of the current month and thus $S < t$, we have to account for the part of the underlying rate that has already been accrued. In this case the futures rate is calculated as

$$f^{1m}(t;S,T) = \frac{1}{N}\sum_{i=1}^{N_0} R_{d_i}(t_i) + \frac{1}{T-S}\mathbb{E}^Q\left[\int_t^T r_s ds|\mathcal{F}_t\right] \tag{2.3.17}$$

where $R_{d_i}(t_i)$ for $i \in 1,...,N_0$ with $S \leq t_1,...,t_{N_0} \leq t$ are realized rates and thus $\mathcal{F}_t$-measurable. The settlement of the one-month federal funds futures is based on the same specifications and the pricing formula is therefore valid for both SOFR and federal funds one-month futures traded at the CME.

Three-month SOFR futures

The three month futures contract is based on the daily compounded reference rate during the contract quarter

$$R^{3m}(S,T) = \frac{1}{T-S}\left(\prod_{i=1}^{N}(1+d_i R_{d_i}(t_i)) - 1\right). \tag{2.3.18}$$

Where $R_{d_i}(t_i)$ for $i \in 1,...,N$ with $S \leq t_1,...,t_N \leq T$ denotes the realized overnight rates in the reference quarter and d_{t_i} the amount of days to which $R_{d_i}(t_i)$ applies. Again, we follow Mercurio (2018) and approximate the daily compounded rate by the continuously compounded rate

$$R^{3m}(S,T) \approx \frac{1}{T-S}\left(e^{\int_S^T r_s ds} - 1\right). \tag{2.3.19}$$

The accuracy of the continuous approximation is studied in Appendix 2.D showing errors of an order less than 10^{-7} for all open contracts. This again is applied mainly for ease of computation. The time t rate of the three-month future starting to accrue at time S and with settlement on time T is then given by

$$f^{3m}(t;S,T) = \frac{1}{T-S}\left(\mathbb{E}^Q\left[e^{\int_S^T r_s ds}|\mathcal{F}_t\right] - 1\right). \tag{2.3.20}$$

When $S < t$ and part of the underlying rate has already accrued we account for this in the pricing formula using discrete compounding

$$f^{3m}(t;S,T) = \frac{1}{T-S}\left(\left(\prod_{i=1}^{N_0}[1+d_i R_{d_i}(t_i)]\right)\mathbb{E}^Q\left[e^{\int_t^T r_s ds}|\mathcal{F}_t\right] - 1\right) \tag{2.3.21}$$

where $R_{d_i}(t_i)$ for $i \in 1, ..., N_0$ with $S \leq t_1, ..., t_{N_0} \leq t$ denotes $\mathcal{F}_t$-measurable realized overnight rates.

2.3.4 Data and estimation

To infer SOFR-based term rates we estimate the models using end of day prices on CME SOFR futures contracts. All futures data is collected through Refinitiv Eikon. The models are fitted using the extended Kalman filter maximum likelihood method described in Appendix 2.C. Code for the extended Kalman filter and relevant pricing functions is available and uploaded at Github.[4] We apply historical futures data starting from the 19th of June 2018 up until the day where the term rates are computed. Term rates are based on a minimum of 250 historical daily futures data observations allowing us to compute term rates from June 2019 and onwards. We calculate the term rates using equation (2.3.4), applying the ACT/360 day count convention and the modified following business day convention on the USNY business day calendar.

The quality of the obtained model estimates and resulting term rates strongly rely on the observed futures prices accurately reflecting market expectations on futures rates. As shown in Heitfield and Park (2019) the majority of the liquidity in the SOFR futures markets is concentrated around the nearest one-month contracts and three-month contracts at a one year horizon. Based on this we use observations of one-month contracts for the seven nearest calendar months as well as the five closest quarterly contracts. The data therefore reflects market expectations covering a period of just over a year. Daily term rates are then calculated using the latest set of filtered state variables together with the optimal set of parameters provided by the Kalman filter. In Appendix 2.C we perform a simulation study testing the efficiency of the Kalman filter maximum likelihood method. The study shows that the parameters related to the risk neutral dynamics and thus determining the term structure are accurately identified by the filter showing no significant bias. It should further be noted that while we construct term rates using end of day quotes in this paper, one can apply the same approach at any point during the day using the Kalman filtering on the prevailing futures prices while using e.g. end of day historical data in the estimation to obtain a relevant term structure.

2.4 Empirical Results

Figure 2.2 presents the SOFR-based term rates obtained using the one-, two-, and three-factor Gaussian models. Particularly at the one-month tenor the models show significant variation in the model implied term rates. Also the graphs show that when market expectations of futures rates are stable implying a flat yield curve all three

[4] `https://github.com/Jacob-Skov/DTSM-SOFR-Futures`

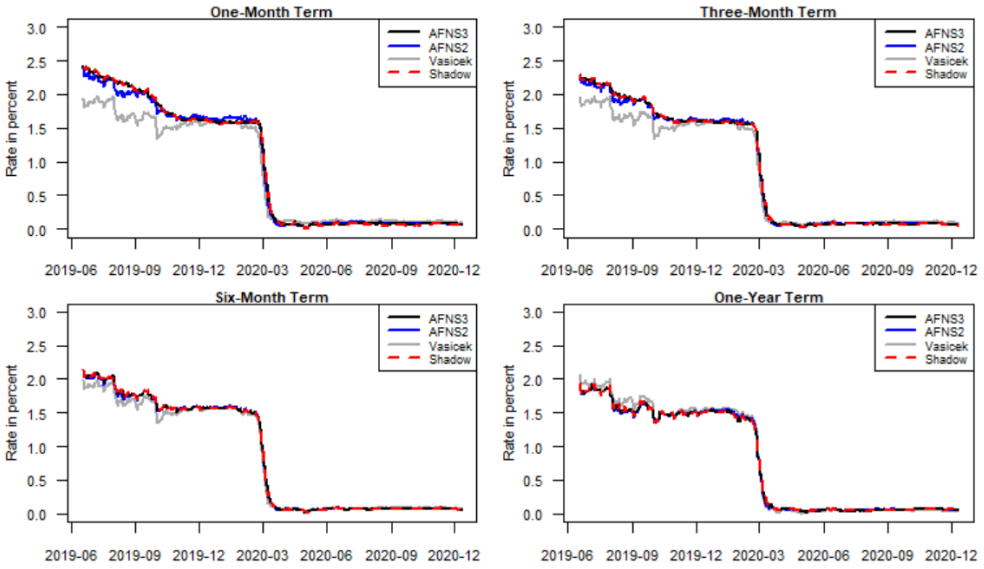

Figure 2.2: *Model implied arbitrage-free term rates for different tenors based on rolling re-estimates from 17th of June 2019.*

Model	One-Month							Three-Month				
	1st	**2nd**	**3rd**	**4th**	**5th**	**6th**	**7th**	**1st**	**2nd**	**3rd**	**4th**	**5th**
Vasicek	18.1	21.5	13.3	7.0	0.0	5.8	10.7	13.0	9.6	11.1	23.5	32.4
AFNS2	4.7	4.3	3.1	2.5	2.3	1.8	1.5	2.1	1.3	1.8	4.3	8.0
AFNS3	3.1	3.1	3.3	2.7	2.1	1.6	1.6	1.0	1.3	1.8	0.9	1.0
Shadow	2.9	3.1	3.3	2.6	2.1	1.6	1.6	0.9	1.3	1.8	0.9	1.8

Table 2.1: *RMSEs of the fitted futures rates based on the final parameter estimates and filtered state variables for each of the models using the full SOFR data sample. All values are in basis points. The final log-likelihood values of the Vasicek, AFNS2, AFNS3 and shadow-rate model respectively are 41826.1, 51050.6, 53247.6 and 53409.3*

models provide near identical term rates. This can be seen during the most recent period after the drastic lowering of rates following COVID-19 due to announcements made by Federal Reserve to keep rates near zero for an extended amount of time.

When assessing the fit of the model implied futures rates to the observed futures rates we consider the root mean square error defined as

$$RMSE(i) = \sqrt{\frac{\sum_{t=1}^{T} \left(f_t^{obs}(i) - f_t(i)\right)^2}{T}}, \tag{2.4.1}$$

where $f_t^{obs}(i)$ denotes the observed futures rate at time t for contract number i and $f_t(i)$ is the corresponding model implied futures rate. Table 2.1 contains the RMSEs of the fitted futures rates for each model. Clearly, the Vasicek model is not able to properly fit the term structure resulting in large deviations from the observed rates. The two-factor model is able to capture most of the variation in the cross section of

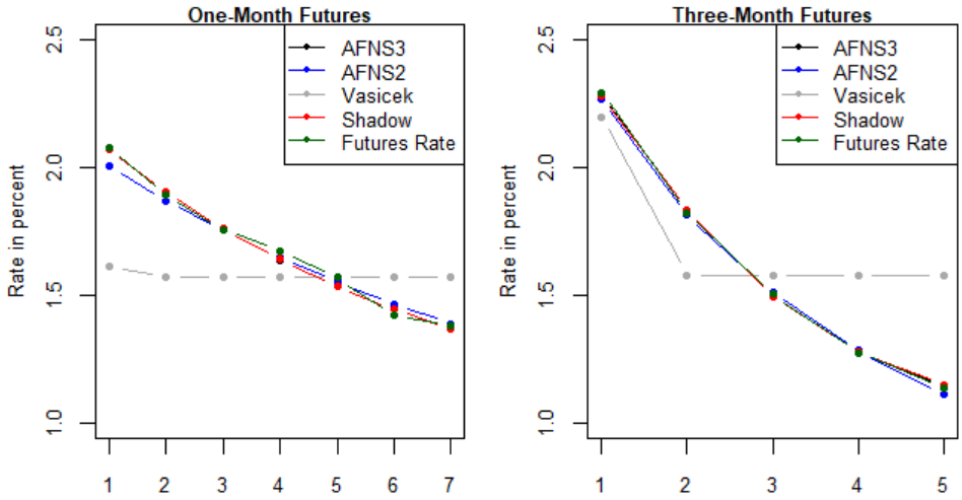

Figure 2.3: *Fitted and observed futures rates for the seven nearest one-month contracts and five nearest three-month contracts as of the 3rd of September 2019.*

futures rates, but does show increasing RMSEs the short and long end of the term structure of futures rates, while the three-factor model provides a close fit across all observed contracts. This is also seen in figure 2.3, which shows the fitted futures rates as of the 3rd of September 2019 together with the market implied futures rates. The futures rates on the particular date indicate a market expectation of a future decrease in SOFR. The graph illustrates the inability of the single-factor model in capturing the term structure of futures rates, while both the two- and three-factor AFNS models perform notably better. The nearest three-month futures rate appears to be reasonably well approximated by the Vasicek model. However, this is only due to the fact that the majority of the underlying overnight rates already have been accrued on this contract. The flat futures rate curve produced by the Vasicek model is a direct consequence of a near zero K^Q estimate, making the state variable act as a level factor under the Q-dynamics.

Since a sufficiently liquid market of linear SOFR derivatives allowing for standard curve construction does not exist, we compare the model implied term rates to the model-independent term rates based on the method presented in Heitfield and Park (2019) published daily on the New York Federal Reserve's website as a benchmark reference.[5] The model-free term rates in Heitfield and Park (2019) are calculated using a step function to parametrize the one-day forward curve, allowing for jumps on dates determined by the target rate announcement dates in the FOMC calender. Expected jump sizes are then recalibrated daily.

Table 2.2 reports statistics on the differences between the indicative term rates

[5] `https://www.federalreserve.gov/econres/notes/feds-notes/indicative-forward-looking-sofr-term-rates-20190419.htm`

Model	Tenor	RMSE	Mean	SD	5%	Q1	Median	Q3	95%
Vasicek	1 Month	23.0	-11.9	19.7	-54.0	-26.5	-0.5	2.7	4.1
	3 Month	15.1	-8.0	12.8	-34.1	-18.3	-1.2	1.8	2.9
	6 Month	6.7	-3.3	5.8	-15.1	-6.9	0.1	0.8	1.7
AFNS2	1 Month	4.8	0.0	4.8	-12.4	-0.7	0.5	1.3	4.9
	3 Month	1.9	-0.2	1.9	-4.3	-0.5	0.1	0.6	2.0
	6 Month	0.7	0.0	0.7	-0.9	-0.2	0.1	0.4	1.1
AFNS3	1 Month	1.7	0.0	1.7	-2.8	-0.7	-0.1	0.6	3.1
	3 Month	1.0	0.1	0.9	-1.0	-0.4	0.0	0.4	2.0
	6 Month	0.7	0.2	0.7	-0.6	-0.3	0.0	0.5	1.4
Shadow	1 Month	1.8	-0.3	1.8	-2.8	-1.3	-0.5	0.5	3.2
	3 Month	0.9	0.1	0.9	-1.3	-0.5	0.0	0.4	1.9
	6 Month	0.7	0.1	0.7	-0.7	-0.3	0.0	0.4	1.3

Table 2.2: *Difference between model implied term rates based on rolling re-estimates and published Federal Reserve indicative term rates.*

published by the Fed and our model implied term rates. Comparing the root mean squared errors across the three models show that the three-factor model provides the closest fit to the model-independent term rates across all tenors. As also indicated by the graphs in figure 2.2 it is especially the shortest tenors that the lower factor models fail to accurately fit.

The SOFR rate is heavily correlated with EFFR (See Figure 2.1) and thus heavily influenced by the targets set by the FOMC, a reasonable assumption would be that a term structure model with a positive probability of jumps on the announcement dates would be necessary to fit the SOFR futures curve especially in the short term. Table 2.2 shows that this feature is in fact not necessary. The AFNS model, without introducing jumps, is able to produce term rates very similar to those of the model free step-function used in Heitfield and Park (2019). This is also seen in figure 2.4, which compares the three-factor AFNS model three-month term rate to the indicative three-month term rate presented in Heitfield and Park (2019) as well as the realized forward-looking compounded SOFR three-month term rate.

Figure 2.5 compares the three-month AFNS model implied SOFR term rate to the three-month-OIS rate and three-month LIBOR. The LIBOR-SOFR three-month term spread reflects a term premium present in the unsecured term borrowing of LIBOR. Following the Great Financial Crisis the premium is driven by a credit risk and funding-liquidity risk premium (see e.g. Backwell et al. (2019)). The spread increases in times of stress as is clearly seen by the sharp increase in LIBOR following COVID-19 while SOFR, being an overnight secured rate, was not affected and like the OIS-rate closely tracked the target range set by the Federal Reserve. Both the ARRC and ISDA recommend calculating the LIBOR-SOFR spread used for legacy contracts using a five-year historical median between the backward-looking compounded average SOFR and LIBOR. However, such a spread would not be consistent with a forward-looking term SOFR. Instead, adding a spread to a forward-

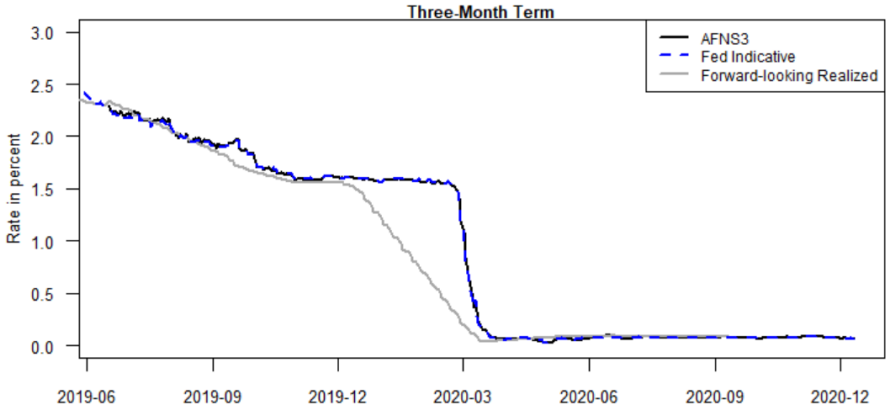

Figure 2.4: *Comparison of forward-looking three-month SOFR term rates.*

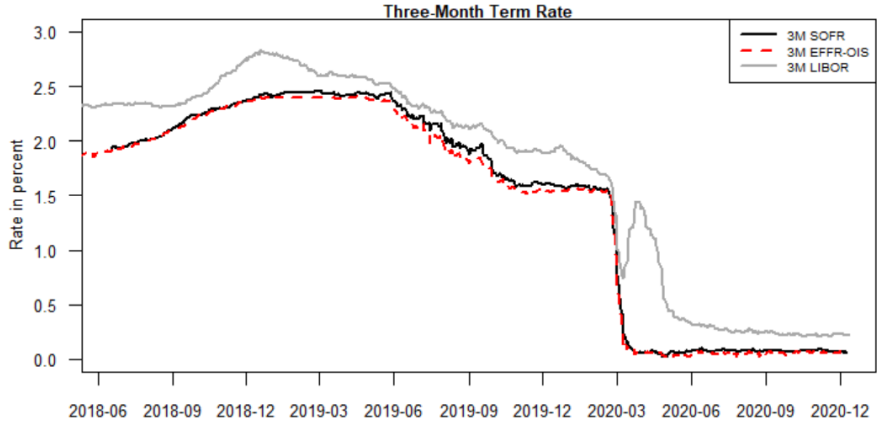

Figure 2.5: *Comparison of forward-looking three-month term rates. The three-month SOFR term rated is based on the final AFNS estimates using the set of filtered state variables.*

looking term SOFR following the same approach would require historical SOFR term rates as presented in this paper.

2.4.1 Federal funds futures implied term rates

As a robustness check we re-estimate our model, using end of day data on federal funds futures traded at the CME instead of SOFR futures. Federal funds futures have traded since 1988 and thus allow us to test the models on a longer time frame. Also, a well developed OIS-market based on federal funds rates exists, which allows us to compare the model implied term rates to actual market term rates. We use data for one-, three- and six-month OIS contracts, which have single end of term payment of exactly $\prod_{i=1}^{N}(1+d_i R_{d_i}^{EFFR}(t_i))-1$, per unit notional with $R_{d_i}^{EFFR}$ being the daily quoted effective federal funds rate. From (2.3.6) it follows that the implied OIS term rate is exactly the EFFR equivalent of the term rate in (2.3.4).

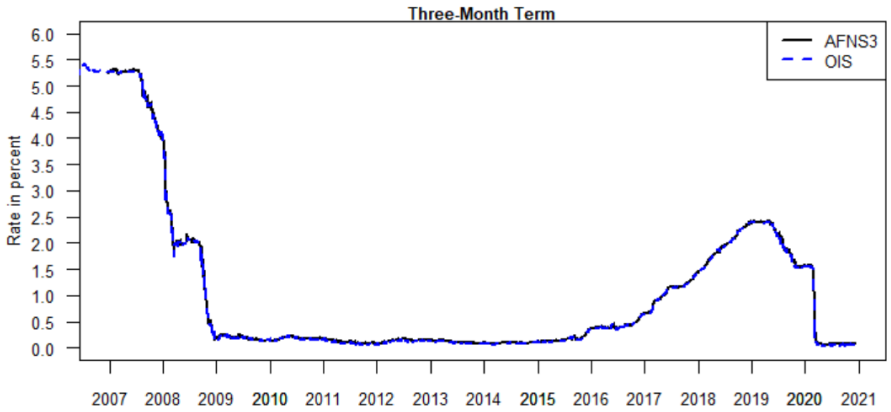

Figure 2.6: *Three-month end of day OIS-rate and model implied three-month three-month term rate based on rolling re-estimates from 3rd of January 2005.*

Model	Tenor	RMSE	Mean	SD	5%	Q1	Median	Q3	95%
Vasicek	1 Month	10.3	-2.3	10.1	-22.5	-2.7	-1.1	0.4	9.9
	3 Month	4.0	0.0	4.0	-6.5	-0.4	0.5	1.3	4.4
	6 Month	5.8	2.6	5.2	-4.5	0.2	2.4	3.8	11.0
AFNS2	1 Month	2.5	0.2	2.5	-3.5	-1.1	0.5	1.4	3.9
	3 Month	1.8	1.1	1.5	-1.1	0.5	1.1	1.6	3.1
	6 Month	1.7	1.2	1.2	-0.5	0.7	1.2	1.6	3.0
AFNS3	1 Month	2.7	1.3	2.4	-1.5	0.6	1.2	1.8	3.9
	3 Month	2.1	1.1	1.8	-1.2	0.4	1.1	1.7	3.4
	6 Month	1.8	1.2	1.3	-0.5	0.7	1.2	1.6	3.0
Shadow	1 Month	2.7	1.3	2.4	-1.5	0.5	1.2	1.9	3.9
	3 Month	2.1	1.1	1.9	-1.5	0.3	1.1	1.7	3.4
	6 Month	2.0	1.1	1.7	-1.8	0.6	1.2	1.6	3.1

Table 2.3: *Differences between model implied term rates based on rolling re-estimates and observed end of day OIS-rates.*

Federal Funds futures are only traded on a one-month contract period with listed contracts covering the 36 first calendar months. As with SOFR-futures most of the traded volume is concentrated around the nearest contracts. We therefore base the estimation on observed end of day prices on the seven nearest one-month futures contracts, thus covering term rates up to six months ahead. The data sample runs from January 2005 until December 2020 and we consider rolling daily estimates beginning in January 2007.

Figure 2.6 plots the model implied term rates at a three month tenor against the corresponding end of day observed OIS-rate. Also in the federal funds case, the three-factor AFNS model is able to closely match the observed OIS-rates even during the drastic rate cuts seen under the financial crisis.

Table 2.3 reports statistics on the difference between model implied and observed OIS term rates. Interestingly, the results favour the two-factor model, which does

provide the closest overall fit as measured by the RMSE, suggesting that two factors is enough to fit the EFFR market. This of course is partly due to the Federal Funds futures data only containing the seven first one-month contracts thus resulting in less daily data points that the model has to fit.[6] We also note that the three-factor models slightly overestimate the term rates compared to the OIS rate, however still tracks the OIS implied term rate well. Refraining from the fact that this is based on end of day data from two different sources, the relatively lower liquidity of the short term OIS-market resulting in a higher spread compared to the futures market could have an impact on the slightly different term structures implied by these markets.

2.4.2 Comparing SOFR and EFFR futures

As a final model-free robustness check we gauge the potential immaturity of the SOFR futures market by comparing the properties of the relatively new market for SOFR futures to the well-established Federal Funds based futures market. Since both the EFFR and SOFR are closely tied to the Federal Funds target range, we would expect that if the SOFR futures market is well functioning you would see similar response in both markets in the wake of the announcements following FOMC meetings. We follow the approach presented in Kuttner (2001) to calculate the unexpected change in the Federal Funds target rate implied by the futures market. Let τ denote the day in the month of the FOMC meeting, N the total number of days in the month and f_τ^{1m} the spot one-month futures rate the day of the FOMC meeting. The unexpected surprise in the futures rate, Δr^u, is then calculated as

$$\Delta r^u = \frac{N}{N-\tau}(f_\tau^{1m} - f_{\tau-1}^{1m}). \tag{2.4.2}$$

When the meeting falls on the first date of the month, we replace $f_{\tau-1}^{1m}$ with the futures rate on the last day of the preceding month. If instead the meeting is at the last day of the month, we calculate the price difference in the futures contract of the following month. Figure 2.7 plots the unexpected change in the target rate implied by SOFR and EFFR futures on all FOMC dates since SOFR futures started trading on CME. The two markets react very similarly to FOMC meetings announcements. The largest difference of 7.5 basis points appeared around the FOMC meeting date in September 2019. This is no surprise as SOFR experienced a drastic spike to above 5 percent on September 17 thus creating uncertainty around the SOFR and impacting the spot one-month futures rate.

Next, we compare risk premia in the two markets following the method presented in Piazzesi and Swanson (2008). For comparability we focus solely on one-month futures contracts. Using end of month data for the six nearest upcoming futures contracts, $n \in \{1, ..., 6\}$, we calculate the ex post realized excess returns of the

[6] A principal component analysis reveals that three factors are required to capture 99.9% of the variation in the SOFR futures data, while only two factors are required for the EFFR futures data.

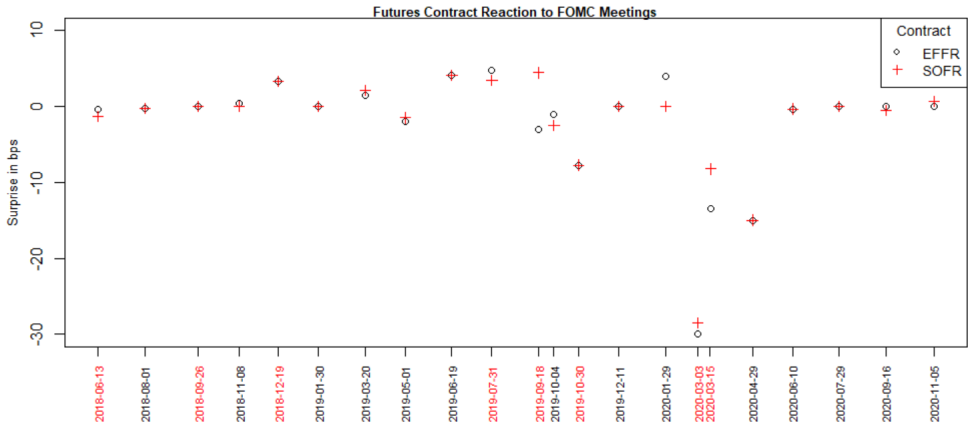

Figure 2.7: *Comparison of price changes on one-month spot EFFR and SOFR futures contracts on FOMC dates. Dates in red mark actual changes in the target rate.*

one-month futures contract, rx_{t+n}^{1m}, as the difference between the time t futures rate of the one-month futures contract, $f_{(n)}^{1m}(t)$, and the ex post realized one-month futures rates, R_{t+n}^{1m},

$$rx_{t+n}^{1m} = f_{(n)}^{1m}(t) - R_{t+n}^{1m}. \tag{2.4.3}$$

We then proceed to run the regression

$$rx_{t+n}^{1m} = \alpha^{(n)} + \varepsilon_{t+n}^{(n)}. \tag{2.4.4}$$

The exercise is performed on both SOFR and EFFR futures based the same data sample starting with end of month futures data from May 2018 when SOFR futures launched on CME and until the end of December 2020. We also consider the full Federal Funds data sample used in the model estimation containing data from January 2005. Table 2.4 contains the estimated constant risk premia for each of the expiries. We can first note that including the full data sample containing the post financial crisis years with little volatility in the Federal Funds overnight rate results in a much smaller risk premium than when using more recent data. But the table also demonstrates very similar risk-premia when comparing SOFR to EFFR futures. Interestingly, it shows a slightly higher premium in the SOFR contracts. One could speculate the reason could be due to liquidity risk premium in the rather new market for SOFR futures or perhaps more likely caused by the observed SOFR spikes. But as the table also shows, the statistical uncertainty is much too great to draw any inference in this regard. Most importantly, for this study, we do not find any evidence to suggest that SOFR futures should not be used in the construction of SOFR term rates.

n	SOFR		EFFR		EFFR Full Sample	
	$\alpha^{(n)}$	Annualized	$\alpha^{(n)}$	Annualized	$\alpha^{(n)}$	Annualized
1m	2.5	30.1	2.3	27.3	1.6	19.0
	(2.5)	(30.0)	(2.3)	(27.8)	(0.6)	(7.4)
2m	7.4	44.5	6.7	40.2	4.3	25.8
	(5.1)	(30.4)	(4.9)	(29.5)	(1.4)	(8.1)
3m	12.6	50.2	11.8	47.1	7.1	28.6
	(6.9)	(27.7)	(6.7)	(26.9)	(2.0)	(7.9)
4m	18.5	55.4	17.4	52.1	10.1	30.3
	(8.4)	(25.3)	(8.3)	(24.8)	(2.6)	(7.7)
5m	25.4	61.0	24.3	58.5	13.2	31.6
	(9.5)	(22.8)	(9.3)	(22.3)	(3.1)	(7.4)
6m	33.3	66.6	32.5	65.0	16.3	32.6
	(10.4)	(20.9)	(10.1)	(20.2)	(3.6)	(7.2)

Table 2.4: *Risk premium for one-month SOFR and EFFR futures contracts using futures data from end of May 2018 until end of December 2020 as well as the full Federal Funds futures sample starting in January 2005. Standard errors are shown in parentheses. Annualized excess returns are obtained by multiplying the excess returns, $rx_{t+n}^{(n)}$, with $1/n$ before running the regression.*

2.4.3 SOFR volatility

The Gaussian short rate distribution of the AFNS model ignores the decrease in volatility resulting from rates being compressed at a lower bound. As of December 2020 the Federal Reserve has never lowered its target rate below zero or expressed willingness in doing so. Therefore, in this paper we assume a zero lower bound of U.S. rates as is often done in shadow-rate models on U.S. data, see e.g. Christensen and Rudebusch (2016). However, towards the end of 2020 Federal Funds futures contracts have priced have priced negative rates in 2021. In the following section we show how the compression of rates at the zero lower bound also impacts the pricing of options on futures. In order to compare the change in value across time figure 2.8 plots the value of a hypothetical at the money call option on a three-month SOFR European futures option with a fixed six month expiry.[7] The option value can then be calculated as

$$C(t, P^{3m}(t;S,T), K, T) = \mathbb{E}^Q \left[e^{-\int_t^T r_s ds} \left(P^{3m}(T;S,T) - K \right)^+ | \mathcal{F}_t \right] \tag{2.4.5}$$

where $P^{3m}(t;S,T)$ denotes the time t price of the three-month SOFR futures contract expiring at time T. Figure 2.8 clearly shows a decrease in the value of the option in the shadow-rate model as the distribution of future short rates becomes truncated at the zero lower bound. This is especially apparent after the rate drop in March 2020 where the option hit a minimum value equal to just 6% of the price of the equivalent option in the AFNS model.

[7] In reality, CME SOFR futures options are American style and thus have an early exercise premium. Flesaker (1993) reports that the the premium is typically less than one basis point for options that are not substantially in the money.

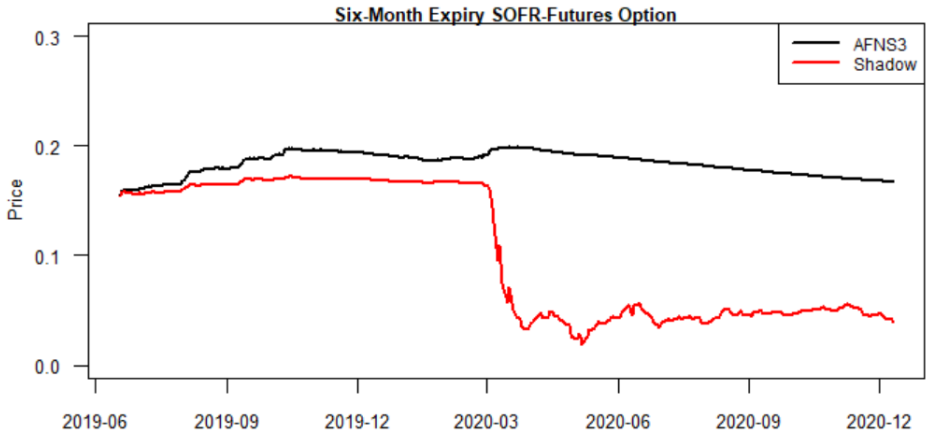

Figure 2.8: *The price of an at the money call option on a hypothetical three-month SOFR futures contract expiring in six months. The prices are quoted in IMM index points and based on daily rolling re-estimations and obtained using Monte Carlo simulations under the risk-neutral measure.*

2.5 SOFR futures convexity adjustment

The convexity adjustment of a futures contract is defined as the difference between the futures rate and an equivalent forward rate. Having estimated a model for the term structure of futures rates, we can compute the convexity adjustment. We follow Mercurio (2018) when defining the convexity adjustment for the one- and three-month SOFR futures. Here we focus solely on the three-factor AFNS model as well as its shadow-rate extension. The one-month adjustment is calculated from the continuously compounded forward rate, $F(t;S,T)$, given by

$$F(t;S,T) = \frac{\log(p(t,S)) - \log(p(t,T))}{T-S}. \tag{2.5.1}$$

Defining the convexity adjustment as the difference between the one-month futures rate and the continuously compounded forward rate, $C^{1m}(t;S,T) := f^{1m}(t;S,T) - F(t;S,T)$, and applying (2.A.10) the one-month adjustment in the AFNS model is

$$C^{1m}(t;S,T) = \frac{A(t,T) - A(t,S)}{T-S}. \tag{2.5.2}$$

We define the three-month convexity adjustment as the difference between the three-month futures rate and the simple forward rate defined as,

$$R^F(t;S,T) = \frac{1}{T-S}\left(\frac{p(t,S)}{p(t,T)} - 1\right). \tag{2.5.3}$$

Similarly the convexity adjustment is defined as $C^{3m}(t;S,T) := f^{3m}(t;S,T) - R^F(t;S,T)$. Then by (2.A.13) in Appendix 2.A, the three-month convexity adjust-

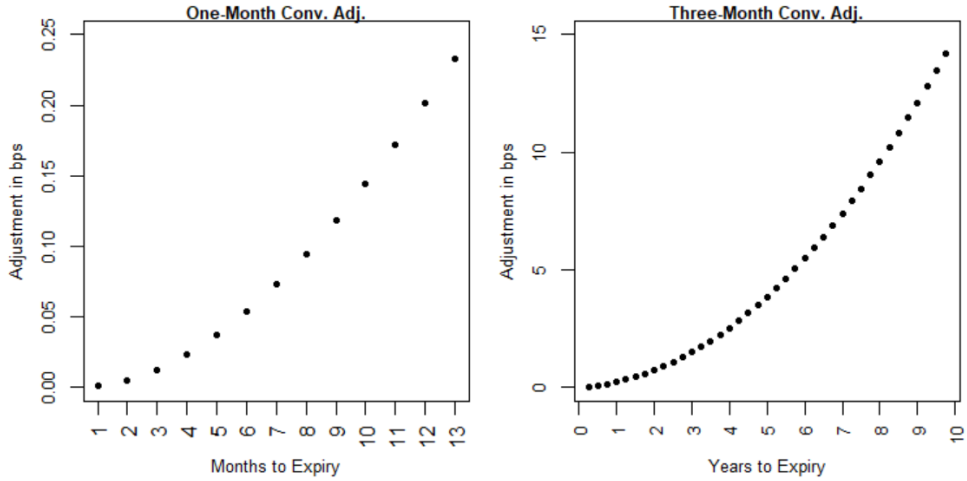

Figure 2.9: *Size of convexity adjustments in the AFNS model as of December 11th 2020 using the final set of SOFR-estimates based on the full sample. The adjustments are plotted for all open SOFR futures contracts traded on the CME.*

ment in the AFNS model is

$$C^{3m}(t;S,T) = \left(R^F(t;S,T) + \frac{1}{T-S}\right)\left(e^{A(t,T)-A(t,S)}e^{A(S,T)}e^{\frac{1}{2}B(S,T)'\mathbb{V}^Q[X_S|\mathcal{F}_t]B(S,T)} - 1\right). \tag{2.5.4}$$

One- and Three-month convexity adjustments in the shadow-rate model are calculated using Monte Carlo simulations. Figure 2.9 plots the AFNS model implied size of the convexity adjustment of the futures rates for the 13 and 39 one- and three-month contracts matching the set of listed SOFR futures on the CME, assuming one is at the beginning of the accrual period of the nearest futures. It clearly shows that using long-dated three-month futures rates as a proxy for the forward rate without any adjustment can lead to sizeable errors. However, when focusing solely on the nearest futures contracts covering the short end of the term structure the convexity adjustment is of very limited scale.

Since the convexity adjustment is model dependent, it changes with the model estimates. To illustrate the range of the size of the adjustment for our data period, we plot convexity adjustments for a selected set of contracts based on rolling re-estimates using SOFR futures data. This is illustrated in figure 2.10, which shows a notable variation in the size of the convexity adjustment for long-dated three-month futures rates.

Given the expression for the one-month convexity adjustment (2.5.2), we see that it is dependent on the estimates of the decay parameter, λ, and the volatility matrix, Σ. As seen in (2.5.4) the three-month convexity adjustment also depends on the level of the discrete forward rate $R^F(t;S,T)$, however, only to a limited extent since the term is small compared to $\frac{1}{T-S} \approx 4$. Given the final set of parameter values

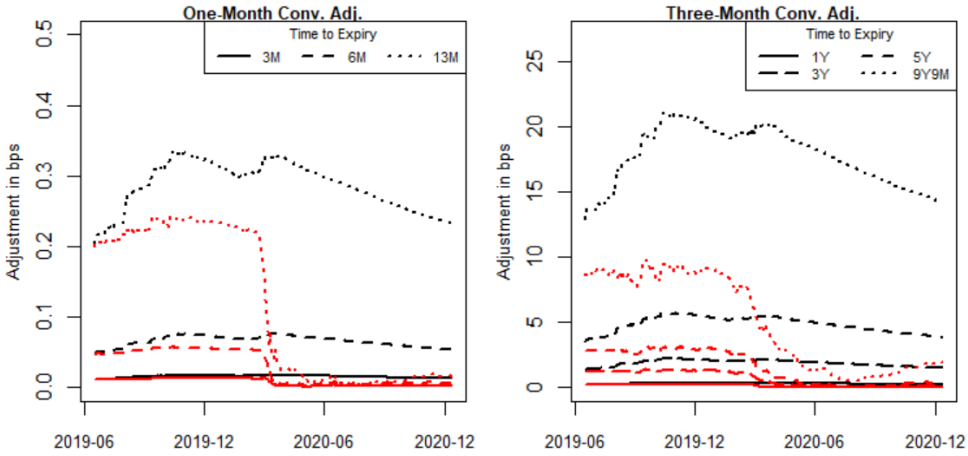

Figure 2.10: *Size of convexity adjustments using rolling re-estimates on SOFR futures data for different fixed time to expiries. The 13 months to expiry one-month and 9 years and 9 months to expiry three-month contracts reflect the last open SOFR futures contracts. The black lines plot the standard AFNS model and the red lines plot the equivalent convexity adjustment in the shadow-rate extension.*

increasing the forward rate by 10% adds less than 0.5 basis point to the convexity adjustment of the furthest futures contract. The main factor driving the variation in the convexity adjustment is the conditional yield volatility under the risk neutral measure as represented by the term $B(S,T)'\mathbb{V}^Q[X_S|\mathcal{F}_t]B(S,T)$ in the three-month convexity adjustment. Thus when rates become increasingly volatile the size of the convexity adjustment also increases. Figure 2.10 also plots the equivalent convexity adjustment of the shadow-rate model. The plots show the convexity adjustment of all contracts dropping close to zero after the FED lowered the target rate in March 2020. The drop reflects a decrease in volatility in the shadow-rate model and highlights that the convexity adjustment is zero when rates are deterministic.

To obtain estimates of the convexity adjustments for a longer sample period containing the global financial crisis, we consider the estimates from the federal funds futures data and plot convexity adjustments as if both one- and three-months contracts equal to those of the SOFR market traded in this market. Figure 2.11 clearly illustrates a spike in the size of the adjustment following the crisis. Subsequently, when rates became compressed against the zero lower bound the convexity adjustment gradually decreases in the Gaussian AFNS model, while in the shadow-rate model we again see a significant drop. Due to the short rate specification in the shadow-rate model, the volatility parameters do not need to decrease to fit the compression in volatility while at the lower bound, thus when the Federal Funds increased the Federal Funds target range away from zero in 2015 the convexity adjustment increases noticeably.

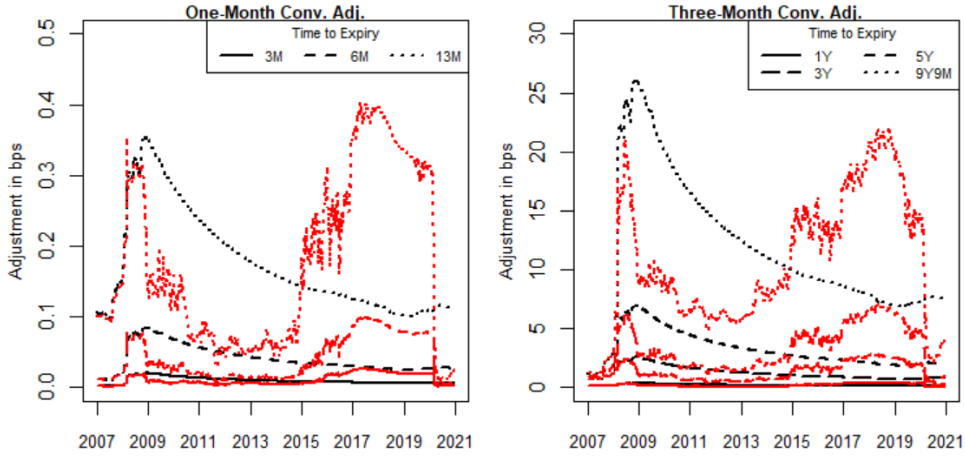

Figure 2.11: *Size of convexity adjustments using rolling re-estimates on federal funds futures data. The 13 months to expiry one-month and 9 years and 9 months to expiry three-month contracts reflect the last open SOFR futures contracts.*

2.6 Conclusion

In this paper we investigate the use of dynamic term structure models for the SOFR futures market using historical data. We find that a standard three-factor arbitrage-free Nelson-Siegel model is able to describe the dynamics of futures prices quite well without explicitly incorporating the expected jumps in the spot rate on FOMC announcement dates. Furthermore, our model is able to produce term rates that are indistinguishable from the indicative rates published by the federal reserve. We furthermore demonstrate that a shadow-rate extension can explicitly capture the volatility compression occurring after a rate drop. Using the models we are able to quantify the size of the convexity adjustment in this market, and determine at what maturity and volatility level such a correction should be implemented.

This provides a framework, which can easily be made to include other derivatives such as SOFR caps, floors and swaptions as these markets become more mature. Future work could extend the empirical analysis to a multi-curve setup. This could include estimating the joint behavior of multiple benchmarks suchs as SOFR, EFFR and LIBOR or some of the more recently proposed benchmarks like AMERIBOR, BSBY or AXI. The estimated models could also be directly used as the SOFR or EFFR components to one of the many existing multi-curve setups (see for example Grbac and Runggaldier (2015) for an overview) for pricing and risk managing derivatives on multiple benchmarks.

2.A AFNS Model Specifications and Results

Here we present the specific parameter restrictions of the AFNS models as well as results needed to price the one- and three-month futures contracts for the AFNS model, similar results can be obtained for the one- and two-factor models. The three-factor Arbitrage-Free Nelson-Siegel model places the following restrictions on the risk neutral dynamics

$$\theta^Q = \begin{pmatrix} 0 \\ 0 \\ 0 \end{pmatrix}, \quad K^Q = \begin{pmatrix} 0 & 0 & 0 \\ 0 & \lambda & -\lambda \\ 0 & 0 & \lambda \end{pmatrix}, \quad \rho_0 = 0, \quad \rho_1 = \begin{pmatrix} 1 \\ 1 \\ 0 \end{pmatrix}. \tag{2.A.1}$$

The state variables are Gaussian with mean and variance

$$\mathbb{E}^Q \left[X_T | \mathcal{F}_t \right] = e^{-K^Q (T-t)} X_t, \tag{2.A.2}$$

$$\mathbb{V}^Q \left[X_T | \mathcal{F}_t \right] = \int_t^T e^{-K^Q (T-s)} \Sigma \Sigma' \left(e^{-K^Q (T-s)} \right)' ds. \tag{2.A.3}$$

Where the matrix exponential can be calculated analytically as

$$e^{-K^Q (T-t)} = \begin{pmatrix} 1 & 0 & 0 \\ 0 & e^{-\lambda (T-t)} & \lambda (T-t) e^{-\lambda (T-t)} \\ 0 & 0 & e^{-\lambda (T-t)} \end{pmatrix}. \tag{2.A.4}$$

Given a diagonal volatility matrix, Σ, we find

$$\mathbb{V}^Q \left[X_T | \mathcal{F}_t \right] = \begin{pmatrix} \sigma_{11}^2 (T-t) & 0 & 0 \\ 0 & \frac{-e^{-2\lambda(T-t)}+1}{2\lambda} \sigma_{22}^2 + \frac{1-e^{-2\lambda(T-t)}((2\lambda(T-t))(\lambda(T-t)+1)+1)}{4\lambda} \sigma_{33}^2 & \frac{e^{-2\lambda(T-t)}(-2\lambda(T-t)-1)+1}{4\lambda} \sigma_{33}^2 \\ 0 & \frac{e^{-2\lambda(T-t)}(-2\lambda(T-t)-1)+1}{4\lambda} \sigma_{33}^2 & \frac{-e^{-2\lambda(T-t)}+1}{2\lambda} \sigma_{33}^2 \end{pmatrix}. \tag{2.A.5}$$

The integral $\int_t^T r_s ds$ is also Gaussian with mean and variance

$$\mathbb{E}^Q \left[\int_t^T r_s ds | \mathcal{F}_t \right] = -B(t,T)' X_t, \tag{2.A.6}$$

$$\mathbb{V}^Q \left[\int_t^T r_s ds | \mathcal{F}_t \right] = \int_t^T \sum_{j=1}^3 \left(\Sigma' B(s,T) B(s,T)' \Sigma \right)_{jj} ds. \tag{2.A.7}$$

Where $B(t,T)$ takes the following form

$$B(t,T) = \begin{pmatrix} -(T-t) \\ -\frac{1-e^{-\lambda(T-t)}}{\lambda} \\ (T-t) e^{-\lambda(T-t)} - \frac{1-e^{-\lambda(T-t)}}{\lambda} \end{pmatrix}. \tag{2.A.8}$$

Define $A(t,T) := \frac{1}{2}\mathbb{V}^Q\left[\int_t^T r_s ds|\mathcal{F}_t\right]$, an analytical formula of $A(t,T)$ is calculated in the original paper Christensen, Diebold, and Rudebusch (2011). Assuming a diagonal volatility matrix the expression simplifies to

$$\begin{aligned}A(t,T) = \sigma_{11}^2\frac{(T-t)^3}{6} + \sigma_{22}^2(T-t)\left(\frac{1}{2\lambda^2} - \frac{1}{\lambda^3}\frac{1-e^{-\lambda(T-t)}}{T-t} + \frac{1}{4\lambda^3}\frac{1-e^{-2\lambda(T-t)}}{T-t}\right)\\ + \sigma_{33}^2(T-t)\Big(\frac{1}{2\lambda^2} + \frac{1}{\lambda^2}e^{-\lambda(T-t)} - \frac{1}{4\lambda}(T-t)e^{-2\lambda(T-t)} - \frac{3}{4\lambda^2}e^{-2\lambda(T-t)}\\ - \frac{2}{\lambda^3}\frac{1-e^{-\lambda(T-t)}}{T-t} + \frac{5}{8\lambda^3}\frac{1-e^{-2\lambda(T-t)}}{T-t}\Big).\end{aligned} \tag{2.A.9}$$

We are now ready to compute the one- and three-month futures rates. The one-month futures rate can be computed as

$$\begin{aligned}f^{1m}(t;S,T) &= \mathbb{E}^Q\left[\frac{1}{T-S}\int_S^T r_s ds|\mathcal{F}_t\right]\\ &= \mathbb{E}^Q\left[\frac{1}{T-S}\int_t^T r_s ds - \frac{1}{T-S}\int_t^S r_s ds\mathcal{F}_t\right]\\ &= \frac{(B(t,S)-B(t,T))'}{T-S}X_t.\end{aligned} \tag{2.A.10}$$

And when $S < t$ such that part of the underlying has already been realized

$$f^{1m}(t;S,T) = \frac{1}{N}\sum_{i=1}^{N_0} R_{d_i}(t_i) - \frac{B(t,T)'}{T-S}X_t. \tag{2.A.11}$$

The three-month futures rate can be computed using the tower property

$$\begin{aligned}\mathbb{E}^Q\left[e^{\int_S^T r_s ds}|\mathcal{F}_t\right] &= \mathbb{E}^Q\left[\mathbb{E}^Q\left[e^{\int_S^T r_s ds}|\mathcal{F}_S\right]|\mathcal{F}_t\right]\\ &= \mathbb{E}^Q\left[e^{A(S,T)-B(S,T)'X_S}|\mathcal{F}_t\right]\\ &= e^{A(S,T)}e^{-B(S,T)'e^{-K^Q(S-t)}X_t + \frac{1}{2}B(S,T)'\mathbb{V}^Q[X_S|\mathcal{F}_t]B(S,T)}.\end{aligned} \tag{2.A.12}$$

such that

$$f^{3m}(t;S,T) = \frac{1}{T-S}\left(e^{A(S,T)}e^{-B(S,T)'e^{-K^Q(S-t)}X_0 + \frac{1}{2}B(S,T)'\mathbb{V}^Q[X_S|\mathcal{F}_t]B(S,T)} - 1\right). \tag{2.A.13}$$

And when $S < t$

$$f^{3m}(t,S,T) = \frac{1}{T-S}\left(\left(\prod_{i=1}^{N_0}[1+d_i R_{d_i}(t_i)]\right)e^{A(t,T)-B(t,T)'X_t} - 1\right). \tag{2.A.14}$$

2.B Pricing the Futures Contracts in a Shadow-Rate Model

Introducing a lower bound on the short rate results in a model where the short rate is no longer Gaussian. Therefore, we can not use the same results used to price the futures contracts in the standard AFNS model. In this section we present formulas necessary to price the one- and three-month futures contracts in a shadow-rate extension of the three-factor AFNS model. We start by listing a few auxiliary results required to calculate the futures rates. Using the results from Appendix 2.A we can calculate the mean of the shadow short rate as

$$\begin{aligned}\mathbb{E}^Q[s_T|\mathcal{F}_t] &= \rho_1' e^{-K^Q(T-t)}X_t \\ &= L_t + e^{-\lambda(T-t)}S_t + \lambda(T-t)e^{-\lambda(T-t)}C_t. \end{aligned} \tag{2.B.1}$$

The variance is given by

$$\mathbb{V}^Q[s_T|\mathcal{F}_t] = \rho_1' \mathbb{V}^Q[X_T|\mathcal{F}_t]\rho_1 \tag{2.B.2}$$

and thus

$$\begin{aligned}\mathbb{V}^Q[s_T|\mathcal{F}_t] = \sigma_{11}^2(T-t) + \sigma_{22}^2\frac{1-e^{-2\lambda(T-t)}}{2\lambda} \\ + \sigma_{33}^2\left(\frac{1-e^{-2\lambda(T-t)}}{4\lambda} - \frac{1}{2}(T-t)e^{-2\lambda(T-t)} - \frac{1}{2}(T-t)^2\lambda e^{-2\lambda(T-t)}\right).\end{aligned} \tag{2.B.3}$$

Where we have assumed a diagonal volatility matrix Σ and used equation (2.A.5). Furthermore, we note that for $s, u > t$

$$Cov^Q[s_u, s_s|\mathcal{F}_t] = \int_t^{u\wedge s} \rho_1' e^{-K^Q(u-\nu)}\Sigma\Sigma'\left(e^{-K^Q(s-\nu)}\right)'\rho_1 d\nu. \tag{2.B.4}$$

Again, assuming a diagonal volatility matrix the covariance can be calculated as

$$\begin{aligned}Cov^Q[s_u, s_s|\mathcal{F}_t] = \sigma_{11}^2((u\wedge s)-t) + \frac{\sigma_{22}^2}{2\lambda}\left(e^{-\lambda(s+u-2(u\wedge s))} - e^{-\lambda(s+u-2t)}\right) \\ + \frac{\sigma_{33}^2}{4\lambda}\Big(e^{-\lambda(s+u-2(u\wedge s))}\left(\lambda(s+u-2(u\wedge s))+1\right) \\ - e^{-\lambda(s+u-2t)}\left(2\lambda^2(s-t)(u-t)+\lambda(s+u-2t)+1\right)\Big).\end{aligned} \tag{2.B.5}$$

The one- and three-month futures rates are computed using results from Priebsch (2013). We follow the notation and denote $\mu_{t,T} = \mathbb{E}^Q[s_T|\mathcal{F}_t]$, $\sigma_{t,T}^2 = \mathbb{V}^Q[s_T|\mathcal{F}_t]$ and $\sigma_{t,u\times s} = Cov^Q[s_u, s_s|\mathcal{F}_t]$. Computing the one-month futures rate requires calculating the first moment of $\int_t^T r_s ds$ under the risk neutral measure. The expectation is given by

$$\mathbb{E}^Q\left[\int_t^T r_s ds|\mathcal{F}_t\right] = \int_t^T \mu_{t,s}\Phi\left(\frac{\mu_{t,s}}{\sigma_{t,s}}\right)\sigma_{t,s}\phi\left(\frac{\sigma_{t,s}}{\mu_{t,s}}\right)ds. \tag{2.B.6}$$

The one-month rate can therefore be computed up to the standard normal CDF, which is then numerically integrated over the remaining duration of the contract. The three-month futures rate is approximated using the power series expansion of the cumulant generating function

$$\log \mathbb{E}^Q \left[e^{\int_t^T r_s ds} | \mathcal{F}_t \right] = \sum_{j=1}^{\infty} \frac{\kappa_j^Q}{j!} \tag{2.B.7}$$

where κ_j^Q is the j^{th} cumulant of $\int_t^T r_s ds$ under the Q-measure. We truncate the series at two terms and use the result that the two first cumulants of any random variable are equal to the two first centered moments. The approximation then becomes

$$\mathbb{E}^Q \left[e^{\int_t^T r_s ds} | \mathcal{F}_t \right] \approx \exp\left(\mathbb{E}^Q \left[\int_t^T r_s ds | \mathcal{F}_t \right] + \frac{1}{2} \mathbb{V}^Q \left[\int_t^T r_s ds | \mathcal{F}_t \right] \right). \tag{2.B.8}$$

Since we have already shown how to compute the first moment in the one-month futures rate, it only remains to compute the second moment to obtain the variance. Again, using results from Priebsch (2013) the expression for the second moment under the risk neutral measure is

$$\begin{aligned}
\mathbb{E}^Q \left[\left(\int_t^T r_s ds \right)^2 | \mathcal{F}_t \right] =& 2 \int_t^T \int_t^s \Bigg\{ \left(\mu_{t,u} \mu_{t,s} + \sigma_{t,u \times s} \right) \Phi_2^d \left(-\zeta_{t,u}, -\zeta_{t,s}; \chi_{t,u \times s} \right) \\
&+ \sigma_{t,s} \mu_{t,u} \phi(\zeta_{t,s}) \Phi \left(\frac{\zeta_{t,u} - \chi_{t,u \times s} \zeta_{t,s}}{\sqrt{1 - \chi_{t,u \times s}^2}} \right) \\
&+ \sigma_{t,u} \mu_{t,s} \phi(\zeta_{t,u}) \Phi \left(\frac{\zeta_{t,s} - \chi_{t,u \times s} \zeta_{t,u}}{\sqrt{1 - \chi_{t,u \times s}^2}} \right) \\
&+ \sigma_{t,u} \sigma_{t,s} \sqrt{\frac{1 - \chi_{t,u \times s}^2}{2\pi}} \phi \left(\sqrt{\frac{\zeta_{t,u}^2 - 2 * \chi_{t,u \times s} \zeta_{t,u} \zeta_{t,s} + \zeta_{t,s}^2}{1 - \chi_{t,u \times s}^2}} \right) \Bigg\} du ds
\end{aligned} \tag{2.B.9}$$

with $\zeta_{t,j} = \frac{\mu_{t,j}}{\sigma_{t,j}}$ for $j = u, s$ and $\chi_{t,u \times s} = \frac{\sigma_{t,u \times s}}{\sigma_{t,u} \sigma_{t,s}}$. Φ_2^d denotes the decumulative bivariate normal distribution function, which satisfies $\Phi_2^d(z_1, z_2; \chi) = 1 - \Phi(z_1) - \Phi(z_2) + \Phi_2(z_1, z_2; \chi)$, where Φ_2 is the cumulative bivariate normal distribution function of two standard normals with covariance χ. As with the first moment the integrand is numerically integrated over both dimensions to obtain the second moment.[8]
Zero coupon bonds in the shadow-rate model are approximated using the series

[8] Computing the double integral can quickly become computationally expensive. In our empirical implementaion we numerically integrate the expression using the Gauss-Kronrod method with five points in each dimension.

Date	One-Month							Three-Month				
	1M	**2M**	**3M**	**4M**	**5M**	**6M**	**7M**	**3M**	**6M**	**9M**	**12M**	**15M**
06/17/19	-0.02	-0.02	-0.01	-0.01	-0.01	0.00	0.00	0.14	0.07	0.04	0.02	0.00
12/11/20	0.00	0.04	0.02	0.06	0.07	0.04	0.03	0.02	0.06	0.02	-0.02	-0.04

Table 2.5: *Difference between the approximated futures rate and Monte Carlo implied futures rate for all contract lengths used in the estimation. All values are in basis points.*

expansion of the cumulant generating function

$$\log \mathbb{E}^Q \left[e^{-\int_t^T r_s ds} | \mathcal{F}_t \right] = \sum_{j=1}^{\infty} (-1)^j \frac{\kappa_j^Q}{j!}. \tag{2.B.10}$$

Again, truncating the series at two terms the approximation becomes

$$P(t,T) = \mathbb{E}^Q \left[e^{-\int_t^T r_s ds} | \mathcal{F}_t \right] = \exp\left(-\mathbb{E}^Q \left[\int_t^T r_s ds | \mathcal{F}_t \right] + \frac{1}{2} \mathbb{V}^Q \left[\int_t^T r_s ds | \mathcal{F}_t \right] \right). \tag{2.B.11}$$

2.B.1 Accuracy of the shadow-rate model futures rate approximation

We test the accuracy of the cumulant based approximation of the futures rates in the shadow-rate model to the futures rates in equation 2.3.16 and 2.3.20. To gauge the size of the error we compare the approximation to futures rates obtained using Monte Carlo simulations under the risk neutral measure. The simulations are based on 100,000 paths with a step size of 1/3600. Table 2.5 contains the error as measured by the difference between the approximation and Monte Carlo value for all maturities used in the estimation. We assume that the prices are observed at the beginning of the nearest futures contract and thus none of the overnight rates have been accrued by the contracts. To evaluate the approximations both away from and at the zero lower bound we consider the estimates and state variables at the beginning of the estimation period as well as the most recent date reflecting a period with rates at their lower bound.

Table 2.5 illustrates that errors on all considered contracts are a fraction of a basis point and far less than the minimum price fluctuation on CME SOFR futures contracts. Thus for estimation purposes the approximation results in accurate futures prices in the shadow-rate model.

2.C Estimation Methodology

The presented models are estimated using a Kalman Filter on end of day futures data. Thus we consider the discretized state process under the P-dynamics given by

$$X_t = \theta^P + e^{-K^P \Delta t}(X_{t-1} - \theta^P) + \int_0^{\Delta t} e^{-K^P u} \Sigma dW_u^P \tag{2.C.1}$$

with Δt set to $1/250$ to approximately reflect the number of daily futures data observations in a year. Rearranging we define the state equation of the Kalman Filter as

$$X_t = \left(I - e^{-K^P \Delta t}\right) \theta^P + e^{-K^P \Delta t} X_{t-1} + \xi_t \tag{2.C.2}$$

with $\xi_t \sim \mathcal{N}(0, Q)$ and covariance, Q, where

$$Q = \int_0^{\Delta t} e^{-K^P u} \Sigma \Sigma' \left(e^{-K^P u}\right)' du. \tag{2.C.3}$$

For any specification of K^P an analytical solution to Q is available by applying the eigendecomposition with V a matrix of the eigenvectors and Λ a vector of the corresponding eigenvalues

$$e^{-K^P u} = e^{-V \Lambda V^{-1} u} = V e^{-\Lambda u} V^{-1}, \tag{2.C.4}$$

we can calculate the covariance matrix as

$$Q = V \left(\int_0^{\Delta t} e^{-\Lambda u} V^{-1} \Sigma \Sigma' (V^{-1})' e^{-\Lambda u} du \right) V'. \tag{2.C.5}$$

Define $G = V^{-1} \Sigma \Sigma' (V^{-1})'$ the entries of the matrix defined by the integral are then

$$\left(\int_0^{\Delta t} e^{-\Lambda u} V^{-1} \Sigma \Sigma' (V^{-1})' e^{-\Lambda u} du \right)_{ij} = \frac{G_{ij}}{\Lambda_{ii} + \Lambda jj} \left(1 - e^{-(\Lambda_{ii} + \Lambda jj)\Delta t}\right). \tag{2.C.6}$$

The prediction step in the Kalman filter is computed as

$$X_{t|t-1} = F_t X_{t-1|t-1} + C_t, \tag{2.C.7}$$

$$P_{t|t-1} = F_t P_{t-1|t-1} F_t' + Q. \tag{2.C.8}$$

Where $F_t = e^{-K^P \Delta t}$ denotes the state transition model and $C_t = \left(I - e^{-K^P \Delta t}\right) \theta^P$ the control input. The standard Kalman filter requires the measurement equation to be affine in the state vector

$$y_t = A_t + B_t X_t + \varepsilon_t \tag{2.C.9}$$

with $\varepsilon_t \sim \mathcal{N}(0, H)$ where H is a diagonal matrix and the transition and measurement errors, ξ_t and ε_t, are independent. The affine measurement equation is only satisfied

for the one-month futures rate approximation. in the case of the three-month futures we apply the method of the extended Kalman filter where the measurement equation is assumed to be on the general form

$$y_t = h(X_t, \Theta) + \varepsilon_t. \tag{2.C.10}$$

A Taylor expansion of h is then done around $X_{t|t-1}$

$$h(X_t, \Theta) \approx h(X_{t|t-1}, \Theta) + \frac{\partial h(X_t, \Theta)}{\partial X_t}\Big|_{X_t = X_{t|t-1}} (X_t - X_{t|t-1}). \tag{2.C.11}$$

Now defining

$$A_t = h(X_{t|t-1}, \Theta) - \frac{\partial h(X_t, \Theta)}{\partial X_t}\Big|_{X_t = X_{t|t-1}} X_{t|t-1}, \tag{2.C.12}$$

$$B_t = \frac{\partial h(X_t, \Theta)}{\partial X_t}\Big|_{X_t = X_{t|t-1}} \tag{2.C.13}$$

the affine approximation becomes

$$y_t \approx A_t + B_t X_t + \varepsilon_t. \tag{2.C.14}$$

The measurement residuals are computed using the time t futures rates data, y_t, and the model implied futures rates.

$$\nu_t = y_t - h(X_t, \Theta). \tag{2.C.15}$$

The residuals have a conditional mean of 0 and conditional variance given by

$$S_t := \mathbb{V}[\nu_t | y_{t-1}, ..., y_1] = H + B_t P_{t|t-1} B_t'. \tag{2.C.16}$$

In the update step the a priori state estimates are updated using the observed time t data

$$X_{t|t} = X_{t|t-1} + K_t \nu_t, \tag{2.C.17}$$

$$P_{t|t} = (I - K_t B_t) P_{t|t-1} \tag{2.C.18}$$

where K_t denotes is the optimal Kalman gain matrix given by

$$K_t = P_{t|t-1} B_t' S_t^{-1}. \tag{2.C.19}$$

The resulting Gaussian log-likelihood for a given set of parameters, Θ, is determined by the conditional mean and variance of the innovations ν_t

$$l(y_1, ..., y_T; \Theta) = -\frac{NT}{2} \log(2\pi) - \frac{1}{2} \sum_{t=1}^{T} \left(\log |S_t| + \nu_t' S_t^{-1} \nu_t \right) \tag{2.C.20}$$

To obtain the optimal set of parameters, $\hat{\Theta}$, we maximize the log-likelihood function using the Nelder-Mead algorithm with a function value tolerance of 0.01. The state variables are required to be stationary under the P-measure and we therefore require the eigenvalues of K^P to be positive.

2.C.1 Efficiency of the extended Kalman filter

The validity of the results heavily relies on the model parameters as well as underlying state variables being accurately estimated by the extended Kalman filter. Therefore, we construct a simulation study to investigate the efficiency of the extended Kalman filter maximum-likelihood method when estimating the model based on data from futures contracts. We assume that the observed futures follow the AFNS model with parameters equal to the final set of parameters obtained for the full SOFR dataset. The underlying state variables are simulated using the discretized P-dynamics

$$X_{t+1} = X_t + K^P(\theta^P - X_t)\Delta t + \sqrt{\Delta t}\Sigma Z_t \tag{2.C.21}$$

with $Z_t \sim \mathcal{N}(0, I_3)$ and Δt set to $1/250$ to reflect the daily observations and the value used in the actual estimation problem. The process is started in the unconditional mean $X_0 = \theta^P$. To reflect the SOFR-estimation the simulated data consists of seven consecutive observations of one-month futures and five consecutive observations of three-month futures. To simplify the study we assume that the contract lengths are 30 and 90 days for all one- and three-month futures. Further, we assume that at all times we observe both the first one- and three-month contract at the beginning of the accrual period, thus we do not have to factor in any rates that have already been accumulated by the contracts. The set of start dates (denoted in ACT/360) for the simulated one- and three-months contracts respectively are therefore $\tau^{1m} = \{0, 30/360, 60/360, 90/360, 120/360, 150/360, 180/360\}$ and $\tau^{3m} = \{0, 90/360, 180/360, 270/360, 360/360\}$. The simulated datasets contain 500 observations reflecting approximately two years of daily data. The futures prices are assumed to be observed without error, but rounded to nearest half basis point representing the minimum price fluctuation on CME SOFR futures.[9] We base the simulation study on 1.000 paths. To avoid misspecification the optimization algorithm is started in the true set of parameter values.

Focusing on the parameters specific to the physical measure, K^P and θ^P, in table 2.6 we note that these parameters are poorly estimated with fairly large standard errors. As shown in Christensen, Lopez, and Rudebusch (2013) this is a common issue when estimating Gaussian term structure models and getting a sensible estimate of the physical drift and mean reversion requires a much longer data sample than what is currently available from the SOFR futures market. However, when turning to the parameters governing the risk-neutral dynamics, λ and Σ, we note that these are estimated close to their respective true values showing no significant bias and a low standard deviation from the true values. This is promising since only the risk-neutral dynamics are relevant when computing the current term structure, while the drift parameters under the physical measure are solely required in e.g. forecasting exercises.

[9] The nearest one and three-month futures contract both have a minimum price fluctuation of 0.25 basis point. We disregard this minor detail here.

Parameter	True Value	Mean	SD	5%	Q1	Median	Q3	95%
k_{11}^P	0.0980	0.0763	0.1331	0.0032	0.0247	0.0512	0.0881	0.2072
k_{22}^P	0.5153	0.4753	0.7928	0.0072	0.0697	0.2855	0.5843	1.5521
k_{33}^P	2.4486	2.1291	2.2305	0.0327	0.3457	1.4599	3.2279	6.5968
θ_1^P	0.0175	0.0093	0.0037	-0.0002	0.0031	0.0051	0.0135	0.0277
θ_2^P	-0.0037	-0.0004	0.0018	-0.0055	-0.0025	-0.0006	0.0012	0.0058
θ_3^P	-0.0012	-0.0003	0.0002	-0.0024	-0.0010	-0.0003	0.0003	0.0020
σ_{11}	0.0054	0.0054	0.0002	0.0051	0.0053	0.0054	0.0055	0.0057
σ_{22}	0.0062	0.0062	0.0003	0.0059	0.0061	0.0062	0.0063	0.0065
σ_{33}	0.0088	0.0088	0.0003	0.0083	0.0086	0.0088	0.0090	0.0093
λ	2.0284	2.0281	0.0047	2.0206	2.0251	2.0281	2.0310	2.0357

Table 2.6: *Estimation results using the Kalman Filter on 500 daily simulated futures observations. The results are based on 1000 simulations.*

State Variable	RMSE	Mean	SD	5%	Q1	Median	Q3	95%
Level	0.3	0.0	0.3	-0.4	-0.2	0.0	0.2	0.4
Slope	0.2	0.0	0.2	-0.4	-0.2	0.0	0.2	0.4
Curve	0.6	0.0	0.6	-1.0	-0.5	0.0	0.4	1.0

Table 2.7: *Statistics on the difference between the true final state variable and the filtered state variable obtained from the Kalman Filter. All values are in basis points.*

In order to produce a valid term structure it is also important that the filtering process is able to accurately reproduce the value of the latent state variable. To test this aspect we compare the true final set of state variables from each simulation with the final filtered set of state variables produced by the Kalman filter. Note that we use the standard Level, Slope and Curve to describe each the three factors of the AFNS model. The results in table 2.7 indicate that the filtered state variables closely track the true values with errors of less than one basis point.

2.D Futures Rate Approximations

In the following we compare exact futures rates to rates obtained from the approximations presented in section 2 and used in the historical estimation. Since we consider Gaussian term structure models exact expressions for the futures rates of both the one- and three-month contracts exist. The results shown here are based on the three-factor AFNS model but can similarly be obtained for the one- and two-factor Gaussian models.

To illustrate the size of the approximation we consider the final set of parameters obtained from the full period of SOFR futures data with the state variable X_t equal to the unconditional mean θ^P. We define the approximation error as the difference between the approximation and the exact futures rate. Figure 2.12 presents the approximation error covering 13 consecutive one-month and 39 consecutive three-month contracts. The size of the error is similar across all consecutive contracts and

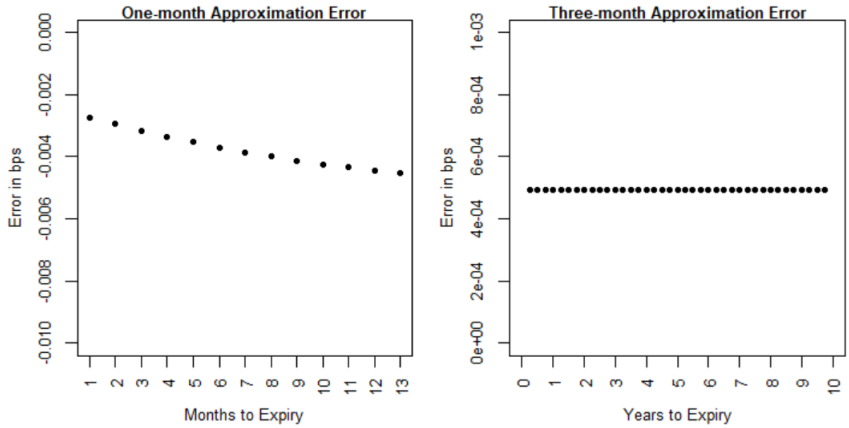

Figure 2.12: *Approximation error for one- and three-month futures rates based on the final SOFR parameter estimates.*

small compared to the minimum price fluctuation of the futures contract. Based on this the approximations do not have any significant impact on the model estimation and resulting term rates.

2.D.1 Exact one-month SOFR futures rate

Recalling that the one month futures rate is given by the discrete average $R(t,T) = \frac{1}{N}\sum_{i=1}^{N}\frac{1}{d_i}\left(\frac{1}{p(t_i,t_i+d_i)}-1\right)$, we can calculate the mean of the average overnight rate during the reference period as

$$\begin{aligned}
f^{1m}(t;S,T) &= \mathbb{E}^Q\left[\frac{1}{N}\sum_{i=1}^{N}\frac{1}{d_i}\left(\frac{1}{p(t_i,t_i+d_i)}-1\right)|\mathcal{F}_t\right] \\
&= \frac{1}{N}\sum_{i=1}^{N}\frac{1}{d_i}\left(\mathbb{E}^Q\left[\frac{1}{\mathbb{E}^Q\left[e^{-\int_{t_i}^{t_i+d_i} r_s ds}|\mathcal{F}_{t_i}\right]}|\mathcal{F}_t\right]-1\right) \\
&= \frac{1}{N}\sum_{i=1}^{N}\frac{1}{d_i}\left(\mathbb{E}^Q\left[\frac{1}{e^{A(t_i,t_i+d_i)+B(t_i,t_i+d_i)'X_{t_i}}}|\mathcal{F}_t\right]-1\right) \\
&= \frac{1}{N}\sum_{i=1}^{N}\frac{1}{d_i}\left(\mathbb{E}^Q\left[e^{-A(t_i,t_i+d_i)-B(t_i,t_i+d_i)'X_{t_i}}|\mathcal{F}_t\right]-1\right) \\
&= \frac{1}{N}\sum_{i=1}^{N}\frac{1}{d_i}\left(e^{-A(t_i,t_i+d_i)}e^{-B(t_i,t_i+d_i)'e^{-K^Q(t_i-t)}X_t+\frac{1}{2}B(t_i,t_i+d_i)'\mathbb{V}^Q[X_{t_i}|\mathcal{F}_t]B(t_i,t_i+d_i)}-1\right)
\end{aligned} \tag{2.D.1}$$

2.D.2 Exact three-Month SOFR futures rate

To gauge the size of the approximation error of the three-month futures rate using the continuous approximation we follow Henrard (2018). Here it is shown that

the three-month futures rate in a Gaussian Heath-Jarrow-Morton setup without approximation is given by

$$f^{3m}(t;S,T) = \frac{1}{T-S}\left(\frac{p(t,S)}{p(t,T)}\prod_{i=1}^{n}\gamma(t_{i-2},t_{i-1},t_{i-1},t_n) - 1\right) \tag{2.D.2}$$

with $t_{-1} = t$, $S = t_0 < t_1 <, ..., < t_{n-1} < t_n = T$ and

$$\gamma(s,t,u,v) = \exp\left(\int_s^t \nu(\tau,v)(\nu(\tau,v) - \nu(\tau,u))'d\tau\right) \tag{2.D.3}$$

where $\nu(t,T)$ defines the $p(t,T)$ bond volatility. By application of the multi-dimensional Itô's lemma with $g(t,X_t) = e^{A(t,T)+B(t,T)'X_t}$ we have the following Q-dynamics

$$\begin{aligned} dp(t,T) = dg(t,X_t) &= r_t p(t,T)dt + \sum_{i=1}^{n}\frac{\partial f}{\partial x_i}\sigma_i dW_t \\ &= r_t p(t,T)dt + \sum_{i=1}^{n} B_i(t,T)e^{A(t,T)+B(t,T)'X_t}\sigma_i dW_t \\ &= r_t p(t,T)dt + p(t,T)\sum_{i=1}^{n} B_i(t,T)\sigma_i dW_t \\ &= r_t p(t,T)dt + p(t,T)\nu(t,T)dW_t, \end{aligned} \tag{2.D.4}$$

with σ_i denoting the row vectors of the volatility matrix, Σ. Thus in the three factor AFNS model with a diagonal volatility matrix the T-bond volatility is

$$\nu(t,T)' = \begin{pmatrix} -(T-t)\sigma_{11} \\ -\frac{1-e^{-\lambda(T-t)}}{\lambda}\sigma_{22} \\ \left((T-t)e^{-\lambda(T-t)} - \frac{1-e^{-\lambda(T-t)}}{\lambda}\right)\sigma_{33} \end{pmatrix}. \tag{2.D.5}$$

The expression for $\gamma(s,t,u,v)$ becomes rather involved for the three-factor model and thus omitted here. It is however a scalar that can be analytically computed.

Chapter 3

Decomposing LIBOR in Transition: Evidence from the Futures Markets

This chapter contains the manuscript *Skov and Skovmand (2022)*.

Abstract

Applying historical data from the USD LIBOR transition period, we estimate a joint model for SOFR, Federal Funds, and Eurodollar futures rates as well as spot USD LIBOR and term repo rates. The framework endogenously models basis spreads between each of the benchmark rates and allows for the decomposition of spreads. Modeling the LIBOR-OIS spread as credit and funding-liquidity roll-over risk, we find that the spike in the LIBOR-OIS spread during the onset of COVID-19 was mainly due to credit risk, while on average credit and funding-liquidity risk contribute equally to the spread.

Keywords: SOFR, LIBOR, Federal Funds Rate, Futures, Roll-Over Risk.

3.1 Introduction

Fixed income markets are currently undergoing a major transition from the well established IBOR rates to overnight transaction-based rates termed Risk-Free rates (RFR) as the primary interest rate benchmark. In the US the Secured Overnight Financing Rate (SOFR) is scheduled to replace USD LIBOR by the middle of 2023. In particular, when facing a transition from LIBOR to SOFR, understanding and modeling what sets LIBOR apart from SOFR from an empirical point of view is of great importance to market participants. Furthermore, the end of LIBOR has

already prompted a wide variety of potential replacements,[1] as SOFR, being a secured overnight rate, does not measure the actual cost of unsecured borrowing at term. In fact, Klingler and Syrstad (2021) show that term rates based on SOFR can be detached from banks marginal funding and highlight the possible problematic implications of this for products such as credit lines during market stress. The introduction of several alternative rates and the ensuing discussions (see for example Bartholomew (2021)), reflect the demand for a rate that captures the actual cost of funding as well as the need to understand and quantify the drivers of the funding costs.

Vast amounts of research in the field of term structure modeling have been devoted to the decomposition of LIBOR. Early studies such as Collin-Dufresne and Solnik (2001), Feldhütter and Lando (2008), and Liu, Longstaff, and Mandell (2006) apply affine arbitrage-free multifactor models to study the impact of liquidity and credit risk on spreads between LIBOR, interest rate swap rates, and treasury yields. The large increase in the spread between LIBOR and a maturity-matched overnight indexed swap (OIS) referencing the Effective Federal Funds Rate (EFFR) during the Great Financial Crisis further brought attention to the drivers of the LIBOR-OIS spread. Michaud and Upper (2008) argue that the lack of relationship between default risk and money market risk premia as well as the impact of central bank liquidity facilities on interbank rates indicate that liquidity is a key component to the size of the spread. Dubecq et al. (2016) use a quadratic term structure model to decompose the EURIBOR-OIS into credit and liquidity risks and evaluate effects of unconventional monetary policy in the euro zone during the crisis. Filipović and Trolle (2013) study the decomposition of the LIBOR-OIS and EURIBOR-OIS spread during the Financial Crisis using credit default swap (CDS) data on LIBOR panel banks to identify a default and non-default component. Similarly, Gallitschke, Seifried, and Seifried (2017) study the decomposition of the LIBOR-OIS into credit and liquidity components using an equilibrium style modeling approach. Backwell et al. (2019) use similar data to decompose the EURIBOR-OIS spread into roll-over risk components. These studies all base their estimation of the LIBOR-OIS spread around swap data.

In this paper we take a different approach and decompose the LIBOR-OIS spread by leveraging the fact that since the introduction of the SOFR futures contract in May of 2018 futures contracts referencing EFFR, SOFR, and LIBOR have traded simultaneously at the Chicago Mercantile Exchange (CME). This allows us to describe the dynamics of the benchmark rates using a joint model for Federal Funds, SOFR, and Eurodollar futures. While the majority of the existing research has focused on the decomposition of the LIBOR-OIS spread during the Financial Crisis, our paper, as a result of the fairly recent introduction of SOFR futures, studies the behaviour

[1] For example the ICE Bank Yield Index (IBYI), Bloomberg Short-Term Bank Yield Index (BSBY), AMERIBOR, and AXI (see Berndt, Duffie, and Zhu (2020))

of the spread in the current transitory interest rate environment and in particular around the onset of the COVID-19 pandemic.

When modeling futures rates, we have to account for the futures convexity adjustment, see e.g. Skov and Skovmand (2021) and Mercurio (2018). This is a model-dependent task, we therefore consider an affine framework for the the joint benchmark dynamics. Modeling term rates, we follow the approach of Alfeus, Grasselli, and Schlögl (2020) and Backwell et al. (2019) and model the LIBOR-OIS spread as a result of roll-over risk. By roll-over risk, we refer to the risk that an entity at a future point in time is not able to roll-over its loan at the prevailing reference rate, due to changes in credit or funding-liquidity risk. An increase in the roll-over risk components of our model thus leads to a steepening in the term structure of money market spreads consistent with the observations in Gorton, Metrick, and Xie (2021) showing that there was a "flight from maturity" during the Great Financial Crisis.

We apply the Kalman filter quasi-maximum likelihood method to estimate the model to the historical record of spot and futures rates with up to one year of maturity. The model fit shows that the model is able to capture the cross-sectional and time variation in the term structure of futures rates for all three benchmark rates. As an additional validity check we show that the model is able to provide close fits to out of sample swap rates on OIS contracts for EFFR and SOFR as well as LIBOR swap contracts. Examining the latent state variables filtered by the model estimation indicates that the FOMC announcement on October 11th 2019 in response to the SOFR surge during September 2019 was effective in bringing down both the repo specific liquidity premium as well as the funding-liquidity component.

Finally, including data on term repos allow us to decompose the three- and six-month LIBOR-OIS spread into a credit and funding-liquidity component. Our framework suggests that the credit and funding components on average each contribute equally to the spread during our sample period. We also find that the large spike in the LIBOR-OIS spread during the outbreak of the COVID-19 crisis was mainly driven by an increase in credit risk.

The paper is structured as follows. In section 3.2 we present the joint affine setup for SOFR, EFFR, LIBOR, and term repos as well as the main formulas required to compute spot and futures rates. Section 3.3 details the data and quasi-maximum likelihood method used to estimate the model. In section 3.4 we discuss the empirical results.

3.2 Constructing a Joint Interest Rate Setup for SOFR, EFFR, Term Repo, and LIBOR

3.2.1 Modeling SOFR and EFFR

We consider a single risk-free short-rate, $r(t)$, defined on the filtered probability space $(\Omega, \mathcal{G}, \{\mathcal{G}\}_{t\geq 0}, Q)$. The risk-neutral measure, Q, is defined by the risk-free continuous savings account numeraire with value process $B(t) = B(0)e^{\int_0^t r(u)du}$. The associated risk-free zero coupon bond price process is given by

$$p(t,T) = B(t)\mathbb{E}^Q\left[B(T)^{-1}|\mathcal{G}(t)\right]. \tag{3.2.1}$$

The spread between the risk-free rate and SOFR is represented by a non-negative process $\psi(t)$. The process captures the systemic specific risk premia in the repo market such as gap risk, induced by varying liquidity of treasury securities, default risk in treasuries, haircuts etc. (see Lou (2021) for an depth discussion of the magnitude of these particular risks and Hu, Pan, and Wang (2021) for an analysis of pricing in the tri-party repo market). The SOFR specific short rate process is therefore given by

$$r^s(t) = r(t) + \psi(t). \tag{3.2.2}$$

For identification reasons we posit dynamics for the SOFR related short rate process $r^s(t)$ directly using a two-factor Gaussian process

$$dr^s(t) = \kappa^r(\theta^s(t) - r^s(t))dt + \sigma^r dW^r(t), \tag{3.2.3}$$

$$d\theta^s(t) = \kappa^\theta(\theta^\theta - \theta^s(t))dt + \sigma^\theta\left(\rho dW^r(t) + \sqrt{1-\rho^2}dW^\theta(t)\right). \tag{3.2.4}$$

While the continuous specification is a limitation given the discontinuous dynamics of the underlying overnight rate, we note that, as shown in Skov and Skovmand (2021), a simple Gaussian setup without jumps is sufficient to obtain a decent fit when modeling futures contracts based on arithmetic or compounded averages of the overnight benchmark as is used in swap and futures contracts referencing SOFR. However, if time series data on the underlying overnight rate fixings were included in the estimation, it would be necessary to extend the model to be able to account for unexpected and expected jumps and spikes observed in the overnight rate. Furthermore, such extensions, consistent with the underlying dynamics, are likely to produce higher likelihood values on estimation dates with actual jumps in the underlying rate. Several recent papers provide frameworks consistent with these characteristics. Andersen and Bang (2020) present a consistent approach to modeling spikes in the overnight SOFR, Gellert and Schlögl (2021) focus on spikes and jumps at known times, and Backwell and Hayes (2022) present a framework incorporating both expected and unexpected jumps in the overnight rate.

The spread between EFFR and the true risk-free rate is represented by an average overnight credit spread reflecting that the EFFR is an unsecured overnight rate. We

denote the non-negative overnight credit spread, $\Lambda(t)$, and the affected short rate

$$r^{FF}(t) = r(t) + \Lambda(t). \tag{3.2.5}$$

$\Lambda(t)$ thus represents the time t overnight credit spread of an average institution able to borrow at the EFFR.

Consider the spread between EFFR and SOFR defined as

$$\zeta(t) := r^{FF}(t) - r^s(t) = \Lambda(t) - \psi(t). \tag{3.2.6}$$

While both the overnight credit component and systemic repo component are non-negative, the spread between the two can turn both positive and negative depending on the size of each component. Furthermore, despite SOFR and EFFR represent a secure and unsecured rate, respectively, it is clear from the data and as we show in this paper that EFFR is not consistently greater than SOFR. The EFFR represents the unsecured rate in the funding market between top tier financial institutions that post reserves at the Fed, and thus approximately reflect the average cost of unsecured overnight funding of US LIBOR panel banks.[2] On the other hand SOFR is derived from repo transactions and thus contains many idiosyncratic aspects specific to the repo market, exemplified most prominently in the SOFR Surge of September 2019. See Lou (2021) for an in depth description of the repo market underlying SOFR. As a consequence we model the spread between EFFR and SOFR using a Gaussian process

$$d\zeta(t) = \kappa^\zeta(\theta^\zeta - \zeta(t))dt + \sigma^\zeta dW^\zeta(t). \tag{3.2.7}$$

Modeling the spread above as opposed to the individual three components $r(t)$, $\Lambda(t)$, and $\psi(t)$ avoids the need of identifying the pure risk free rate $r(t)$, since a proper proxy for this rate is not available in the context of our model nor identified by our data. We stress that while we are unable to identify the individual components, our approach of directly modeling the SOFR specific short rate, $r^s(t)$, and the EFFR-SOFR spread process, $\zeta(t)$, still allow us to ascribe the correct underlying components to the equivalent secured and unsecured term rates as we describe in section 3.2.3 and 3.2.3.

3.2.2 Modeling the LIBOR rate

In modeling LIBOR we use a multi-curve model construction. The literature on multi-curve models is vast, and we refer to Grbac and Runggaldier (2015) for an overview of the literature. In particular, we follow a structure similar to Alfeus,

[2]We note that the participants in the Federal Funds market are not limited to the US LIBOR panel banks, but consist of a larger set of institutions with accounts at the Federal Reserve banks. This includes US commercial banks, US branches of foreign banks, savings and loan organizations, and government-sponsored enterprises. The EFFR therefore only approximately reflects the cost of overnight unsecured funding of the panel banks.

Grasselli, and Schlögl (2020) and ascribe the spread between overnight and term unsecured borrowing to roll-over risk. This approach is similar in spirit to the so-called renewal approach in Collin-Dufresne and Solnik (2001), which was also applied in a different context in Filipović and Trolle (2013). Thus, we consider a time t representative member of the LIBOR panel able to finance itself at both the overnight unsecured rate, EFFR, as well as on a fixed term basis with LIBOR. Roll-over risk then represents the risk of a time t representative member not being able to roll-over its overnight unsecured financing at a time u with $u > t$. We denote the time u roll-over risk infinitesimal spread of a time t representative LIBOR panel member by $\gamma_t(u)$, and thus the total unsecured funding rate of this representative entity at time $u \geq t$

$$r_t^f(u) = r^{FF}(u) + \gamma_t(u). \tag{3.2.8}$$

Since such an entity is assumed to be able to finance itself using both unsecured overnight and term borrowing at time t we require that $\gamma_t(t) = 0$. However, for any $u > t$ the entity fixed at time t may no longer be representative of the LIBOR panel. As such there is a risk of the the event $\gamma_t(u) > 0$ occurring. I.e a roll-over risk event where the entity is unable to refinance its debt at the current market benchmark rate. The representative entity we consider in our model is therefore not to be understood as fixed, but potentially changing for every time t that is considered.

The roll-over risk spread, $\gamma_t(u)$, can be decomposed into two separate components, a credit-downgrade component and a funding-liquidity component. The credit-downgrade component denoted $\lambda_t(u)$ reflects the credit deterioration of the time t representative entity compared to the time u updated reference panel. The funding-liquidity component captures the risk that the entity is not able to roll-over its debt at the reference rate without it being due to a decrease in credit quality. Such freezes in lending liquidity or the fear thereof are best associated with the Financial Crisis or perhaps more recently during the repo squeeze in 2019. Thus, we model the total roll-over risk spread expressed as the sum of both credit-downgrade and funding-liquidity risk

$$\gamma_t(u) = \lambda_t(u) + \phi_t(u). \tag{3.2.9}$$

The rate which applies to funding an unsecured loan over the period $[t, T]$ using the unsecured overnight rate therefore contains both the overnight average credit spread as well as the roll-over risk specific components. Thus, for any time u with $t \leq u \leq T$ the funding rate, $r_t^f(u)$, consists of

$$r_t^f(u) = r(u) + \Lambda(u) + \lambda_t(u) + \phi_t(u). \tag{3.2.10}$$

Since the roll-over risk specific components are interpreted as future shocks in either credit quality or funding-liquidity and initiated at zero, we model these as pure jump processes. The credit component dynamics for $u \geq t$ are assumed to given as

$$d\lambda_t(u) = -\beta^\lambda \lambda_t(u)du + dJ_t^\lambda(u), \quad \lambda_t(t) = 0, \tag{3.2.11}$$

and similarly the funding-liquidity component for $u \geq t$ is assumed to be given as

$$d\phi_t(u) = -\beta^{\phi}\phi_t(u)du + dJ_t^{\phi}(u), \quad \phi_t(t) = 0. \tag{3.2.12}$$

In both cases the jump sizes are assumed exponentially distributed with a fixed mean of 2%. Furthermore, we will assume zero recovery at default throughout the paper. The recovery rate and mean jump size are interchangeable with the intensity level and thus these quantities are fixed in order to be able to identify the intensity processes.[3] The jumps in the credit-downgrade component, $J_t^{\lambda}(u)$, are assumed to have a stochastic intensity process modeled using a two-factor square-root process

$$d\xi(t) = \kappa^{\xi}(\eta(t) - \xi(t))dt + \sigma^{\xi}\sqrt{\xi(t)}dW^{\xi}(t), \tag{3.2.13}$$

$$d\eta(t) = \kappa^{\eta}(\theta^{\eta} - \eta(t))dt + \sigma^{\eta}\sqrt{\eta(t)}dW^{\eta}(t). \tag{3.2.14}$$

For the intensity of the jumps, $J_t^{\phi}(u)$, in the funding-liquidity component, we apply a single square-root process

$$d\nu(t) = \kappa^{\nu}(\theta^{\nu} - \nu(t))dt + \sigma^{\nu}\sqrt{\nu(t)}dW^{\nu}(t). \tag{3.2.15}$$

As an identifying restriction (see the following section 3.2.3), we assume that $r(u)$, $\phi_t(u)$ and in turn $\nu(u)$ are independent of the underlying systemic repo risk process $\psi(u)$. The model is now fully specified under the risk neutral measure Q and we can formulate the state vector process $X_t(u) := (r^s(u), \theta^s(u), \zeta(u), \lambda_t(u), \phi_t(u), \xi(u), \eta(u), \nu(u))'$ for $u \geq t$. As demonstrated in Appendix 3.A this defines an affine process in the sense of Duffie, Pan, and Singleton (2000) for each t, with dynamics

$$dX_t(u) = K^Q\left(\theta^Q - X_t(u)\right)du + \Sigma D(X_t(u), t)dW^Q(u) + dJ_t(u) \tag{3.2.16}$$

the elements of which are explicitly defined in Appendix 3.A. When estimating the model to the historical record of data, we also require the dynamics under the physical measure P. The physical and risk-neutral measures are related through the market price of risk, $\mu(t)$, by

$$dW^Q(t) = dW^P(t) + \mu(t)dt. \tag{3.2.17}$$

Since the components driving the roll-over risk are initiated at zero at each observation date, we do not model their time series properties and therefore only specify a market price of risk for the remaining state variables. Estimating the drift specific parameters under P is severely challenged by the fairly short sample of data on contracts referencing SOFR. We therefore consider a simple completely affine market price of risk structure given by

$$\mu(t) = \left(\mu^r, \mu^{\theta}, \mu^{\zeta}, \mu^{\xi}\sqrt{\xi(t)}, \mu^{\eta}\sqrt{\eta(t)}, \mu^{\nu}\sqrt{\nu(t)}\right)'. \tag{3.2.18}$$

[3]Related studies such as Filipović and Trolle (2013) and Backwell et al. (2019) follow a similar approach in order to identify the intensity process.

3.2.3 Term Rates with Roll-Over Risk

In this section we outline how to compute fair secured (repo) and unsecured (LIBOR) term rates, following an approach similar to Backwell et al. (2019). The fair term rates are determined by equating the present value of a term loan at the secured or unsecured term rate to the present value of a strategy in which the loan is rolled-over at the equivalent secured or unsecured overnight benchmark rate on an overnight, and in our model abstraction, continuous basis. As stated in the previous section the analysis is done from the point of view of a so called LIBOR representative entity. That is, an entity, which is able to borrow and lend at LIBOR at present, but may not be able to at a future time.

Term LIBOR

In order to compute the fair term LIBOR, we start by considering the present value of continuously rolling over a loan from time t to time T at the unsecured funding rate in (3.2.10)

$$\begin{aligned} U(t,T) &= B(t)E^Q\left[\frac{1}{B(T)}e^{\int_t^T r_t^f(u)du}1_{(\tau_t>T)}|\mathcal{G}_t\right] \\ &= B(t)E^Q\left[e^{\int_t^T \phi_t(u)+\lambda_t(u)+\Lambda(u)du}1_{(\tau_t>T)}|\mathcal{G}_t\right] \\ &= B(t)E^Q\left[e^{\int_t^T \phi_t(u)du}|\mathcal{F}_t\right]. \end{aligned} \tag{3.2.19}$$

The last equality follows from the results on the intensity based credit risk approach in Appendix 3.B with $\mathcal{F}_t \subseteq \mathcal{G}_t$. If instead the entity is able to borrow unsecured over the period $[t,T]$ at a rate $L(t,T)$, then the present value of the repayment is given by

$$B(t)E^Q\left[\frac{1}{B(T)}1_{(\tau_t>T)}\left(1+(T-t)L(t,T)\right)|\mathcal{G}_t\right]. \tag{3.2.20}$$

Next, we define the value of the defaultable zero coupon

$$\begin{aligned} Q(t,T) &= B(t)E^Q\left[\frac{1}{B(T)}1_{(\tau_t>T)}|\mathcal{G}_t\right] \\ &= B(t)E^Q\left[e^{-\int_t^T r(u)+\lambda_t(u)+\Lambda(u)du}|\mathcal{F}_t\right] \\ &= B(t)E^Q\left[e^{-\int_t^T r^s(u)+\zeta(u)+\lambda_t(u)du}|\mathcal{F}_t\right]. \end{aligned} \tag{3.2.21}$$

Where again we have used the intensity based credit risk approach as well as the relation $r(u)+\Lambda(u) = r^s(u)+\zeta(u)$ to obtain processes identified in the model setup. The present value of the unsecured term loan in (3.2.20) can then be expressed as

$$\left(1+(T-t)L(t,T)\right)Q(t,T). \tag{3.2.22}$$

The repayment of the roll-over risky account and the term loan must reflect the same present value in order to preclude arbitrage opportunities for the representative

entity. Thus, we equate (3.2.19) and (3.2.22) to get the fair spot LIBOR rate

$$\begin{aligned} L(t,T) &= \frac{1}{T-t}\left(\frac{U(t,T)}{Q(t,T)} - 1\right) \\ &= \frac{1}{T-t}\left(\frac{E^Q\left[e^{\int_t^T \phi_t(u)du}|\mathcal{F}_t\right]}{E^Q\left[e^{-\int_t^T r^s(u)+\zeta(u)+\lambda_t(u)du}|\mathcal{F}_t\right]} - 1\right). \end{aligned} \tag{3.2.23}$$

The term LIBOR is consistent with our interpretation of the EFFR as the rate at which a LIBOR panel bank is able to fund itself unsecured on a running basis. Indeed, as the term aspect vanishes the rate matches the rate of the overnight unsecured benchmark. Specifically, assuming differentiability with respect to T and applying the definition $\lambda_t(t) = \phi_t(t) = 0$

$$\begin{aligned} \lim_{T\to t} L(t,T) &= \frac{\partial}{\partial T}\left(\frac{E^Q\left[e^{\int_t^T \phi_t(u)du}|\mathcal{F}_t\right]}{E^Q\left[e^{-\int_t^T r^s(u)+\zeta(u)+\lambda_t(u)du}|\mathcal{F}_t\right]} - 1\right)\Bigg|_{T=t} \\ &= \frac{\partial}{\partial T}\, E^Q\left[e^{\int_t^T \phi_t(u)du}|\mathcal{F}_t\right]\Big|_{T=t} - \frac{\partial}{\partial T}\, E^Q\left[e^{-\int_t^T r^s(u)+\zeta(u)+\lambda_t(u)du}|\mathcal{F}_t\right]\Big|_{T=t} \\ &= r^s(t) + \zeta(t) + \lambda_t(t) + \phi_t(t) \\ &= r^{FF}(t). \end{aligned} \tag{3.2.24}$$

The spot LIBOR is calculated using the affine model specifcation as

$$L(t,T) = \frac{1}{T-t}\left(e^{A^L(T-t)+B^L(T-t)'X_t(t)} - 1\right) \tag{3.2.25}$$

where $A^L(T-t)$ and $B^L(T-t)$ solve the spot LIBOR specific equations specified in Appendix 3.A. We note that while we consider jump processes, $J_t^\lambda(u)$ and $J_t^\phi(u)$, for each t, the intensities of $J_t^\lambda(u)$ and $J_t^\phi(u)$ are driven by the same time-homogeneous processes for every t. The resulting LIBOR expression therefore only depends on time to maturity as also seen by $A^L(T-t)$ and $B^L(T-t)$ depending only on $T-t$ and not directly on t.

Term repo rate

A repo loan, is a loan that is fully mitigated by credit risk since a secure underlying asset, i.e. a treasury instrument is posted as collateral with the counterparty. To determine the fair term Repo rate, $R^{repo}(t,T)$, we can thus follow a similar approach as before. A reasonable assumption is that the same entity that is a time-t representative of the LIBOR panel also has access to a sufficiently large pool of treasury instruments and therefore is able to fund itself using repo transactions on a running, and in our model abstraction, continuous basis. This means it can fund itself at a continuous rate that disregards credit spreads altogether due to posting

of the underlying asset with the counterparty. The funding rate of the entity on a continuous repo loan is therefore

$$r_t^{repo}(u) = r(u) + \psi(u) + \phi_t(u). \tag{3.2.26}$$

Recall that $\psi(u)$ captures the systemic specific risk premia in the repo market, also present in the SOFR rate defined in Equation (3.2.2). Similarly, $\phi_t(u)$ represents the funding-liquidity spread also present in the LIBOR rate. We first consider the present value of a repo strategy where one unit of currency is rolled-over at the continuous repo rate $r_t^{repo}(u)$ from t to T. The time t value is then given by

$$B(t)E^Q\left[\frac{1}{B(T)}e^{\int_t^T r_t^{repo}(u)du}|\mathcal{F}_t\right] = E^Q\left[e^{\int_t^T \psi(u)+\phi_t(u)du}|\mathcal{F}_t\right]. \tag{3.2.27}$$

Alternatively, the entity can borrow over the entire period using a term repo. The time t value of the time T repayment of the repo loan is

$$\begin{aligned} &B(t)E^Q\left[\frac{1}{B(T)}\left(1+(T-t)R^{repo}(t,T)\right)|\mathcal{F}_t\right] \\ &= B(t)E^Q\left[\frac{1}{B(T)}|\mathcal{F}_t\right]\left(1+(T-t)R^{repo}(t,T)\right). \end{aligned} \tag{3.2.28}$$

Again, requiring equal present values of each approach by setting (3.2.27) equal to (3.2.28) implies

$$R^{repo}(t,T) = \frac{1}{T-t}\left(\frac{E^Q\left[e^{\int_t^T \psi(u)+\phi_t(u)du}|\mathcal{F}_t\right]}{E^Q\left[e^{-\int_t^T r(u)du}|\mathcal{F}_t\right]} - 1\right). \tag{3.2.29}$$

Analogously to the LIBOR case, one can show that our definition of the term repo rate is consistent with our interpretation of SOFR as the secured overnight funding rate in the sense that

$$\lim_{T\to t} R^{repo}(t,T) = r^s(t). \tag{3.2.30}$$

Since the individual $r(u)$ and $\psi(u)$ processes are not identified in our model, we approximate the true term repo rate in (3.2.29) to obtain an expression that can be calculated using processes identified by the model. The approximation assumes independence between $\psi(u)$ and $\phi_t(u)$ as well as $r(u)$ and $\psi(u)$. Furthermore, it ignores a convexity adjustment for $\psi(t)$ by applying the approximation $E^Q\left[\frac{1}{e^{\int_t^T \psi(u)du}}|\mathcal{F}_t\right] \approx \frac{1}{E^Q\left[e^{\int_t^T \psi(u)du}|\mathcal{F}_t\right]}$. The resulting term repo approximation can then be calculated as

$$R^{repo}(t,T) \approx \frac{1}{T-t}\left(\frac{E^Q\left[e^{\int_t^T \phi_t(u)du}|\mathcal{F}_t\right]}{E^Q\left[e^{-\int_t^T r^s(u)du}|\mathcal{F}_t\right]} - 1\right). \tag{3.2.31}$$

We detail the derivation of the approximation in Appendix 3.C and study its validity by creating an upper and lower bound for the true term repo rate. The bounds show that, given our model estimates, the resulting approximation error is less than 0.02 and 0.08 basis points for the three- and six-month repo contracts considered in the estimation. Again, the approximate term repo rate is calculated using the affine model specification

$$R^{repo}(t,T) \approx \frac{1}{T-t}\left(e^{A^{repo}(T-t)+B^{repo}(T-t)'X_t(t)}-1\right). \tag{3.2.32}$$

Where $A^{repo}(T-t)$ and $B^{repo}(T-t)$ solve the term repo specific equations (See Appendix 3.A).

3.2.4 Futures Contracts

Futures contracts traded at the CME are quoted as $100(1-R(S,T))$ where $R(S,T)$ denotes the contract specific futures rate, which comes in the four different variants as described below. Following standard results (see e.g. Hunt and Kennedy (2004)) the value of a futures contract with a random payoff is given by the risk-neutral expectation of the non-discounted payoff. Applying this to interest rate futures the time t futures rate is given by

$$f(t;S,T) = \mathbb{E}^Q\left[R(S,T)|\mathcal{F}_t\right]. \tag{3.2.33}$$

Eurodollar futures

Eurodollar futures contracts reference a future three-month LIBOR fixing. The Eurodollar futures rate is therefore given by

$$f^{ED}(t;S,T) = \mathbb{E}^Q\left[L(S,T)|\mathcal{F}_t\right]. \tag{3.2.34}$$

Inserting the spot LIBOR expression in (3.2.25) we have

$$\begin{aligned} f^{ED}(t;S,T) &= \frac{1}{T-S}\mathbb{E}^Q\left[\left(e^{A^L(T-S)+B^L(T-S)'X_S(S)}-1\right)|\mathcal{F}_t\right] \\ &= \frac{1}{T-S}\mathbb{E}^Q\left[\left(e^{A^L(T-S)+\hat{B}^L(T-S)'X_t(S)}-1\right)|\mathcal{F}_t\right]. \end{aligned} \tag{3.2.35}$$

In the last equation we recall that the jump specific elements, $\lambda_S(S)$ and $\phi_S(S)$ in $X_S(S)$ are zero by definition. Thus, we let $\hat{B}^L(T-S)$ be identical to $B^L(T-S)$, but with zeros in the jump specific elements. The Eurodollar futures rates is then calculated as

$$f^{ED}(t;S,T) = \frac{1}{T-S}\left(e^{A^{ED}(S-t)+B^{ED}(S-t)'X_t(t)}-1\right). \tag{3.2.36}$$

Where $A^{ED}(S-t)$ and $B^{ED}(S-t)$ solve the Eurodollar futures specific Riccati equations (see Appendix 3.A) with initial conditions $A^{ED}(0) = A^L(T-S)$ and $B^{ED}(0) = \hat{B}^L(T-S)$ with $T-S = 91/360$.

Three-month SOFR futures

The three-month SOFR futures rate, $R^{s,3m}(S,T)$, is computed as the daily compounded SOFR fixings during the reference quarter

$$R^{s,3m}(S,T) = \frac{1}{T-S}\left(\prod_{i=1}^{N}\left(1+d_i R^s_{d_i}(t_i)\right)-1\right), \tag{3.2.37}$$

with $R^s_{d_i}(t_i)$ for $i \in 1,...,N$ with $S \leq t_1,...,t_N \leq T$ denoting the realized SOFR fixings in the reference quarter and d_i the day count fraction multiplied amount of days to which $R^s_{d_i}(t_i)$ applies.[4] When computing the futures rate we consider the continuous approximation of the futures rate

$$R^{s,3m}(S,T) \approx \frac{1}{T-S}\left(e^{\int_S^T r^s(u)du}-1\right). \tag{3.2.38}$$

The errors induced by this approximation are studied in detail in Appendix D in Skov and Skovmand (2021) and they are found to be of no economic significance. Given the approximation, the three-month SOFR futures rate can be computed as

$$\begin{aligned} f^{s,3m}(t;S,T) &= \mathbb{E}^Q\left[\frac{1}{T-S}\left(e^{\int_S^T r^s(u)du}-1\right)|\mathcal{F}_t\right] \\ &= \frac{1}{T-S}\mathbb{E}^Q\left[\mathbb{E}^Q\left[\left(e^{\int_S^T r^s(u)du}-1\right)|\mathcal{F}_S\right]|\mathcal{F}_t\right] \\ &= \frac{1}{T-S}\mathbb{E}^Q\left[\left(e^{A^{s,3m}(T-S)+B^{s,3m}(T-S)'X_S(S)}-1\right)|\mathcal{F}_t\right] \\ &= \frac{1}{T-S}\left(e^{A^{s,f}(S-t)+B^{s,f}(S-t)'X_t(t)}-1\right). \end{aligned} \tag{3.2.39}$$

Where $A^{s,3m}(T-S)$, $B^{s,3m}(T-S)$, $A^{s,f}(S-t)$, and $B^{s,f}(S-t)$ all solve Riccati equations presented in Appendix 3.A with initial conditions $A^{s,3m}(0) = B^{s,3m}(0) = 0$, $A^{s,f}(0) = A^{s,3m}(T-S)$, and $B^{s,f}(0) = B^{s,3m}(T-S)$ with $T-S = 91/360$ reflecting the accrual days in the three-month SOFR futures contract. It is important to emphasize that while the LIBOR fixing is a forward looking term rate and thus $\mathcal{F}_S$-measurable, the SOFR futures rate is based on a backward-looking compounded rate and therefore only $\mathcal{F}_T$-measurable. Thus, for $S < t < T$ we have to account for the part of the underlying that has already been accrued

$$f^{s,3m}(t;S,T) = \frac{1}{T-S}\left(\left(\prod_{i=1}^{N_0}\left[1+d_i R^s_{d_i}(t_i)\right]\right)e^{A^{s,3m}(T-t)+B^{s,3m}(T-t)'X_t(t)}-1\right) \tag{3.2.40}$$

where $R^s_{d_i}(t_i)$ for $i \in 1,...,N_0$ with $S \leq t_1,...,t_{N_0} \leq t$ are the $\mathcal{F}_t$-measurable realized SOFR fixings.

[4] E.g. for Fridays $d_i = 3/360$ while $d_i = 1/360$ on days with a normal business day the following day.

One-month SOFR futures

The one-month SOFR futures rate is based on the arithmetic average of the daily SOFR fixings during the contract month

$$R^{s,1m}(S,T) = \frac{1}{T-S}\sum_{i=1}^{N} d_i R^s_{d_i}(t_i), \tag{3.2.41}$$

with N the total number of days in the month and $R^s_{d_i}(t_i)$ for $i \in 1,...,N$ with $S \leq t_1,...,t_N \leq T$ the published SOFR. For any date for which the rate is not published the last preceding rate is used. As in Mercurio (2018) we approximate the discrete average by an integral of the instantaneous short rate

$$R^{s,1m}(S,T) \approx \frac{1}{T-S}\int_S^T r^s(u)du. \tag{3.2.42}$$

Again, the errors induced by this approximation are studied in detail in Appendix D in Skov and Skovmand (2021) and found to be of no economic significance. The one-month SOFR futures rate can therefore be computed as follows

$$f^{s,1m}(t;S,T) = \mathbb{E}^Q\left[\frac{1}{T-S}\int_S^T r^s(u)du|\mathcal{F}_t\right]. \tag{3.2.43}$$

The expectation is calculated explicitly in Appendix 3.A. For spot contracts when $S < t < T$ a part of the total futures rate has already fixed, which we account for by letting

$$f^{s,1m}(t;S,T) = \frac{1}{T-S}\sum_{i=1}^{N_0} d_i R^s_{d_i}(t_i) + \mathbb{E}^Q\left[\frac{1}{T-S}\int_t^T r^s(u)du|\mathcal{F}_t\right] \tag{3.2.44}$$

where $R^s_{d_i}(t_i)$ for $i \in 1,...,N_0$ with $S \leq t_1,...,t_{N_0} \leq t$ are the realized SOFR fixings.

Federal funds futures

The Federal Funds futures contract has a one-month reference period and shares the same specifications as the one-month SOFR futures contract, however referencing the daily EFFR fixings. The approach to deriving the futures rate is therefore analogous to the previous section, and we get for $t \leq S < T$

$$f^{FF}(t;S,T) = \mathbb{E}^Q\left[\frac{1}{T-S}\int_S^T r^{FF}(u)du|\mathcal{F}_t\right]. \tag{3.2.45}$$

Again, we refer to Appendix 3.A for an explicit expression of the expectation.

3.3 Data and Estimation

Our dataset is collected through Refinitiv. It consists of daily observations on spot three- and six-month LIBOR fixings, the three- and six-month term repo for

treasuries, Eurodollar futures, one- and three-month SOFR futures, and Federal Funds futures. Liquidity in the interest rate futures markets is generally concentrated in the contracts closest to expiry. Since the focus of this study is also the short end of the term structure, we include contracts with up to around one year of maturity.[5] Volume in the futures market for SOFR contracts at CME has steadily increased since its beginning in May 2018. Heitfield and Park (2019) present data for the first year of trading in SOFR futures showing liquidity in the five nearest one-month contracts and nine nearest three-month contracts. Following this we include the five nearest one-month and five nearest three-month SOFR futures contracts in the data sample. The market for Eurodollar futures is massive and contracts are liquid out to a maturity of five years, however, in order to obtain an identical range to the SOFR contracts we include the four nearest Eurodollar contracts. Federal funds futures contracts are traded one and a half years out. We include the 12 nearest contracts in our estimation.[6] Our data sample begins in June 2018 when SOFR futures started trading at the CME and runs until October 2021 resulting in a total of 840 daily observations.

Based on the futures contracts included in the estimation, we note that our model estimation covers the term structure of the benchmark rates out to maturities of approximately one year. In this study, we thus solely focus on the short-term joint dynamics of the interest rate benchmarks. The short-term focus is unavoidable since our study relies on the coexistence of derivatives referencing actual independent fixings for both SOFR and LIBOR, which are only available during the transition period. Furthermore, the cessation of US LIBOR was initially announced to happen by the end of 2021, this was then extended on November 30, 2020 to June 30, 2023 for all maturities except the one-week and two-month LIBOR. Therefore, the implied rate by any derivative referencing LIBOR traded before November 30, 2020 and maturing after 2021 as well as any derivative traded after November 30, 2020 and maturing after June 2023 will reflect the LIBOR fallback language rather than the actual cost of interbank funding (see section 3.4.6 for further details on the Eurodollar futures LIBOR fallback methodology).

There are several reasons for looking at the futures market when modeling the short end of the term structure. First, the futures market is by far the most liquid short term market referencing the benchmark rates. Second, a historical record of contracts referencing SOFR is only available in the futures market. Third, since the futures contracts are exchange traded instruments the data consists of actual traded futures prices unlike OTC derivatives such as caps or swaps where data depends on quoted broker prices. Finally, using futures contracts we do not have to take into account the discounting rate (see Equaion 3.2.33). This is especially relevant during

[5]Since futures contracts have fixed expiration dates the time to maturity of the included contracts will vary across different observation dates in our sample.

[6]Daily volumes on all futures contracts can be found at `https://www.cmegroup.com/`

our data sample since the price alignment interest (PAI) used by LCH and CME in e.g. swaps changed in October 2020 from EFFR to SOFR.

When estimating the model we transform the observed spot LIBOR rates into equivalent yields

$$y^L(t,T) = \frac{1}{T-t}\log\left(1+(T-t)L(t,T)\right) \tag{3.3.1}$$

As with the spot LIBOR rates we also transform the term repo

$$y^{repo}(t,T) = \frac{1}{T-t}\log\left(1+(T-t)R^{repo}(t,T)\right). \tag{3.3.2}$$

Following Bikbov and Chernov (2005) we also consider a similar transformation to obtain Eurodollar futures yields

$$y^{ED}(t;S,T) = \frac{1}{T-S}\log\left(1+(T-S)f^{ED}(t;S,T)\right), \tag{3.3.3}$$

as well as three-month SOFR futures yields

$$y^{s,3m}(t;S,T) = \frac{1}{T-S}\log\left(1+(T-S)f^{s,3m}(t;S,T)\right). \tag{3.3.4}$$

The transformations imply that the spot and futures rates are affine in the state variables and thus allow us to apply the standard Kalman filter when estimating the model (see Appendix 3.D for details on the Kalman filter). The Federal Funds and one-month SOFR futures rate approximations in Equation (3.2.45) and (3.2.43) are already affine in the state variables, therefore a similar transform is therefore not required for these contracts.

3.4 Empirical Results

In this section we examine the consistency of the model outputs with observed data as well as estimates and latent variables. We then proceed to use our framework to decompose the spot three-and six-month LIBOR and compare risk premia in the futures markets.

3.4.1 Model fit

To validate that the model is able to capture the variation in futures and spot rates across our sample period, we compare the fitted values to the observed values. Figure 3.1 plots the futures rates for a subset of the SOFR contracts in our data sample. The futures expiry dates are fixed dates, thus the time to maturity for each of the plotted contracts vary through the sample. E.g. the expiry of the nearest SOFR futures contract varies from one day to three months, while the second nearest SOFR futures contract has an expiry range between three and six months and so on. The resulting fit reflects the results presented in Skov and Skovmand (2021) showing

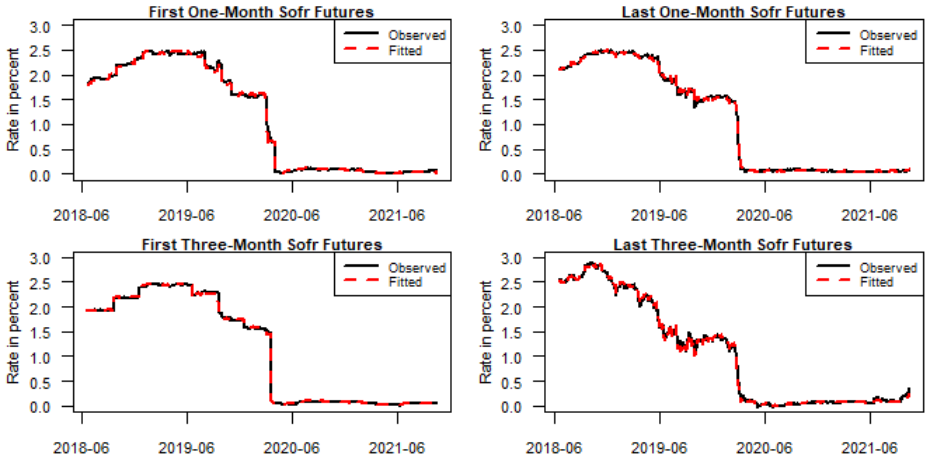

Figure 3.1: *In sample fit of the first and last one- and three-month SOFR futures contracts.*

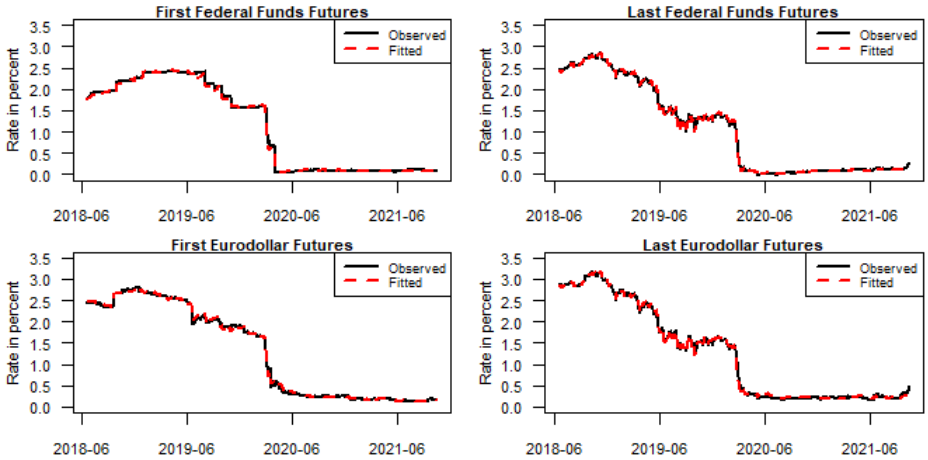

Figure 3.2: *In sample fit of the first and last Federal Funds and Eurodollar futures contracts*

that two Gaussian factors are enough to capture the majority of the variation in the SOFR futures market up to a one year maturity.

The Eurodollar and Federal Funds futures rates are plotted in figure 3.2. Focusing on the spot Eurodollar futures rate, we note the spike during the onset of the COVID-19 crisis reflecting the spike in spot LIBOR as seen in figure 3.3. However, the increase is far less pronounced in the later contracts indicating that the Eurodollar futures market predicted the spike in LIBOR to be fairly short-lived.

In addition to futures contracts, we also include spot LIBOR and term repo in the estimation. The fit of these rates is plotted in Figure 3.3. We see that the roll-over risk approach is able to capture the large spike in the LIBOR while also matching

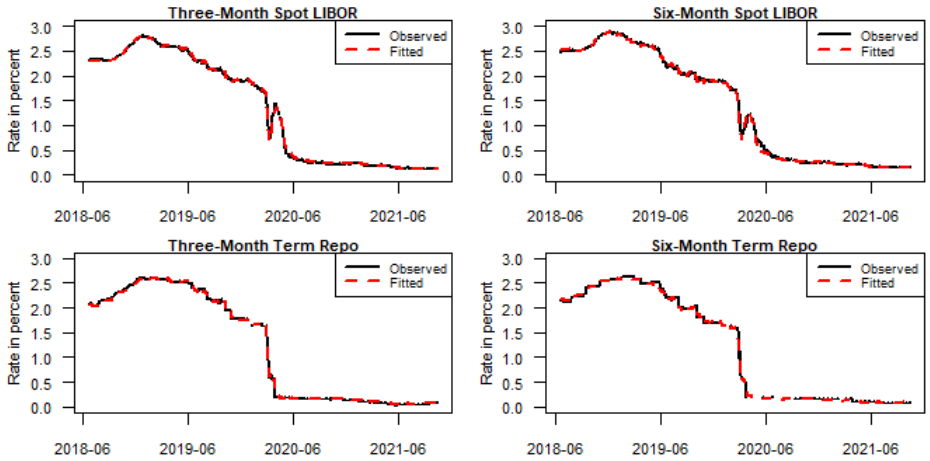

Figure 3.3: *In sample fit of three- and six-month spot LIBOR and repo rates.*

	SOFR Futures	EFFR Futures	ED Futures	Spot LIBOR	Term Repo
RMSE	2.2	2.0	2.9	2.5	2.4

Table 3.1: *RMSEs of the fitted rates for the full sample. All values are in basis points.*

the term repo rate during the period in March 2020. We also note that term repos are fairly illiquid contracts, which is clearly seen from the observed six-month term repo data series showing multiple missing values, particularly during the market stress just after the onset of the COVID crisis. However, missing values are easily overcome during the filtering used in the estimation (see Appendix 3.D).

Table 3.1 shows the fitted root mean squared errors (RMSE). When computing the RMSEs, we consider the actual futures and spot rates instead of the yield transformations used in the estimation. The RMSEs further demonstrate that the model provides a close fit across futures contracts on all three benchmarks.

3.4.2 Estimates

Table 3.2 presents the estimated parameter values and standard deviations. First, we note that the process governing the spread between the overnight rates SOFR and EFFR has an estimated mean level, θ^{ζ}, equal to zero together with a low volatility, σ^{ζ}, reflecting the high level of correlation between SOFR and the effective Federal Funds rate. Turning to the roll-over risk specific estimates, we see that the intensity process is rather volatile, however, with a quick mean reversion, while the stochastic mean process is more stable as also seen from the state variables in figure 3.4. The large estimate of β^{ϕ} indicates that the funding-liquidity specific shocks are expected to quickly revert back to a normal state again. The parameters related to the market price of risk are estimated with significant standard errors, however, this is

Mean Reversion	Estimate	Mean	Estimate	Volatility	Estimate	Risk Premium	Estimate
κ^r	1.2394			σ^r	0.0032	μ^r	-1.3117
	(0.0039)				(0.0000)		(1.4424)
κ^θ	0.0273	θ^θ	0.0306	σ^θ	0.0071	μ^θ	0.0003
	(0.0017)		(0.0012)		(0.0001)		(0.5767)
κ^ζ	0.5945	θ^ζ	0.0000	σ^ζ	0.0006	μ^ζ	-0.1095
	(0.0808)		(0.0000)		(0.0001)		(1.0250)
κ^ξ	8.2375			σ^ξ	2.8610	μ^ξ	0.8202
	(0.1714)				(0.1607)		(1.1110)
κ^η	0.1299	θ^η	0.0163	σ^η	0.7715	μ^η	0.1451
	(0.0405)		(0.3187)		(0.0571)		(0.4502)
κ^ν	1.6624	θ^ν	2.4408	σ^ν	3.1921	μ^ν	-0.2445
	(0.0651)		(0.3218)		(0.2297)		(0.4180)
β^λ	5.1952						
	(0.0742)						
β^ϕ	37.3898						
	(3.9829)						

Table 3.2: *Parameter estimates with standard deviations in parentheses. The correlation parameter, ρ, is estimated at* 0.0650 (0.0276)*. The estimated values of the filtering parameters and their standard deviations in basis points are* $\sigma_{SOFR} = 2.3094$ (0.0139)*,* $\sigma_{EFFR} = 2.0621$ (0.0095)*, and* $\sigma_{LIBOR} = 2.8949$ (0.0164)*. The maximized log-likelihood value is* 170,331*.*

as expected given the fairly short sample size.

3.4.3 State variables

To investigate the drivers of the interest rate benchmarks, we plot the path of the filtered state variables during the data period in figure 3.4. The period reflects a decrease in short term interest rate expectations as seen by the downward trend of the stochastic mean $\theta^s(t)$, which even turns slightly negative during the first half of 2020. The $\zeta(t)$ process related to the spread between the overnight benchmarks, SOFR and EFFR, is concentrated around zero reflecting both positive and negative spreads between the two rates. During the SOFR surge on September 17, SOFR increased to above 5 percent.[7] We note that the spread process also turns negative during the same period indicating an increase in the underlying systemic repo risk component. The decomposition thus shows that neither of the underlying spreads, $\psi(t)$ and $\Lambda(t)$, dominate the other one during the entire sample. This further emphasizes that even though SOFR is a secured rate unlike the EFFR, SOFR should not be thought of as being closer to a "pure" risk free rate than the EFFR. Turning to the roll-over risk specific variables represented by the jump intensity processes in the instantaneous funding rate. The process $\xi(t)$ relating to the credit downgrade component with its stochastic drift term $\eta(t)$ and $\nu(t)$ the intensity of jumps in the

[7]See Anbil, Anderson, and Senyuz (2020) for details on what happened during the SOFR surge. Copeland, Duffie, and Yang (2021) argue that the spikes in SOFR were a result of the reduced aggregate reserves following the balance-sheet normalization between 2017 and September 2019.

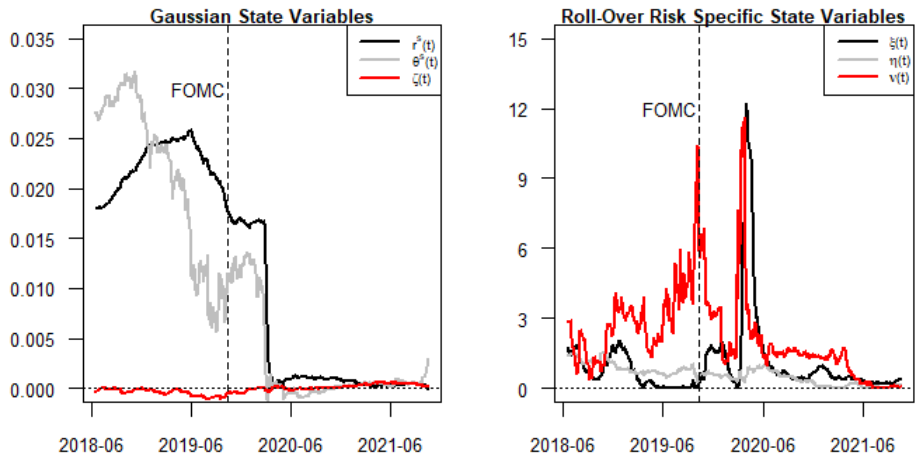

Figure 3.4: *The plot displays the filtered state variables impacting to the overnight benchmark rates during the sample period from June 2018 to October 2021. The vertical line marks the October 11th FOMC meeting.*

funding-liquidity spread are plotted in the right hand panel of figure 3.4. In the period up to the SOFR surge of September 2019 the model identifies a general liquidity-spread increase through the rise in the intensity process $\nu(t)$, as well as an increase in SOFR relative to EFFR as the $\zeta(t)$ process moves into negative territory. All the while the credit-downgrade intensity $\xi(t)$ hovers around zero in the same period. On October 11th 2019 following the SOFR surge the Fed announced that it would conduct operations in the term and overnight repo market.[8] After the announcement, we see an immediate increase in the SOFR-EFFR spread component suggesting a decrease in the systemic repo risk premium. Furthermore, the funding-liquidity component also decreases significantly. The decomposition therefore indicates that the actions of the Fed did help to decrease risk premia both in the overnight and term rate market.[9] Further, looking at the overnight SOFR fixings since the announcement,[10] spikes in SOFR have largely disappeared indicating that the Fed policy was indeed effective in eliminating SOFR spikes.

The COVID-19 related events of early March 2020 resulted in a massive spread between term LIBOR and the Federal Funds rate. Figure 3.4 shows that the increase in risk was, unlike the events following the SOFR surge, not just isolated to funding-liquidity risk. It affected the average overnight credit spread, as well as both the credit-downgrade and funding-liquidity risk. This can be seen in the clear spikes

[8] See `https://www.federalreserve.gov/newsevents/pressreleases/monetary20191011a.htm`

[9] Allen, Carletti, and Gale (2009) create a model for interbank liquidity and the intervention of central banks. Likewise, Christensen, Lopez, and Rudebusch (2014) find that the Fed's Term Auction Facility (TAF) helped to reduce risk premia in interbank lending rates during the Financial Crisis.

[10] A dynamically updated series of SOFR can be found at `https://fred.stlouisfed.org/series/SOFR`

Maturity	SOFR-OIS	EFFR-OIS	3M-IRS	6M-IRS
1Y	0.7	0.9	1.4	1.9

Table 3.3: *RMSEs of the fitted swap rates for the full sample. All values are in basis points. SOFR swap data is only available from July 2020.*

in both intensity processes $\nu(t)$, and $\xi(t)$ during the same period. Likewise, the low LIBOR-OIS spread in the second half of 2021 results in close to zero intensity processes.

3.4.4 Comparing with swap contracts

As an additional validity check of the model, we perform an out of sample test of the model by comparing short-term observed swap rates with model implied rates. We detail the pricing of OIS and IRS contracts in Appendix 3.A.

The model endogenously models the spread between different LIBOR tenors as a result of roll-over risk. Therefore, we also test the ability of the model to extrapolate the spot six-month rate to swaps of greater maturity referencing the six-month LIBOR fixing. To obtain data on the six-month LIBOR IRS we use that the basis swap rate, $BS^{3M,6M}(t,T)$, reflects the difference in fixed rates of two IRS referencing different LIBOR tenors. Swap rates referencing the six-month LIBOR fixing are then calculated as

$$IRS^{6M}(t,T) = IRS^{3M}(t,T) + BS^{3M,6M}(t,T). \tag{3.4.1}$$

Figure 3.5 and table 3.3 displays the fitted swap rates along with their RMSEs, and shows a tight fit reflecting a swap and futures market that is well in line with each other. Swap data could of course be added to the estimation data, likely resulting in a closer fit to the swap market. Furthermore, the swap market is traded at far greater maturities compared to futures thus allowing for modeling of the mid to long term maturities of the term structure as in Filipović and Trolle (2013) and Backwell et al. (2019). We restrict the scope of our estimation to futures contracts due to the limited liquidity of the SOFR swap market during our sample period. But also, as discussed in section 3.3, because LIBOR derivatives expiring after June 2023 will reference SOFR plus the ISDA fixed fallback spread and thus not reflect actual expectations of interbank funding.

When decomposing the LIBOR-OIS spread into its roll-over risk components it is essential that the model correctly ascribes credit risk in the LIBOR panel to the roll-over risk credit component $\lambda_t(u)$. We investigate the decomposition by comparing the model-implied CDS-spread for an average LIBOR panel bank to the observed CDS spreads for the LIBOR panel banks. In particular, we construct the time series of CDS-spreads by trimming and averaging CDS-quotes for all banks in the current

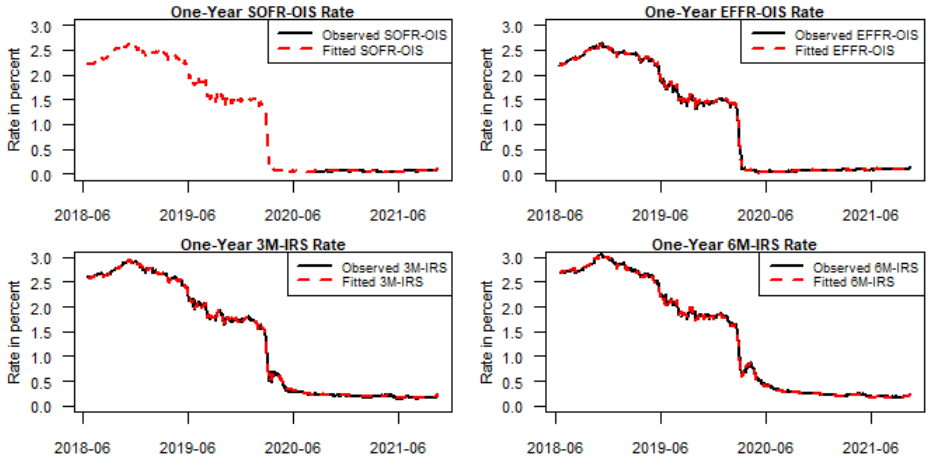

Figure 3.5: *Observed and model implied one-year swap rates. SOFR swap data is only available from July 2020.*

USD LIBOR panel using the LIBOR specific methodology.[11] We focus on the the shortest on-the-run CDS contract, which has a six month tenor, however, due to the biannual roll dates for these contracts the effective maturity varies between six months and a full year. Since we cannot identify the overnight average credit spread $\Lambda(t)$ using our dataset, we are only able to calculate the fair CDS-spread implied from the roll-over risk specific credit component. We detail the calculation of the fair swap spread in Appendix 3.A. Figure 3.6 plots the model implied spread against the observed LIBOR panel CDS spread. In addition to excluding the overnight average credit component there are multiple reasons why we would not expect the model to produce an exact fit to the CDS spread. First, any idiosyncrasies in the short-term CDS market will not be reflected by the model fit without including these contracts in the estimation. Second, Since our estimation only includes data on the spot three- and six-month repo the decomposition of roll-over risk beyond the six-month tenor will be depend on an extrapolation. However, despite this the plot clearly still shows that the decomposed credit component captures variation in credit risk for the LIBOR panel banks. This is also apparent from the correlation of 75.2% between changes in the monthly averages of the credit-downgrade intensity process, $\xi(t)$, and the observed average CDS spread.

3.4.5 Decomposing roll-over risk in spot LIBOR

In order to investigate the cost of unsecured interbank term funding present in LIBOR, we use our model to decompose the roll-over risk components in the spot three- and six-month LIBOR. As previously mentioned the LIBOR-OIS spread contains both

[11] The current USD LIBOR methodology and panel banks can be found at `https://www.theice.com/iba/libor`

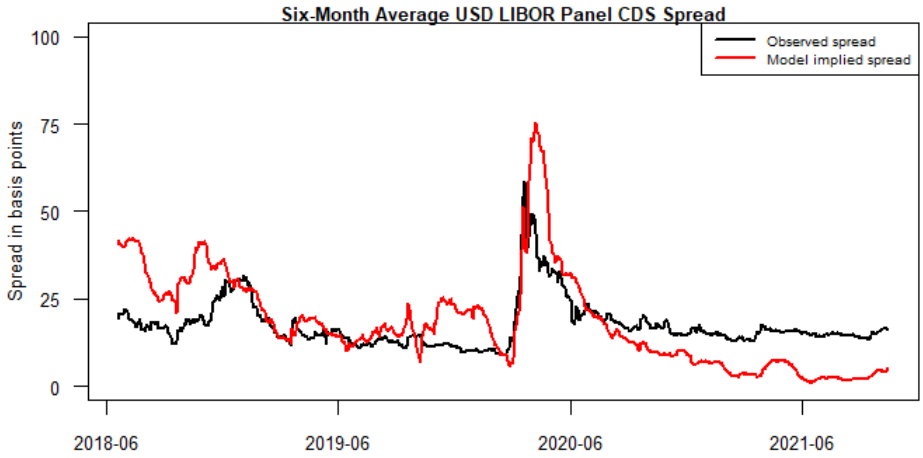

Figure 3.6: *Observed and model implied six month CDS spread based on the decomposed roll-over risk credit component.*

credit and funding-liquidity risks, which cannot be separated using only data on EFFR and LIBOR. Previous studies such as Filipović and Trolle (2013) and Backwell et al. (2019) use CDS data on LIBOR panel banks in order to identify the credit component and thus separate the roll-over risk specific components. These studies attempt to identify the entire term structure of the IRS-OIS spread. Due to the short term nature of this study, we focus solely on the decomposition of the three- and six-month spot LIBOR-OIS spread, however, CDS contracts are only traded at maturities of six months or longer with most of the liquidity concentrated in the five year maturity contract.[12] Furthermore, using five-year CDS contracts Junge and Trolle (2015) find that liquidity risk accounts for 24% of CDS spreads on average. To avoid the liquidity premium and mismatch in maturities, we take a different approach and include data on the three- and six-month term repo rate. A similar method is used in Smith (2010) who applies the three-month LIBOR-repo spread to identify the credit component in LIBOR. As we formalize in section 3.2.3 the term repo rate is a secured rate and therefore unaffected by the overnight average credit spread as well as credit-downgrade risk. However, it is a term loan and thus still contains funding-liquidity risk as well as the systemic repo risk premium. As an identification strategy we assume that funding-liquidity risk impacts the LIBOR and term repo market equally through the same funding-liquidity risk spread $\phi_t(u)$. We note that in contrast to the previously mentioned studies in Filipović and Trolle (2013) and Backwell et al. (2019) such a decomposition of the term repo is only applicable since we have included data on SOFR, allowing us to define the value of the overnight

[12]Due to the biannual roll dates for CDS contracts the actual contract maturities are usually greater than the quoted tenors. E.g. the actual expiry of the shortest CDS contract varies between six months and up to an entire year. See Boyarchenko, Costello, and Shachar (2019) for details on the CDS market.

rolled-over secured loan in Equation (3.2.27), which accounts for the systemic repo risk premium captured by $\psi(t)$. Furthermore, this allows us to remain agnostic about the size of the average overnight credit risk level and in turn the actual underlying risk-free rate unlike previous studies where the overnight average credit spread has been assumed either as a fixed level of e.g. 5 basis points (as in Filipović and Trolle (2013) and Alfeus, Grasselli, and Schlögl (2020)) or extrapolated from credit default swap contracts (as in Backwell et al. (2019)).

Figure 3.7 plots the decomposed three- and six-month LIBOR-OIS spreads. First, we note that the large spike in the spread in March 2020 was mainly driven by a large increase in credit-downgrade risk. This observation also aligns with studies of the LIBOR-OIS spread during the great financial such as King, Lewis, et al. (2020) who find that at the peak of the crisis the spread was dominated by credit risk. During normal periods, however, we find that the funding component is equally relevant in explaining the spread. Considering the entire sample period the credit component explains 51.2% of the three-month LIBOR-OIS spread and 53.9% of the six-month spread. Comparing with similar studies, Filipović and Trolle (2013) find that the impact of the non-default component is greater than the credit component for the spot three-month spread in both the USD and euro market. Similarly, Schwarz (2019) show that her liquidity measure dominates the impact of credit on the EURIBOR-OIS spread during both the Financial and European Debt Crisis. Thus, we find a slightly larger impact from the credit component on the LIBOR-OIS spread using our data sample and method. We note that the market for term repo lending, especially the six-month repo loan, is fairly illiquid and thus the observed repo rate may reflect an added market liquidity premium.[13] The term repo may therefore contain both market and funding-liquidity risk.[14] Such a premium would result in the model decomposition overestimating the roll-over risk funding-liquidity component in the LIBOR-OIS spread and thus underestimating the size of the credit component.

The figure further plots a regression based decomposition of the credit component. We regress the three- and six-month LIBOR-OIS spread on the equivalent LIBOR-repo spread

$$Spread_t^{OIS} = \alpha + \beta \times Spread_t^{repo} + \varepsilon_t. \tag{3.4.2}$$

The estimate of the three-month regression coefficient β^{3m} is 0.9652 (0.0236) and for the six-month spot LIBOR decomposition we obtain β^{6m} is 0.8528 (0.0314). We compute the regression based credit component as $\beta \times Spread_t^{repo}$ to ensure that the credit component spread is zero when the LIBOR-repo spread is zero. The regression shows a similar decomposition to the model mainly diverging in the second half of 2019 where the LIBOR-repo spread went slightly negative. A negative LIBOR-repo

[13] Volume data for term repos published by the OFR can be found at `https://www.financialresearch.gov/short-term-funding-monitor/datasets/repo/`

[14] see Brunnermeier and Pedersen (2009) for details on the close relationship between market and funding-liquidity

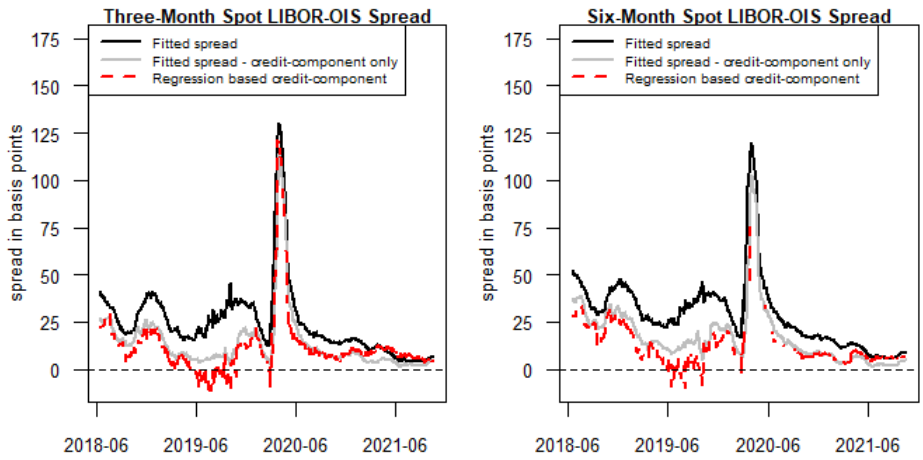

Figure 3.7: *Decomposed three- and six-month LIBOR-OIS spreads.*

spread is inconsistent with our roll-over risk interpretation of the spread and likely due to market liquidity in the term repo market. Our model specification clearly precludes negative LIBOR-repo (as well negative as LIBOR-OIS) spreads, which is also apparent from the model based decomposition of the LIBOR-OIS spread.

3.4.6 Comparing risk premia in futures markets

Assuming that the LIBOR transition follows its current trajectory and three-month USD LIBOR fixings cease after June 30, 2023 the Eurodollar futures market referencing the LIBOR fixings will also end. Furthermore, the fallback method proposed by CME for all Eurodollar futures contracts maturing after the LIBOR cessation date is to convert Eurodollar futures contracts into the corresponding SOFR futures contracts plus the fixed ISDA fallback spread.[15] The ISDA fallback spread has already been fixed at 26.161 basis points for three-month USD LIBOR.[16] In this section we compare the risk premia in the new futures market for three-month SOFR contracts to the Eurodollar contracts that these are meant to replace. Any results involving the physical measure are of course impacted by a level of uncertainty due to the fairly large standard deviations of the market price of risk related parameters as displayed in table 3.2. In order to compare the risk premia in these markets, we consider the zero cost portfolio of buying one Eurodollar futures contract and simultaneously selling the equivalent three-month SOFR futures contract. The constructed portfolio should be insensitive to changes in the underlying risk-free rate, but sensitive to the

[15]The CME proposed fallback for Eurodollar contracts is available at `https://www.cmegroup.com/content/dam/cmegroup/notices/ser/2021/02/SER-8720.pdf` and `https://www.cmegroup.com/education/files/webinar-fallbacks-for-eurodollars.pdf?itm_source=rates_recap_article&itm_medium=hypertext&itm_campaign=rates_recap&itm_content=022021`

[16]The fixed fallback spreads can be found at `https://assets.bbhub.io/professional/sites/10/IBOR-Fallbacks-LIBOR-Cessation_Announcement_20210305.pdf`

spread processes between SOFR and LIBOR fixings. As previously mentioned, due to the forward-looking nature of the LIBOR rate, the Eurodollar contract settles at the beginning of the interest rate period, while the equivalent SOFR contract settles at the end of the reference period. The SOFR contract therefore remains risky through the entire period. To account for the mismatch, we calculate the risk premium at time t of the constructed portfolio as the difference between the time t value of the portfolio and the expected value at the beginning of the reference period of the contracts denoted by time S.

$$RP(t;S,T) = f^{ED}(t;S,T) - f^{s,3m}(t;S,T) - E^P\left[f^{ED}(S;S,T) - f^{s,3m}(S;S,T)|\mathcal{F}_t\right] \tag{3.4.3}$$

As also mentioned in Piazzesi and Swanson (2008) Equation (3.4.3) is not a completely accurate representation of the expected excess return of the portfolio. This is due to the daily mark to market of futures contracts. However, they find that the simplification is insignificant to the size of the risk premium and thus we follow the same approach.

Due to the varying expiry of the actual futures contracts, we cannot compare the risk premium of the portfolio equally across observation dates. Instead, we consider a set of standardized contracts with fixed maturities for each observations date. In particular we will consider contracts for each quarter ahead such that $S - t \in \{90/360, 180/360, 270/360, 360/360\}$.

We note that the completely affine market price of risk specification in Equation (3.2.18) results in the risk-neutral mean reversion matrix being identical to the physical mean reversion for the Gaussian part of the state variables. Since we model the SOFR and Federal Funds futures rates purely as Gaussian processes this implies that the risk premium on these contracts is essentially constant. The time variation in risk premia observed for our constructed portfolio is therefore purely driven by risk premia related to the roll-over risk specific processes.

Figure 3.8 plots the resulting annualized risk premium from the strategy.[17] The portfolio clearly reflects a positive risk premium due to the added risk in the three-month LIBOR fixing compared to the equivalent compounded SOFR rate. the most recent period characterized by the fairly low LIBOR-OIS spread (and equally low LIBOR-SOFR spread) is also reflected in a modest risk premium. The plot also shows that part of the large spike in March 2020 was driven by a significant spike in the risk premia related to interbank lending. Finally, we note that the FOMC announcement on October 11th, was effective in part by successfully reducing the risk premia in interbank lending.

Table 3.4 plots the full sample average annualized risk premia for each contract

[17] Annualized risk premia are obtained by dividing the premium with the holding period of the constructed portfolio, i.e. $S - t$

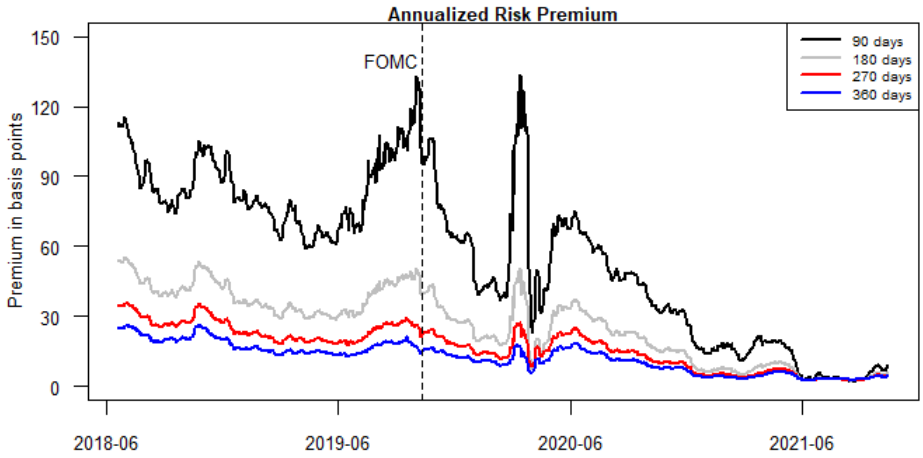

Figure 3.8: *The figure plots the annualized risk premium for the constructed portfolio given different holding periods. The vertical line marks the October 11th FOMC meeting.*

$(S-t)$	3M SOFR	Eurodollar	1M SOFR	Federal Funds
90 days	32.1	88.4	34.9	35.5
180 days	28.6	54.6	31.0	31.6
270 days	25.8	42.5	27.8	28.3
360 days	23.4	35.7	25.1	25.6

Table 3.4: *Model implied annualized expected excess returns for SOFR, Eurodollar and Federal Funds futures contracts.*

from holding the contract until the beginning of the accrual period. The average annualized risk premium is positive, but decreasing in time to maturity for all contracts. For the one-months contracts we also note that the SOFR and Federal Funds futures are near identical in risk premium for our sample, which is also to be expected given the close to zero $\mu^{\zeta} = -0.1095$ estimate. This aligns with the model-free analysis in Skov and Skovmand (2021) showing very similar excess average returns of one-month SOFR and EFFR futures contracts.

3.5 Conclusion

In this paper, we have presented an affine multicurve framework, which jointly models SOFR, EFFR, LIBOR, and term repos while ascribing economic interpretation to the spreads between each of the different rates. The framework thus provides a unified approach for risk managing the LIBOR transition. In particular the model would have many potential use cases such as pricing bespoke tenors, calculating the value transfer of shifting from LIBOR to SOFR as well as pricing nonlinear derivatives involving multiple benchmark rates. The LIBOR benchmark allows financial institutions to gain exposure to the roll-over risk premium embedded in the cost of funding at

term. Such exposure is not easily obtained elsewhere. As we show some of it is obtainable through exposure to credit risky instruments pricing, but a significant component is not, as seen through our decomposition of the LIBOR-OIS spread. The decomposition shows that the spike in the LIBOR-OIS spread during March 2020 was largely driven by an increase in the credit premium, however, during the full sample period we find that the funding-liquidity component is on average equally important in explaining the spread. Beyond 2023, as LIBOR is discontinued, the model components would still be identifiable with the LIBOR specific data swapped by one of the likely contenders to replace it. Furthest along is possibly the BSBY, which already has futures contracts traded at the CME, but as of writing with very sparse liquidity. However, even in the absence of a liquid derivatives market there is considerable information gained simply by including spot rate data in the model, as is also demonstrated in this paper.

3.A Pricing in the Affine Setup

We write the dynamics of the state process under the Q-measure on matrix form

$$dX_t(u) = K^Q \left(\theta^Q - X_t(u)\right) du + \Sigma D(X_t(u), t) dW^Q(u) + dJ_t(u) \tag{3.A.1}$$

where $X_t(u) = (r^s(u), \theta^s(u), \zeta(u), \lambda_t(u), \phi_t(u), \xi(u), \eta(u), \nu(u))'$ is the vector of state variables. The drift specifications are given by

$$K^Q = \begin{bmatrix} \kappa^r & -\kappa^r & 0 & 0 & 0 & 0 & 0 & 0 \\ 0 & \kappa^\theta & 0 & 0 & 0 & 0 & 0 & 0 \\ 0 & 0 & \kappa^\zeta & 0 & 0 & 0 & 0 & 0 \\ 0 & 0 & 0 & \beta^\lambda & 0 & 0 & 0 & 0 \\ 0 & 0 & 0 & 0 & \beta^\phi & 0 & 0 & 0 \\ 0 & 0 & 0 & 0 & 0 & \kappa^\xi & -\kappa^\xi & 0 \\ 0 & 0 & 0 & 0 & 0 & 0 & \kappa^\eta & 0 \\ 0 & 0 & 0 & 0 & 0 & 0 & 0 & \kappa^\nu \end{bmatrix}, \quad \theta^Q = \begin{bmatrix} \theta^\theta \\ \theta^\theta \\ \theta^\zeta \\ 0 \\ 0 \\ \theta^\eta \\ \theta^\eta \\ \theta^\nu \end{bmatrix}. \tag{3.A.2}$$

And the volatility specification becomes

$$\Sigma = \begin{bmatrix} \sigma^r & 0 & 0 & 0 & 0 & 0 & 0 & 0 \\ \sigma^\theta \rho & \sigma^\theta \sqrt{1-\rho^2} & 0 & 0 & 0 & 0 & 0 & 0 \\ 0 & 0 & \sigma^\zeta & 0 & 0 & 0 & 0 & 0 \\ 0 & 0 & 0 & 0 & 0 & 0 & 0 & 0 \\ 0 & 0 & 0 & 0 & 0 & 0 & 0 & 0 \\ 0 & 0 & 0 & 0 & 0 & \sigma^\xi & 0 & 0 \\ 0 & 0 & 0 & 0 & 0 & 0 & \sigma^\eta & 0 \\ 0 & 0 & 0 & 0 & 0 & 0 & 0 & \sigma^\nu \end{bmatrix}, \quad D(X(t), t) = \operatorname{diag}\left(\begin{bmatrix} 1 \\ 1 \\ 1 \\ 0 \\ 0 \\ \sqrt{\xi(t)} \\ \sqrt{\eta(t)} \\ \sqrt{\nu(t)} \end{bmatrix} \right) \tag{3.A.3}$$

where $\text{diag}(v)$ is a diagonal matrix with the elements in v on the diagonal. Finally, $J_t(u) \in \mathbb{R}^8$ and $W^Q(u) \in \mathbb{R}^8$ are defined as

$$W^Q(u) = \left(W^r(u), W^\theta(u), W^\zeta(u), 0, 0, W^\xi(u), W^\eta(u), W^\nu(u)\right)', \tag{3.A.4}$$

$$J_t(u) = \left(0, 0, 0, J_t^\lambda(u), J_t^\phi(u), 0, 0, 0\right)'. \tag{3.A.5}$$

Based on this the ODEs referenced in section 3.2 and used when computing the futures and spot rates can be expressed in a general framework of ODEs satisfying

$$\frac{\partial B_1(\tau)}{\partial \tau} = -\kappa^r B_1(\tau) - [R]_1, \tag{3.A.6}$$

$$\frac{\partial B_2(\tau)}{\partial \tau} = -\kappa^\theta B_2(\tau) + \kappa^r B_1(\tau) - [R]_2, \tag{3.A.7}$$

$$\frac{\partial B_3(\tau)}{\partial \tau} = -\kappa^\zeta B_3(\tau) - [R]_3, \tag{3.A.8}$$

$$\frac{\partial B_4(\tau)}{\partial \tau} = -\beta^\lambda B_4(\tau) - [R]_4, \tag{3.A.9}$$

$$\frac{\partial B_5(\tau)}{\partial \tau} = -\beta^\phi B_5(\tau) - [R]_5, \tag{3.A.10}$$

$$\frac{\partial B_6(\tau)}{\partial \tau} = -\kappa^\xi B_6(\tau) + \frac{1}{2}(B_6(\tau)\sigma^\xi)^2 + \frac{B_4(\tau)}{0.02^{-1} - B_4(\tau)} - [R]_6, \tag{3.A.11}$$

$$\frac{\partial B_7(\tau)}{\partial \tau} = -\kappa^\eta B_7(\tau) + \kappa^\eta B_6(\tau) + \frac{1}{2}(B_7(\tau)\sigma^\eta)^2 - [R]_7, \tag{3.A.12}$$

$$\frac{\partial B_8(\tau)}{\partial \tau} = -\kappa^\nu B_8(\tau) + \frac{1}{2}(B_8(\tau)\sigma^\nu)^2 + \frac{B_5(\tau)}{0.02^{-1} - B_5(\tau)} - [R]_8, \tag{3.A.13}$$

$$\frac{\partial A(\tau)}{\partial \tau} = (K^Q\theta^Q)'B(\tau) + \frac{1}{2}B(\tau)'\sigma_0\sigma_0'B(\tau), \tag{3.A.14}$$

Where $R \in \mathbb{R}^8$ is specific to each of the ODEs and $[R]_i$ denotes the i^{th} element in R. σ_0 is the volatility related to the Gaussian processes

$$\sigma_0 = \begin{bmatrix} P_{3\times3} & 0_{3\times5} \\ 0_{5\times3} & 0_{5\times5} \end{bmatrix}, \quad P_{3\times3} = \begin{bmatrix} \sigma^r & 0 & 0 \\ \sigma^\theta\rho & \sigma^\theta\sqrt{1-\rho^2} & 0 \\ 0 & 0 & \sigma^\zeta \end{bmatrix}. \tag{3.A.15}$$

3.A.1 Spot and futures rates

We now list the different specifications of R used to solve the ODEs presented in section 3.2. In order to solve the LIBOR specific ODEs, we note that

$$E^Q\left[e^{\int_t^T \phi_t(u)du}\middle|\mathcal{F}_t\right] = e^{A^U(T-t)+B^U(T-t)'X_t(t)} \tag{3.A.16}$$

where $A^U(T-t)$ and $B^U(T-t)$ solve the general set of ODEs with $R = (0,0,0,0,-1,0,0,0)'$ and initial conditions $A^U(0) = B^U(0) = 0$. Similarly, we calculate the denominator as

$$E^Q\left[e^{-\int_t^T r^s(u)+\zeta(u)+\lambda_t(u)du}\middle|\mathcal{F}_t\right] = e^{A^Q(T-t)+B^Q(T-t)'X_t(t)} \tag{3.A.17}$$

and again $A^Q(T-t)$ and $B^Q(T-t)$ solve the general set of ODEs with $R = (1,0,1,1,0,0,0,0)'$ and initial conditions $A^Q(0) = B^Q(0) = 0$. Finally, the LIBOR specific expressions are calculated as $A^L(T-t) = A^U(T-t) - A^Q(T-t)$ and $B^L(T-t) = B^U(T-t) - B^Q(T-t)$. Likewise, for the term repo contract we first note that

$$E^Q\left[e^{-\int_t^T r^s(u)du}|\mathcal{F}_t\right] = e^{A^s(T-t)+B^s(T-t)'X_t(t)} \tag{3.A.18}$$

where $A^s(T-t)$ and $B^s(T-t)$ solve the general set of ODEs with $R = (1,0,0,0,0,0,0,0)'$ and initial conditions $A^s(0) = B^s(0) = 0$. Thus, we compute the term repo using the expressions $A^{repo}(T-t) = A^U(T-t) - A^s(T-t)$ and $B^{repo}(T-t) = B^U(T-t) - B^s(T-t)$.

The SOFR accumulating account used to price the three-month SOFR futures contract is calculated with $A^{s,3m}(\tau)$ and $B^{s,3m}(\tau)$, which solve the general set of ODEs with $R = (-1,0,0,0,0,0,0,0)'$. The Eurodollar and three-month SOFR futures specific ODEs $A^{ED}(\tau)$ and $B^{ED}(\tau)$ as well as $A^{s,f}(\tau)$ and $B^{s,f}(\tau)$ both solve the general ODEs with $R = (0,0,0,0,0,0,0,0)'$, however, with the different initial conditions given in section 3.2.4 and 3.2.4, respectively.

For the one-month SOFR futures rate, we first apply the Fubini theorem to change the order of integration

$$\mathbb{E}^Q\left[\frac{1}{T-S}\int_S^T r^s(u)du|\mathcal{F}_t\right] = \frac{1}{T-S}\int_S^T \mathbb{E}^Q\left[r^s(u)|\mathcal{F}_t\right]du. \tag{3.A.19}$$

We note that the risk-neutral expectation of the Gaussian subset of the state variables is given by

$$\mathbb{E}^Q\left[X_t(u)|\mathcal{F}_t\right] = \begin{bmatrix} \theta^\theta + e^{-(u-t)\kappa^r}\left(r(t)-\theta^\theta\right) - \frac{\kappa^r\left(e^{-(u-t)\kappa^r}-e^{-(u-t)\kappa^\theta}\right)}{\kappa^r-\kappa^\theta}\left(\theta(t)-\theta^\theta\right) \\ \theta^\theta + e^{-(u-t)\kappa^\theta}\left(\theta(t)-\theta^\theta\right) \\ \theta^\zeta + e^{-(u-t)\kappa^\zeta}\left(\zeta(t)-\theta^\theta\right) \end{bmatrix}. \tag{3.A.20}$$

For the SOFR futures rate, we only need the integral of the first coordinate, which we define as

$$\begin{aligned} I^r(t;S,T) =& \int_S^T \theta^\theta + e^{-(u-t)\kappa^r}\left(r(t)-\theta^\theta\right) - \frac{\kappa^r\left(e^{-(u-t)\kappa^r}-e^{-(u-t)\kappa^\theta}\right)}{\kappa^r-\kappa^\theta}\left(\theta(t)-\theta^\theta\right)du \\ =& (T-S)\theta^\theta + \frac{e^{-(S-t)\kappa^r}-e^{-(T-t)\kappa^r}}{\kappa^r}\left(r(t)-\theta^\theta\right) \\ &+ \frac{\kappa^r\left(e^{-(S-t)\kappa^\theta}-e^{-(T-t)\kappa^\theta}\right) - \kappa^\theta\left(e^{-(S-t)\kappa^r}-e^{-(T-t)\kappa^r}\right)}{\kappa^\theta(\kappa^r-\kappa^\theta)}\left(\theta(t)-\theta^\theta\right). \end{aligned} \tag{3.A.21}$$

Thus, the expectation is

$$\mathbb{E}^Q\left[\frac{1}{T-S}\int_S^T r^s(u)du|\mathcal{F}_t\right] = \frac{1}{T-S}I^r(t;S,T) \tag{3.A.22}$$

For the Federal Funds futures rate, we include the integral over the expectation of the SOFR-EFFR spread process

$$\begin{aligned} I^\zeta(t;S,T) &= \int_S^T \theta^\zeta + e^{-(u-t)\kappa^\zeta}\left(\zeta(t)-\theta^\theta\right)du \\ &= (T-S)\theta^\zeta + \frac{e^{-(S-t)\kappa^\zeta}-e^{-(T-t)\kappa^\zeta}}{\kappa^\zeta}\left(\zeta(t)-\theta^\zeta\right). \end{aligned} \tag{3.A.23}$$

Such that the expectation is calculated as

$$\mathbb{E}^Q\left[\frac{1}{T-S}\int_S^T r^{FF}(u)du|\mathcal{F}_t\right] = \frac{1}{T-S}\left(I^r(t;S,T)+I^\zeta(t;S,T)\right). \tag{3.A.24}$$

3.A.2 Swap rates

This section presents the results required to compute the swap rates in section 3.4.4. On October 16, 2020, the London Clearing House (LCH) and Chicago Mercantile Exchange (CME) changed the Price Alignment Interest (PAI) on cleared swaps from EFFR to SOFR. For the sake of simplicity, we assume SOFR to be the collateral rate for the entire sample period.[18] To ease the notation, we define the pseudo zero coupon bond referencing SOFR $p^s(t,T) := \mathbb{E}\left[e^{-\int_t^T r^s(u)du}|\mathcal{F}_t\right]$, which we compute as

$$p^s(t,T) = e^{A^s(T-t)+B^s(T-t)'X_t(t)}, \tag{3.A.25}$$

where we reiterate that $A^s(T-t)$ and $B^s(T-t)$ solve the Riccati equations with $R = (1,0,0,0,0,0,0,0)'$ and initial conditions $A^s(0)=0$ and $B^s(0)=0$. The floating leg SOFR-rate is calculated from the daily compounded SOFR analogously to the three-month SOFR futures contract in Equation (3.2.37). Again, we consider the continuous approximation, which we denote $R^s(T_{i-1},T_i)$. In the USD market SOFR OIS payments occur at a similar frequency for each leg and once a year for all contracts with a maturity of one year or greater. We denote the payment dates by T_i for $i=1,...,n$ and $\delta = T_i - T_{i-1}$ with $T_n = T$. The fair SOFR OIS rate, $OIS^s(t,T)$, is then given by

$$OIS^s(t,T) = \frac{1-p^s(t,T_n)}{\sum_{i=1}^n \delta p^s(t,T_i)} \tag{3.A.26}$$

[18] See Rutkowski and Bickersteth (2021) for an in depth study on pricing SOFR derivatives under differential funding cost.

Applying the same continuous approximation for the standard OIS contract referencing EFFR, the resulting OIS rate satisfies

$$OIS^{FF}(t,T) = \frac{\sum_{i=1}^{n} \delta \mathbb{E}^Q \left[e^{-\int_t^{T_i} r^s(u)du} R^{FF}(T_{i-1},T_i) | \mathcal{F}_t \right]}{\sum_{i=1}^{n} \delta p^s(t,T_i)}. \tag{3.A.27}$$

Where $R^{FF}(T_{i-1},T_i)$ denotes the continuous approximation of the floating leg EFFR-rate. We note that OIS contracts referencing SOFR and EFFR follow identical conventions. In order to calculate the expectation in the nominator we rewrite it as

$$\begin{aligned} &\mathbb{E}^Q \left[e^{-\int_t^{T_i} r^s(u)du} R^{FF}(T_{i-1},T_i) | \mathcal{F}_t \right] \\ &= \frac{1}{\delta} \mathbb{E}^Q \left[e^{-\int_t^{T_i} r^s(u)du} e^{\int_{T_{i-1}}^{T_i} r^{FF}(u)du} | \mathcal{F}_t \right] - \frac{p^s(t,T_i)}{\delta}. \end{aligned} \tag{3.A.28}$$

Focusing on the term on the left we have

$$\begin{aligned} &\frac{1}{\delta} \mathbb{E}^Q \left[e^{-\int_t^{T_i} r^s(u)du} e^{\int_{T_{i-1}}^{T_i} r^{FF}(u)du} | \mathcal{F}_t \right] \\ &= \frac{1}{\delta} \mathbb{E}^Q \left[e^{-\int_t^{T_{i-1}} r^s(u)du} \mathbb{E}^Q \left[e^{\int_{T_{i-1}}^{T_i} \zeta(u)du} | \mathcal{F}_{T_{i-1}} \right] | \mathcal{F}_t \right]. \end{aligned} \tag{3.A.29}$$

The inner expectation can be solved using the general set of ODEs where $R = (0,0,-1,0,0,0,0,0)'$

$$\mathbb{E}^Q \left[e^{\int_{T_{i-1}}^{T_i} \zeta(u)du} | \mathcal{F}_{T_{i-1}} \right] = e^{A^{aux}(\delta) + B^{aux}(\delta) X_{T_{i-1}}(T_{i-1})} \tag{3.A.30}$$

with initial conditions $A^{aux}(0) = 0$ and $B^{aux}(0) = 0$. This allows us to compute the entire expectation as

$$\mathbb{E}^Q \left[e^{-\int_t^{T_{i-1}} r^s(u)du} e^{A^{aux}(\delta) + B^{aux}(\delta)' X_{T_{i-1}}(T_{i-1})} | \mathcal{F}_t \right] = e^{A^{OIS}(T_{i-1}-t) + B^{OIS}(T_{i-1}-t) X_t(t)} \tag{3.A.31}$$

where $A^{OIS}(T_{i-1}-t)$ and $B^{OIS}(T_{i-1}-t)$ again solve the general set of ODEs with $R = (1,0,0,0,0,0,0,0)$ and initial conditions $A^{OIS}(0) = A^{aux}(\delta)$ and $B^{OIS}(0) = B^{aux}(\delta)$.

Next, we consider an IRS referencing the LIBOR fixings. The standard USD IRS references the three-month LIBOR with the floating leg payment frequency matching the LIBOR fixing. The payment dates on the fixed leg are semi-annually. We denote the floating leg payment dates T_i^L for $i = 1, ..., n$ with $T_i^L - T_{i-1}^L = \delta^L$ and the fixed leg payment dates T_i^{fix} for $i = 1, ..., m$ with $T_i^{fix} - T_{i-1}^{fix} = \delta^{fix}$. Finally, we assume identical dates for the final payment such that $T_n = T_M = T$. The IRS rate ensuring zero initial value of the swap is

$$IRS(t,T) = \frac{\sum_{i=1}^{n} \delta^L \mathbb{E}^Q \left[e^{-\int_t^{T_i^L} r^s(u)du} L(T_{i-1}^L, T_i^L) | \mathcal{F}_t \right]}{\sum_{i=1}^{m} \delta^{fix} p^s(t,T_i)}. \tag{3.A.32}$$

Following the approach of the OIS we rewrite the expectation as

$$\mathbb{E}^Q\left[e^{-\int_t^S r^s(u)du}L(T_{i-1}^L,T_i^L)|\mathcal{F}_t\right]=\frac{1}{\delta^L}\mathbb{E}^Q\left[e^{-\int_t^S r^s(u)du}\frac{U(T_{i-1}^L,T_i^L)}{Q(T_{i-1}^L,T_i^L)}|\mathcal{F}_t\right]-\frac{p^s(t,T_i^L)}{\delta^L}. \tag{3.A.33}$$

Focusing on the term on the left, we have

$$\begin{aligned}
&\frac{1}{\delta^L}\mathbb{E}^Q\left[e^{-\int_t^{T_i^L} r^s(u)du}\frac{U(T_{i-1}^L,T_i^L)}{Q(T_{i-1}^L,T_i^L)}|\mathcal{F}_t\right]\\
=&\frac{1}{\delta^L}\mathbb{E}^Q\left[\mathbb{E}^Q\left[e^{-\int_t^{T_i^L} r^s(u)du}\frac{U(T_{i-1}^L,T_i^L)}{Q(T_{i-1}^L,T_i^L)}|\mathcal{F}_{T_{i-1}^L}\right]|\mathcal{F}_t\right]\\
=&\frac{1}{\delta^L}\mathbb{E}^Q\left[e^{-\int_t^{T_{i-1}^L} r^s(u)du}p^s(T_{i-1}^L,T_i^L)\frac{U(T_{i-1}^L,T_i^L)}{Q(T_{i-1}^L,T_i^L)}|\mathcal{F}_t\right].
\end{aligned} \tag{3.A.34}$$

The expectation is then calculated similarly to the Eurodollar futures rate in Equation (3.2.36). Thus, we compute the term as

$$\frac{1}{\delta^L}e^{A^{IRS}(T_{i-1}^L-t)+B^{IRS}(T_{i-1}^L-t)'X_t(t)}, \tag{3.A.35}$$

where $A^{IRS}(T_{i-1}^L-t)$ and $B^{IRS}(T_{i-1}^L-t)$ solve the general ODEs with $R=(1,0,0,0,0,0,0,0)'$ and initial conditions given by $A^{IRS}(0)=A^s(\delta^L)+A^U(\delta^L)-A^Q(\delta^L)$ and $B^{IRS}(0)=B^s(\delta^L)+B^U(\delta^L)-B^Q(\delta^L)$ except for the the jump elements with $J_t^\lambda(u)$ and $J_t^\phi(u)$, which have their initial conditions set equal to zero reflecting the renewal of the LIBOR panel.

Credit default swaps

We calculate the fair CDS spread on a unit notional contract providing protection over the period $[t;T]$ while assuming zero recovery at default. The value of the protection leg is

$$\mathbb{E}^Q\left[e^{-\int_t^{\tau_t} r^s(u)du}1_{(\tau_t\leq T)}|\mathcal{G}_t\right], \tag{3.A.36}$$

and for the payment leg

$$\sum_{i=1}^n C(T_i-T_{i-1})\mathbb{E}^Q\left[e^{-\int_t^{T_i} r^s(u)du}1_{(T_i<\tau_t)}|\mathcal{G}_t\right] \tag{3.A.37}$$

$$+\sum_{i=1}^n C\mathbb{E}^Q\left[(\tau_t-T_{i-1})e^{-\int_t^{\tau_t} r^s(u)du}1_{(T_{i-1}<\tau_t\leq T_i)}|\mathcal{G}_t\right], \tag{3.A.38}$$

where C denotes the spread, $T_0=t$ and T_i for $i=1,..,n$ are the quarterly payment dates with $T_n=T$. as in Lando (2009), we have that the value of the protection leg is given by

$$\int_t^T \mathbb{E}^Q\left[(\Lambda(u)+\lambda_t(u))e^{-\int_t^u r^s+\Lambda(u)+\lambda_t(u)du}|\mathcal{F}_t\right]du. \tag{3.A.39}$$

When calculating the integrand we note that $\Lambda(u)$ is unidentified in our model and thus omitted in the calculation of the CDS spread (see section 3.4.4), that is we set $\Lambda(u) = 0$. The integrand is then computed using the extended transform in Duffie, Pan, and Singleton (2000)

$$(a(u-t) + b(u-t)'X_t(t))\, e^{A^{cds}(u-t)+B^{cds}(u-t)'X_t(t)} \tag{3.A.40}$$

where $A^{cds}(u-t)$ and $B^{cds}(u-t)$ solve the ODEs in Equation (3.A.6))-(3.A.14) with initial conditions $A^{cds}(0) = 0$ $B^{cds}(0) = 0$ and $R = (1,0,0,1,0,0,0,0)'$ while $a(\tau)$ and $b(\tau)$ satisfy the modified ODEs

$$\frac{\partial b_1(\tau)}{\partial \tau} = -\kappa^r b_1(\tau), \tag{3.A.41}$$

$$\frac{\partial b_2(\tau)}{\partial \tau} = -\kappa^\theta b_2(\tau) + \kappa^r b_1(\tau), \tag{3.A.42}$$

$$\frac{\partial b_3(\tau)}{\partial \tau} = -\kappa^\zeta b_3(\tau), \tag{3.A.43}$$

$$\frac{\partial b_4(\tau)}{\partial \tau} = -\beta^\lambda b_4(\tau), \tag{3.A.44}$$

$$\frac{\partial b_5(\tau)}{\partial \tau} = -\beta^\phi b_5(\tau), \tag{3.A.45}$$

$$\frac{\partial b_6(\tau)}{\partial \tau} = -\kappa^\xi b_6(\tau) + B_6(\tau) b_6(\tau) (\sigma^\xi)^2 + \frac{0.02^{-1} b_4(\tau)}{(0.02^{-1} - B_4(\tau))^2}, \tag{3.A.46}$$

$$\frac{\partial b_7(\tau)}{\partial \tau} = -\kappa^\eta b_7(\tau) + \kappa^\eta B_6(\tau) + B_7(\tau) b_7(\tau) (\sigma^\eta)^2, \tag{3.A.47}$$

$$\frac{\partial b_8(\tau)}{\partial \tau} = -\kappa^\nu b_8(\tau) + B_8(\tau) b_8(\tau) (\sigma^\nu)^2 + \frac{0.02^{-1} b_5(\tau)}{(0.02^{-1} - B_5(\tau))^2}, \tag{3.A.48}$$

$$\frac{\partial a(\tau)}{\partial \tau} = (K^Q \theta^Q)' b(\tau) + B(\tau)' \sigma_0 \sigma_0' b(\tau), \tag{3.A.49}$$

with initial conditions $a(0) = 0$ and $b(0) = (0,0,0,1,0,0,0,0)'$. We can then numerically integrate the integrand in (3.A.40) to obtain the value of the protection leg. For the payment leg we calculate the expectation in the first sum in Equation (3.A.37) as

$$\mathbb{E}^Q \left[e^{-\int_t^{T_i} r^s(u) du} 1_{(T_i < \tau_t)} | \mathcal{G}_t \right] = e^{A^{cds}(T_i - t) + B^{cds}(T_i - t)' X_t(t)}. \tag{3.A.50}$$

For the expectation in the second sum, Equation (3.A.38), we have

$$\begin{aligned} &\mathbb{E}^Q \left[(\tau_t - T_{i-1}) e^{-\int_t^{\tau_t} r^s(u) du} 1_{(T_{i-1} < \tau_t \leq T_i)} | \mathcal{G}_t \right] \\ &= \int_{T_{i-1}}^{T_i} (u - T_{i-1}) \left(a(u-t) + b(u-t)' X_t(t) \right) e^{A^{cds}(u-t) + B^{cds}(u-t)' X_t(t)} du. \end{aligned} \tag{3.A.51}$$

3.B The Intensity Based Credit Risk Approach

In order to price credit risky instruments, we follow Filipović and Trolle (2013) and extend the doubly stochastic framework to accommodate default times for each

arbitrary time t. Thus, we consider the filtration $\mathcal{F}_t = \sigma(X(s)|0 \leq s \leq t)$ and an i.i.d. sequence of exponentially distributed random variables $E_t \sim \text{Exp}(1)$ independent of the filtration $\mathcal{F}_t$. For each t we then define the random default times by

$$\tau_t = \inf\left\{T > t | \int_t^T \Lambda(u) + \lambda_t(u)du \geq E_t\right\}, \tag{3.B.1}$$

and denote the filtration generated by all default indicator processes as $\mathcal{H}_t$. The random times τ_t are stopping times with respects to the enlarged filtration $\mathcal{G}_t = \mathcal{F}_t \vee \mathcal{H}_t$. Following standard results on the intensity based approach (see e.g. Lando (2009)) and assuming zero recovery, any $\mathcal{F}_T$-measurable integrable random variable, X, satisfies

$$\mathbb{E}^Q\left[X1_{(\tau_t > T)}|\mathcal{G}_t\right] = \mathbb{E}^Q\left[Xe^{-\int_t^T \Lambda(u)+\lambda_t(u)du}|\mathcal{F}_t\right]. \tag{3.B.2}$$

3.C The Term Repo Approximation

In this appendix we investigate the accuracy of the approximation in Equation (3.2.31) to the true term repo rate, which we recall is given by

$$R^{repo}(t,T) = \frac{1}{T-t}\left(\frac{E^Q\left[e^{\int_t^T \psi(u)+\phi_t(u)du}|\mathcal{F}_t\right]}{E^Q\left[e^{-\int_t^T r(u)du}|\mathcal{F}_t\right]} - 1\right). \tag{3.C.1}$$

It is clear from this expression that we are unable compute the repo rate without identifying the underlying risk-free rate, $r(u)$ and the repo specific risk premium, $\psi(u)$, separately. However, applying Jensen's inequality, we can construct both an upper and lower bound for $R^{repo}(t,T)$ using only processes identified in our model, which allows us to evaluate the maximum possible error of the approximation in (3.2.31).

First, we note that the approximation used in the paper is in fact a lower bound. To see this, assume independence between $\psi(u)$ and $\phi_t(u)$ as well as $r(u)$ and $\psi(u)$

as in section 3.2.3. Focusing on the fraction we have

$$\begin{aligned}
\frac{E^Q\left[e^{\int_t^T \psi(u)+\phi_t(u)du}|\mathcal{F}_t\right]}{E^Q\left[e^{-\int_t^T r(u)du}|\mathcal{F}_t\right]} &= \frac{E^Q\left[e^{\int_t^T \phi_t(u)du}|\mathcal{F}_t\right] E^Q\left[e^{\int_t^T \psi(u)du}|\mathcal{F}_t\right]}{E^Q\left[e^{-\int_t^T r(u)du}|\mathcal{F}_t\right]} \\
&= \frac{E^Q\left[e^{\int_t^T \phi_t(u)du}|\mathcal{F}_t\right]}{E^Q\left[e^{-\int_t^T r(u)du}|\mathcal{F}_t\right] \frac{1}{E^Q\left[e^{\int_t^T \psi(u)du}|\mathcal{F}_t\right]}} \\
&\geq \frac{E^Q\left[e^{\int_t^T \phi_t(u)du}|\mathcal{F}_t\right]}{E^Q\left[e^{-\int_t^T r(u)du}|\mathcal{F}_t\right] E^Q\left[\frac{1}{e^{\int_t^T \psi(u)du}}|\mathcal{F}_t\right]} \\
&= \frac{E^Q\left[e^{\int_t^T \phi_t(u)du}|\mathcal{F}_t\right]}{E^Q\left[e^{-\int_t^T r^s(u)du}|\mathcal{F}_t\right]}. \qquad (3.C.2)
\end{aligned}$$

Next, in order to calculate an upper bound, we assume independence between $\psi(u) + \phi_t(u)$ and $r(u)$, which yields

$$\begin{aligned}
\frac{E^Q\left[e^{\int_t^T \psi(u)+\phi_t(u)du}|\mathcal{F}_t\right]}{E^Q\left[e^{-\int_t^T r(u)du}|\mathcal{F}_t\right]} &= E^Q\left[e^{\int_t^T \psi(u)+\phi_t(u)du}|\mathcal{F}_t\right] \frac{1}{E^Q\left[e^{-\int_t^T r(u)du}|\mathcal{F}_t\right]} \\
&\leq E^Q\left[e^{\int_t^T \psi(u)+\phi_t(u)du}|\mathcal{F}_t\right] E^Q\left[\frac{1}{e^{-\int_t^T r(u)du}}|\mathcal{F}_t\right] \\
&= E^Q\left[e^{\int_t^T r^s(u)+\phi_t(u)du}|\mathcal{F}_t\right]. \qquad (3.C.3)
\end{aligned}$$

Thus, combining Equation (3.C.2) and (3.C.3) we obtain

$$\frac{E^Q\left[e^{\int_t^T \phi_t(u)du}|\mathcal{F}_t\right]}{E^Q\left[e^{-\int_t^T r^s(u)du}|\mathcal{F}_t\right]} \leq \frac{E^Q\left[e^{\int_t^T \psi(u)+\phi_t(u)du}|\mathcal{F}_t\right]}{E^Q\left[e^{-\int_t^T r(u)du}|\mathcal{F}_t\right]} \leq E^Q\left[e^{\int_t^T r^s(u)+\phi_t(u)du}|\mathcal{F}_t\right] \qquad (3.C.4)$$

Because of the Gaussian specification of the $r^s(u)$ and $\zeta(u)$ processes, the spread between the upper and lower bound is constant across the entire sample for each of the considered maturities. Specifically, given our model estimates, we find that the spread between the upper and lower bound approximation of the term repo rate is 0.02 basis points for the three-month repo and 0.08 basis points for the six-month repo. Furthermore, due to the low volatility of the $\zeta(u)$ process (see table 3.2), we expect the underlying $\psi(u)$ to display an equally low volatility. This implies that the ignored convexity adjustment in (3.C.2) is negligible and thus the lower bound is a very close approximation to the actual term repo rate.

3.D The Kalman Filter

We estimate the model using quasi-maximum likelihood method with the Kalman Filter on spot LIBOR and end of day futures data. When estimating the time series property of the model, we consider the reduced state process $X(t) \in \mathbb{R}^6$ excluding the roll-over risk jump variables and thus we omit the subscript. Having defined a completely affine market price of risk the implied drift parameters under the P-measure are obtained from

$$K^P = \hat{K}^Q - \hat{\Sigma}\text{diag}(\mu)\delta^2, \tag{3.D.1}$$

$$\theta^P = (K^P)^{-1}[\hat{K}^Q\hat{\theta}^Q + \hat{\Sigma}\text{diag}(\mu)\delta^1] \tag{3.D.2}$$

where $\hat{\theta}^Q$, $\hat{K}^Q$ and $\hat{\Sigma}$ refer to the Q-parameters in Equation (3.A.2) and (3.A.3) excluding the fourth and fifth row and column specific to the roll-over risk jump variables and

$$\mu = \left(\mu^r, \mu^\theta, \mu^\zeta, \mu^\xi, \mu^\eta, \mu^\nu\right)', \quad \delta^1 = (1,1,1,0,0,0)', \quad \delta^2 = \text{diag}\left((0,0,0,1,1,1)'\right). \tag{3.D.3}$$

The state transition equation is given by

$$X(t_i) = \left(I - e^{-K^P\Delta t}\right)\theta^P + e^{-K^P\Delta t}X(t_{i-1}) + \omega(t_i) \tag{3.D.4}$$

with $\Delta t = t_i - t_{i-1}$ set to $1/252$ to approximately reflect the number of daily futures data observations in a year. We approximate the transition densities with a Gaussian distribution and thus assume $\omega(t_i) \sim \mathcal{N}(0, Z(t_i))$. Multiple papers such as Duan and Simonato (1999) have conducted Monte Carlo studies demonstrating that the quasi maxixmum likelihood procedure obtained when approximating the transition density in the square-root process by a normal density produces reliable estimates. The conditional covariance matrix, $Z(t_i)$, is equal to

$$Z(t_i) = \int_{t_{i-1}}^{t_i} e^{-K^P u}\hat{\Sigma}D(\mathbb{E}\left[X(u)|\mathcal{F}(t_{i-1})\right], u)D(\mathbb{E}\left[X(u)|\mathcal{F}(t_{i-1})\right], u)'\hat{\Sigma}'\left(e^{-K^P u}\right)' du. \tag{3.D.5}$$

We compute $Z(t_i)$ analytically using the methods presented in Christensen, Lopez, and Rudebusch (2015). Next, we define the measurement equation which, given our yield transformations in section 3.3, is affine in the state variables

$$y(t_i) = A(t_i) + B(t_i)'X(t_i) + \varepsilon(t_i), \quad \varepsilon(t_i) \sim \mathcal{N}(0, H(t_i)). \tag{3.D.6}$$

We consider independent measurement errors with separate error distributions for secured, Federal Funds, and LIBOR rates. Thus, we define $H(t_i)$ as a diagonal matrix with measurement error variances σ^2_{SOFR} for SOFR and term repo observations, σ^2_{EFFR} for Federal Funds futures observations, and σ^2_{LIBOR} for spot LIBOR and

Eurodollar observations. Let $X(t_i|t_j) = \mathbb{E}[X(t_i)|y(t_j), ..., y(t_1)]$ and $P(t_i|t_j) = \mathbb{V}[X(t_i)|y(t_j), ..., y(t_1)]$ for $j \leq i$ denote the conditional expectation and variance. The prediction step of the kalman filter is then

$$X(t_i|t_{i-1}) = FX(t_{i-1}|t_{i-1}) + C, \tag{3.D.7}$$

$$P(t_i|t_{i-1}) = FP(t_{i-1}|t_{i-1})F' + Z(t_i). \tag{3.D.8}$$

Where $F = e^{-K^P \Delta t}$ denotes the state transition model and $C = \left(I - e^{-K^P \Delta t}\right) \theta^P$ the control input. In the update step the a priori state estimates are updated using the time t_i observations

$$X(t_i|t_i) = X(t_i|t_{i-1}) + K(t_i)\nu(t_i), \tag{3.D.9}$$

$$P(t_i|t_i) = (I - K(t_i)B(t_i))P(t_i|t_{i-1}). \tag{3.D.10}$$

Where we have defined the optimal Kalman gain matrix as

$$K(t_i) = P(t_i|t_{i-1})B(t_i)'(S(t_i))^{-1} \tag{3.D.11}$$

with $S(t_i)$ the variance of the prefit residuals

$$S(t_i) = H + B(t_i)P(t_i|t_{i-1})B(t_i)'. \tag{3.D.12}$$

Approximating the transition densities by a Gaussian quasi log-likelihood for a given set of parameters, Θ, the log-likelihood is given by

$$l(y(t_1), ..., y(t_T); \Theta) = \sum_{i=1}^{T} \left(-\frac{N}{2} \log(2\pi) - \frac{1}{2} \left(\log |S(t_i)| + \nu(t_i)'(S(t_i))^{-1}\nu(t_i) \right) \right) \tag{3.D.13}$$

with N the number of observations at each date and T the amount of dates in out data sample. To obtain the optimal set of parameters, $\hat{\Theta}$, we maximize the quasi log-likelihood function using the Nelder-Mead algorithm with a function value tolerance of 0.01. The state variables are required to be stationary under the P-measure and we therefore require the eigenvalues of K^P to be positive.

The futures market calendar differs slightly from the LIBOR publishing dates. In the estimation we consider all dates with futures resulting in dates with missing spot LIBOR data. Furthermore, the six-month repo rate is rather illiquid and thus there are days in our time series for which we have no six-month repo quote, particularly around March 2020. The missing observations are easily accommodated in the kalman filter by considering an $N(t_i) \times N$-matrix $W(t_i)$ where N is the total amount of observations including missings and $N(t_i)$ is the actual amount of observations at time t_i. $W(t_i)$ is then a subset of I_N such that $y^\star(t_i) = W(t_i)y(t_i)$ is the set of non-missing observations. The measurement equation is then simply replaced by

$$y^\star(t_i) = A^\star(t_i) + B^\star(t_i)'X(t_i) + \varepsilon^\star(t_i), \quad \varepsilon^\star(t_i) \sim \mathcal{N}(0, H^\star(t_i)), \tag{3.D.14}$$

where $A^\star(t_i) = W(t_i)A(t_i)$, $B^\star(t_i) = W(t_i)B(t_i)$ and $H^\star(t_i) = W(t_i)HW(t_i)'$. Finally, we change N in the likelihood contributions to reflect the actual number of observations on a given date $N(t_i)$.

Chapter 4

Term Structure Modeling of SOFR: Evaluating the Importance of Scheduled Jumps

This chapter contains the manuscript *Schlögl, Skov, and Skovmand (2023)*.

Abstract

As interest rate benchmarks move from LIBOR to overnight Risk-Free Rates (RFR), it has become increasingly important for models to accurately capture the interest rate dynamics at the overnight tenor. Overnight rates closely track central bank policy rate decisions resulting, in highly discontinuous dynamics around scheduled meeting dates. In this paper, we construct a dynamic term structure model, which accounts for the discontinuous short-rate dynamics. We show that the model is able to jointly fit the overnight US policy rate, SOFR and SOFR futures rates through the recent Fed hiking cycle. Comparing our model with a standard continuous time-homogeneous short-rate model, we find several indications that our model avoids the clear misspecification of the continuous model, in particular with regard to the short-rate dynamics around meeting dates of the Federal Open Market Committee (FOMC). This effect begins to disappear as the term of the rates under consideration is increased, suggesting that diffusive dynamics are a reasonably accurate reflection of the evolution of market expectations embodied in longer-term interest rates.

Keywords: SOFR, Jumps, FOMC, Futures.

4.1 Introduction

Since Vasicek (1977), time-homogeneous affine term structure models have been the main tool when estimating dynamic term structure models. However, the push by regulators during recent years to move from LIBOR to overnight Risk-Free Rates (RFR) as the main benchmarks in fixed income products has increased the importance of accurately modeling rates at the overnight tenor. Overnight rates are highly dependent on central bank policy rates, which predominantly change on dates that are scheduled in advance and known to the market participants. Time-homogeneous and diffusive models ignore these scheduled announcement effects and therefore cannot be expected to accurately capture the dynamics of the policy rate and consequently the overnight benchmark.

Our focus is the Secured Overnight Financing Rate (SOFR), the USD RFR benchmark scheduled to replace USD LIBOR following its June 2023 cessation deadline. Studying the historical changes in SOFR following Federal Open Market Committee (FOMC) meetings, we argue that the primary US policy rate determining the level of SOFR is the Interest on Reserve Balances (IORB). We then construct an affine dynamic term structure model, which jointly models IORB, overnight SOFR and SOFR futures rates. In our framework, the dynamics of IORB are modeled as a time-inhomogeneous pure jump process consisting of both scheduled and unscheduled jumps reflecting the scheduled and unscheduled meetings of the FOMC. modeling IORB as a pure jump process, the filtered IORB short-rate path of the estimated model is consistent with the observed piecewise constant dynamics.

SOFR is computed using aggregate data from the overnight treasury repo market. It is therefore not entirely piecewise constant between FOMC announcements, but also affected by the general funding conditions in the overnight treasury repo market. We model the additional diffusive dynamics of SOFR by considering a stochastic SOFR-IORB spread. Our framework thus models the variation in SOFR futures rates as reflecting changes in expectations about future changes in the underlying policy rate as measured by the IORB as well as a stochastic SOFR-IORB spread.

Previous papers have also studied the effect of central bank policy rate announcements on the term structure. Piazzesi (2005) provides an early attempt to model the Federal Funds target rate accounting for the FOMC meeting calendar. In her model the target rate follows a pure jump process driven by Poisson processes, with jumps during FOMC meetings triggered by elevated jump intensities. More recently, inspired by the UK LIBOR Transition, Backwell and Hayes (2022) propose and estimate a pure jump multicurve model for GBP LIBOR and SONIA OIS rates. In their model overnight, SONIA is included as a direct observation of the SONIA short-rate state variable, while term rates are modeled using a set of auxiliary state variables determining the distribution of future expected and unexpected jumps.

Gellert and Schlögl (2021) put forward a model for SOFR in the Heath-Jarrow-Morton framework in which the target rate is piecewise constant between FOMC meeting dates while forward rates evolve diffusively due to the changing market expectations about future FOMC decisions driven by underlying Wiener processes. Brace, Gellert, and Schlögl (2022) extend the model with stochastic volatility to also fit options on SOFR futures.[1] While these studies also include the scheduled central bank announcements, our paper is the first to seek to include data on the overnight policy and benchmark rates, not as a direct observation of a state variable, but as a part of the estimation sample. Furthermore, the model we construct falls within the traditional class of affine term structure models. The tractable nature of this framework allows us to include option data as well as futures data in the estimation sample.

In the empirical section of the paper we compare our jump model to an instance of the standard time-homogeneous continuous affine term structure models. The models are estimated on daily overnight rate, futures rate data using maximum-likelihood estimation in conjunction with the Kalman filter. While the continuous model is able to fit the cross-section of futures rates fairly well, as also shown in Skov and Skovmand (2021), this is no longer the case when overnight rates are introduced in the estimation sample. Studying the individual log-likelihood contributions we find that, unlike the jump model, estimating the continuous model results in significant deterioration of the log-likelihood contributions on observation dates with changes in the overnight policy rate following FOMC announcements. The misspecification also results in the continuous model being unable to jointly fit overnight and futures rates during the Fed hiking cycle in 2022, whereas the time-inhomogeneous jump model is consistent with both overnight and futures rates. Comparing real-time policy rate forecasts produced by both models we find that the jump model performs better at short horizons (one month) while the forecasts become similar when considering longer forecast periods. Finally, accounting for the FOMC meeting calendar is not only important when modeling overnight rates, but also in contracts with shorter tenors such as the one-month futures or during the accumulation period of contracts set in arrears as is the case in both one- and three-month SOFR futures and the one-month SOFR futures option.

The paper is structured as follows. Section 4.2 studies the dynamics of SOFR in relation to overnight US policy rates. Next, in section 4.3 We present the time-inhomogeneous affine jump framework used to jointly model IORB and SOFR. Section 4.5 details the data and estimation used in the empirical analysis while the results are discussed in Section 4.6.

[1] Scheduled or expected jumps are also referred to in the literature as stochastic discontinuities. Recently, Multiple theoretical papers have also studied the modeling of stochastic discontinuities in relation to term structure modeling see e.g. Keller-Ressel, Schmidt, and Wardenga (2019), Fontana et al. (2020), and Fontana, Grbac, and Schmidt (2022).

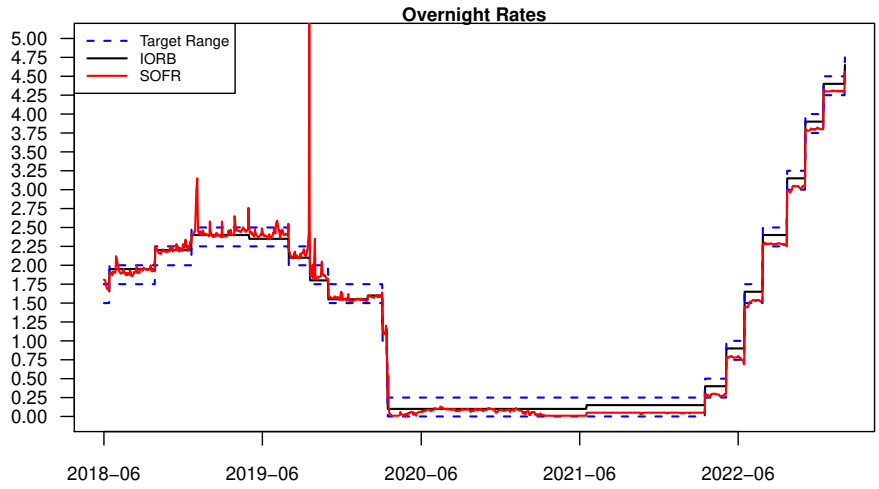

Figure 4.1: *Overnight SOFR, IORB and the upper and lower bound of the Federal Funds Target Range during our sample period.*

4.2 Policy Rates, FOMC Announcements and SOFR

Two of the primary policy rates set by the Federal Reserve are the Federal Funds Target Range and the Interest Rate on Reserve Balances (IORB). The Federal Funds Target Range indicates an acceptable interval for the Effective Federal Funds Rate (EFFR). The IORB replaces the Interest Rate on Required Reserves (IORR) and Interest Rate on Excess Reserves (IOER), which were discontinued on July 29, 2021.[2] The last time IORR and IOER differed was in 2008 and thus before our data sample. With IORR and IOER identical during our entire data period, we will refer to all three rates during our sample simply as IORB.

Figure 4.1 plots the Target Range, IORB, and SOFR. The plot suggests a stochastic spread between SOFR and each of the policy rates. Note that, while mostly within the target range, SOFR fixes both below and above IORB. Also, while spikes in SOFR were frequent during the start of our data period, there have been no significant spikes in SOFR since the October 11, 2019 Fed announcement to conduct operations in the overnight repo market.[3] Importantly, we see that SOFR closely tracks the changes in the policy rates set by the Federal Reserve. Since the nineties, changes in the policy rates have historically been announced following the eight annual scheduled FOMC meetings, with few exceptions of changes after unscheduled meetings during crises such as the Great Financial Crisis or the beginning of the COVID-19 pandemic. This suggests that correctly modeling the jumps in policy rates around FOMC meetings is crucial when modeling the dynamics of overnight SOFR.

[2]See `https://www.federalreserve.gov/newsevents/pressreleases/bcreg20210602a.htm`
[3]See `https://www.federalreserve.gov/newsevents/pressreleases/monetary20191011a.htm`

FOMC Date	$\Delta Target\ Range$	$\Delta IORB$	$\Delta SOFR$	$\Delta EFFR$
June 13, 2018	25	20	19	20
September 28, 2018	25	25	24	25
December 19, 2018	25	20	11	20
May 1, 2019	0	−5	−4	−4
July 31, 2019	−25	−25	−36	−26
September 18, 2019	−25	−30	−60	−35
October 30, 2019	−25	−25	−6	−24
January 29, 2020	0	5	5	5
*March 3, 2020	−50	−50	−41	−50
*March 15, 2020	−100	−100	−84	−85
June 16, 2021	0	5	4	4
March 16, 2022	25	25	25	25
May 4, 2022	50	50	49	50
June 15, 2022	75	75	75	75
July 27, 2022	75	75	75	75
September 21, 2022	75	75	74	75
November 2, 2022	75	75	75	75
December 14, 2022	50	50	52	50
February 1, 2023	25	25	25	25

Table 4.1: *Changes in overnight policy and market rates around FOMC announcements. * denotes unscheduled meetings. Dates in red have $\Delta Target\ Range \neq \Delta IORB$. All values are in basis points.*

Studying the rate changes following FOMC announcements further, Table 4.1 lists the Target Range and IORB changes made by the Fed and the corresponding change in SOFR as well as EFFR on the day following the FOMC announcement during our sample period. The table suggests that the primary policy rate affecting the level of both SOFR and EFFR is the IORB and not the Target Range. E.g., following the scheduled meeting on June 13, 2018 the target range increased by 25 basis points, while IORB only increased by 20 basis points, which caused an increase in SOFR and EFFR by 19 and 20 basis points, respectively. Furthermore, unlike the target range, changes in the IORB are not restricted to the well-known increments in multiples of 25 basis points, but may change by as little as 5 basis points.[4]

4.3 Modeling the Joint Dynamics of IORB and SOFR

We fix the filtered probability space $(\Omega, \mathcal{F}, \{\mathcal{F}_t\}_{t\geq 0}, Q)$ and specify the dynamics directly under the risk-neutral Q-measure defined by the continuously compounded savings account numeraire. To reflect the piecewise constant dynamics of IORB we

[4]For a brief discussion on how the IOER emerged as the key policy rate set by the Fed, see Gellert and Schlögl (2021).

model the IORB-specific short-rate as a pure jump process

$$dr_t = J_t^D dN_t^D + dJ_t^P \tag{4.3.1}$$

where N_t^D is defined as a deterministic counting process reflecting the deterministic jump dates. The set of deterministic jump dates $\{\tau_1, ..., \tau_M\}$ are denoted as $\mathcal{T}$ and identified as the days following the scheduled FOMC meetings when the potential changes in IORB become effective. Furthermore, J_t^P is a pure jump process with jump arrival intensity ν_t^P and iid jump sizes $Z_1, Z_2, ...$ capturing unscheduled jumps in the target rate. We assume that the scheduled jumps, J_t^D, have an exponentially affine jump size distribution with parameters determined by affine transformations of the underlying state process X_t^j. The dynamics of X_t^j are modeled using a standard n-dimensional time-homogeneous continuous affine process

$$dX_t^j = \theta^j(K^j - X_t^j)dt + \Sigma^j D(X_t^j)dW_t^j \tag{4.3.2}$$

where $D(X_t^j)$ is a diagonal matrix with $D(X_t^j)_{ii} = \sqrt{\alpha_i + \beta_i' X_t^j}$. We note that X_t^j must be specified such that the parameters of the jump size distribution stay in the space that they are defined on. Thus, in our framework the joint specification of J_t^D and X_t^j dictates the term structure of scheduled FOMC meeting jumps. The specification of r_t implies that it is an affine time-inhomogeneous process. Since there is no diffusion term in the dynamics of r_t it remains constant between jumps and the time t risk-neutral expectation of the IORB for any future time point $u > t$ is given by the current rate and expected sum of future jumps

$$\mathbb{E}_t^Q[r_u] = r_t + \sum_{j=\eta(t)}^{\eta(u)-1} \mathbb{E}_t^Q\left[J_{\tau_j}^D\right] + \mathbb{E}_t^Q\left[\sum_{i=N_t^P}^{N_u^P-1} Z_i\right] \tag{4.3.3}$$

with $\eta(t) = \{j \in \mathbb{N} | \tau_{j-1} \leq t < \tau_j\}$ and N_t^P the amount of realized unscheduled jumps at time t. Having described the dynamics of the IORB, we model the SOFR specific short-rate, denoted r_t^s, as the sum of IORB and an affine stochastic spread process, s_t, such that

$$r_t^s = r_t + s_t. \tag{4.3.4}$$

Given that spikes in SOFR were only present during the beginning of our sample and seem to have disappeared in recent years, we do not attempt to incorporate spikes in our modeling of the dynamics of SOFR. We refer to Andersen and Bang (2020) for a potential way to treat spikes in SOFR.

4.3.1 Model specification

To obtain a working specification of our framework, we will assume that the size of scheduled jumps is normally distributed with state-dependent mean and constant variance

$$J_t^D \sim \mathcal{N}(\gamma^Q + \Gamma^{Q'} X_{t-}^j, \omega^2). \tag{4.3.5}$$

Furthermore, we let $\gamma^Q = 0$ and $\Gamma^Q = (1,0)'$ and specify $X_t^j = (\xi_t, \theta_t)'$ as a two-factor Gaussian process

$$d\xi_t = \kappa^\xi(\theta_t - \xi_t)dt + \sigma^\xi dW_t^\xi, \tag{4.3.6}$$

$$d\theta_t = \kappa^\theta(\theta^\theta - \theta_t)dt + \sigma^\theta\left(\rho dW_t^\xi + \sqrt{1-\rho^2}dW_t^\theta\right). \tag{4.3.7}$$

The the joint specification of J_t^D and X_t^j implies that the mean jump sizes are modeled by ξ_t, which in turn evolves stochastically around the central tendency factor θ_t. Having specified a Gaussian distribution for the scheduled jumps and ignoring the unscheduled jumps, our model can be seen as a special case of the framework presented in Kim and Wright (2014). However, rather than modeling the target rate specifically, that paper models government bond yields using a diffusive term for the short-rate while considering scheduled jumps on dates with employment report announcements. Next, we assume that the unscheduled jumps J_t^P arrive at a constant intensity ν^P and specify the corresponding jump size distributions $Z_1, Z_2, ...$ as normal with mean μ^P and volatility σ^P. Lastly, since the spread between SOFR and IORB is both negative and positive during our sample, we model it using a simple one-factor Gaussian process

$$ds_t = \theta^s(\kappa^s - s_t)dt + \sigma^s dW_t^s. \tag{4.3.8}$$

Defining the joint process $X_t = (r_t, \xi_t, \theta_t, s_t)'$, our model specification constitutes a four-factor model for the joint dynamics of IORB and SOFR.[5] We relate the dynamics under the physical and risk-neutral measures through the likelihood process

$$\frac{dL_t}{L_{t-}} = \Psi\left(J_t^D, X_{t-}^j\right)dN_t^D + \Lambda' dW_t^P. \tag{4.3.9}$$

Given the fairly short sample size, we consider a parsimonious risk premium specification providing a close link between the risk-neutral and physical dynamics. First, we specify a completely affine market price of risk specification for the diffusive state variables. Thus, we define the market price of risk as $\Lambda = \left(\lambda^\xi, \lambda^\theta, \lambda^s\right)'$ such that the diffusive dynamics under the physical and risk-neutral measures are related through

$$dW_t^Q = dW_t^P + \Lambda dt. \tag{4.3.10}$$

[5]Another possible choice, which would preserve the affine property of r_t, would be to use scaled Poisson distributions for the up and down jumps, i.e., $J_t^D \sim s \cdot \left(Pois(\gamma^u + \Gamma^{u'} X_{t-}^j) - Pois(\gamma^d + \Gamma^{d'} X_{t-}^j)\right)$. The realized IORB jump sizes during our sample presented in Section 4.2 suggest that we would need to set $s = 0.0005$ to be able to capture the realized changes in the IORB during our sample. While this implies a discrete jump size distribution, which may seem more realistic, estimating such a model results in large values of the rate parameters controlling the Poisson distributions. Thus, while on average the sum of these would reflect the scheduled jumps given a sufficiently flexible state process, the simulated paths would result in frequent and large up/down jumps in the target rate dissimilar to the observed path. Specifying Poisson jumps also implies that the rate parameter in each Poisson distribution needs to stay positive, meaning that we cannot model X_t^j using a Gaussian process, which reduces the tractability of the model. Nonetheless, the pricing formulas in Appendix 4.A are easily modified to allow for Poisson jumps with state-dependent parameters driven by independent square-root processes, for example.

Second, we consider an essentially affine scheduled jump risk premium extension as in Kim and Wright (2014)

$$\Psi\left(J_t^D, X_{t-}^j\right) = \exp\left(-\Upsilon \frac{J_t^D - (\gamma^P + \Gamma^{P'} X_{t-}^j))}{\omega} - \frac{1}{2}\Upsilon^2\right) - 1 \tag{4.3.11}$$

with $\Upsilon = \phi + \Phi X_{t-}^j$. This implies that the physical jump distribution is $J_t^D \sim \mathcal{N}(\gamma^P + \Gamma^{P'} X_{t-}^j, \omega^2)$ with $\gamma^P = \gamma^Q + \omega\phi$ and $\Gamma^P = \Gamma^Q + \omega\Phi$. We further restrict the scheduled jump risk specification by $\phi = 0$ and $\Phi = (\Phi_1, 0)'$ such that $\gamma^P = 0$ and $\Gamma^P = (\Gamma_1^P, 0)'$. With these restrictions the jump risk premium effectively scales the effect of ξ_t on the mean jump size under the physical measure. This allows us to directly evaluate the impact of the jump risk premium by comparing the estimated value of Γ_1^P with the fixed value $\Gamma_1^Q = 1$ under the risk-neutral measure. In order to identify the dynamics of the unscheduled jumps under both measures we do not allow for a risk premium on the unscheduled jumps, see Section 4.5.3 for further discussion.

4.3.2 A continuous specification

In order to compare the proposed jump model, we also consider the class of standard time-homogeneous continuous models. Specifically, we consider the maximally identifiable three-factor Gaussian model from Dai and Singleton (2000) as a continuous model for the dynamics of IORB. The IORB related short-rate is therefore affine in the latent state variables $r_t = \rho_0 + \rho_1 \cdot X_t$, which evolve as

$$dX_t = K^Q\left(\theta^Q + X_t\right)dt + \Sigma dW_t^Q. \tag{4.3.12}$$

As in Kim and Wright (2014) we rotate the specification such that the third variable defines the short-rate. The parameterization then becomes

$$K^Q = \begin{bmatrix} K_{11} & 0 & 0 \\ K_{21} & K_{22} & 0 \\ K_{31} & K_{32} & K_{33} \end{bmatrix}, \quad \theta^Q = \begin{bmatrix} 0 \\ 0 \\ 0 \end{bmatrix}, \quad \Sigma = \begin{bmatrix} c & 0 & 0 \\ 0 & c & 0 \\ \sigma_{31} & \sigma_{32} & \sigma_{33} \end{bmatrix}, \quad \rho = \begin{bmatrix} 0 \\ 0 \\ 1 \end{bmatrix}. \tag{4.3.13}$$

Where c is a scaling constant, which we fix at 0.01. Similarly to the jump specification, we define the SOFR specific short rate as the sum of the target rate and a stochastic spread process driven by a single-factor Gaussian process $r_t^s = r_t + s_t$. Likewise, we also specify a completely affine market price of risk specification with $\Lambda = (\lambda_1, \lambda_2, \lambda_3, \lambda^s)'$ such that the diffusive dynamics again are related by

$$dW_t^Q = dW_t^P + \Lambda dt. \tag{4.3.14}$$

The jump and continuous specifications are thus both four-factor models for the joint dynamics of IORB and SOFR, however, we note that the continuous specification contains an extra diffusive Brownian motion term.

4.4 SOFR futures and futures options

Interest rate futures referencing SOFR are traded on the CME. The futures price at expiration is $100\,(1 - R(S,T))$ with $R(S,T)$ denoting the futures rate. The mark-to-market feature implies that the futures price is a martingale under the risk-neutral measure (see e.g. Hunt and Kennedy (2004)). The present value of the futures contract is therefore given by the risk-neutral expectation

$$F(t;S,T) = \mathbb{E}_t^Q \left[100\,(1 - R(S,T))\right]. \tag{4.4.1}$$

Contracts referencing both a one- and three-month backward-looking rate are available. Denoting the realized SOFR fixings $R^s_{t_i}$, the one-month futures rate is determined as the arithmetic average during the contract month

$$R^{1m}(S,T) = \frac{1}{T-S}\sum_{i=1}^{N}\frac{1}{360}R^s_{t_i} \tag{4.4.2}$$

with $S \leq t_1, ..., t_N \leq T$. The three-month futures rate is given by the compounded average of the overnight fixings

$$R^{3m}(S,T) = \frac{1}{T-S}\left(\prod_{i=1}^{N}\left(1 + d_i R^s_{t_i}\right) - 1\right) \tag{4.4.3}$$

with d_i the number of days until the next fixing multiplied by the day count fraction.

Futures contracts provide multiple advantages when studying the short end of the term structure. Specifically, SOFR futures data contains the earliest record of historical data on SOFR linked derivatives and the most liquidly traded short term SOFR contracts. Furthermore, since futures are exchange-traded products, our data consists of actual traded prices instead of quotes from brokers, as is often the case with data on over-the-counter products such as Overnight Index Swaps (OIS). Finally, spot-starting OIS rates involve compounding of the underlying overnight rate throughout the entire period of the swap and thus the compounding period increases as the maturity of the contract increases. In contrast, the futures rate is a direct measurement of risk-neutral SOFR expectations during the reference period of the contract, which is always either one or three months. This feature becomes increasingly important when we want to be able to properly differentiate between the ability of each model in fitting the term structure of SOFR around FOMC meetings.

Options on SOFR futures are available on both the one- and three-month underlying futures contracts. A key difference between the one- and three-month SOFR option is the expiration date of the option. The option referencing the three-month futures expires on the Friday before the third Wednesday of the contract month when the underlying three-month futures starts to accumulate its rate. The one-month futures option expires at the end of the contract month of the underlying one-month

futures contract. The one-month SOFR futures therefore allows one to study the option behaviour as the backward-looking rate fixes, however, as of writing trading is only active in the three-month futures options. Like the futures contract, the three-month SOFR futures option also provides the earliest record of traded SOFR derivatives with optionality. Trading in SOFR futures options has greatly increased during 2022, as the US LIBOR cessation date approaches, and in November 2022 open interest in SOFR futures options has surpassed open interest in Eurodollar futures options.[6] Finally, while the undiscounted SOFR futures contract is a martingale under the risk-neutral measure due to the mark-to-market feature, the SOFR futures option payoff requires discounting. However, since October 2020 SOFR has been the price alignment interest (PAI) at CME and thus SOFR futures options can be accurately priced using a single-curve setup.

4.5 Data and Estimation

In this section we describe the data set and assumptions made in our model estimation as well as the estimation method.

4.5.1 FOMC meeting data

We obtain the historical and future scheduled FOMC calendar from the Federal Reserve website.[7] Meetings are scheduled approximately a year in advance. Since we only consider maturities up to around one year we use the actual historical scheduled FOMC date.[8] Our jump model does not include any FOMC meeting calendar uncertainty. Instead, we model the target rate jumps following unscheduled meetings as unscheduled jumps. Therefore, we also do not consider any changes or unscheduled meetings in the FOMC meeting calendar. This means that unscheduled meetings such as those that happened on March 3 and 15, 2020 are not a part of our FOMC calendar. Similarly, the meeting on March 18, 2020, which was cancelled, is also not removed from our FOMC calendar data.

4.5.2 Overnight, futures and futures option data

First, we collect the overnight SOFR and IORB data used in the estimation from the website of the Federal Reserve Bank of St. Louis. Next, we obtain futures data

[6] See `https://news.bloomberglaw.com/capital-markets/sofr-options-wagers-outnumber-eurodollars-for-the-first-time-1?context=search&index=6`

[7] See `https://www.federalreserve.gov/monetarypolicy/fomccalendars.htm`

[8] We note that our framework can easily be extended to longer maturities simply by extrapolating the FOMC dates. Scheduled FOMC meeting announcements are always on Wednesdays, with the potential target rate change the day after on Thursday and thus in order to obtain the future scheduled meeting dates for e.g. 2024, one can choose the Wednesdays closest to the equivalently scheduled meeting date in 2023. The exact timing of the meeting dates are far less important for the model estimation when considering meetings further than a year out, and thus extrapolating the dates has little impact.

from Refinitiv Eikon. Our data sample consists of daily data starting in June 2018 (following the introduction of SOFR futures on CME) and ending in February 2023, resulting in a total of 1178 SOFR futures trading days. Since we study the effect of FOMC meetings, we focus on the short end of the term structure. Furthermore, futures contracts close to expiry are usually the most liquidly traded. Therefore, we consider futures contracts with a maturity up to around a year. Futures contracts referencing SOFR are available as both one-month and three-month contracts. We include the seven nearest one-month SOFR futures contracts and five nearest quarterly three-month SOFR futures contracts. In Section 4.6.6 we extend the sample with recent data on SOFR futures options. Similarly to futures contracts, options on futures close to expiry are also the most liquid, in particular futures options expiring within a year. Based on this, we include the four nearest quarterly SOFR futures options. These have only recently become liquid and our options data sample therefore starts June 1, 2022, consisting of 170 observations, which include options. Since the main focus is estimate SOFR variance and not fit the actual smile, for each option maturity we only consider the out-of-the-money call option closest to being at-the-money for each contract maturity. Furthermore, we only consider options with an open interest larger than 100. Finally, we exclude options with a quoted price less than 0.02, which tend to be less accurate due to the minimum price fluctuation of the contracts. This usually impacts the nearest options when the options are close to expiry. SOFR futures options are American options. We therefore adjust option prices for the early exercise premium as in Broadie, Chernov, and Johannes (2007) and Bikbov and Chernov (2005) by calculating the Black-implied volatility including the early exercise feature using a binomial tree. We then calculate the approximated European option price by inserting the obtained implied volatility in the European version of the Black formula. When calculating both the American Black-implied volatility and the subsequent European option price we need to fix a constant rate for discounting. Here, we use the fitted SOFR curve from the estimation without options to obtain the prevailing SOFR term rate between the observation date and the maturity date of the option. Since we only include OTM options with up to a year of maturity the American feature has little impact on the price of the option. The median size of the American premium measured in implied volatility is 0.4 basis points, while the observed implied volatilities range from 48 to 180 basis points, with a median size of 124 basis points.

4.5.3 Maximum-likelihood and the Kalman filter

We estimate the models using maximum-likelihood in conjunction with the Kalman filter. This involves casting each model in its state space representation consisting of a transition and measurement equation. The method is frequently used in the estimation of dynamic term structure models, we therefore leave out the exact

steps of the Kalman filtering process.[9] Focusing on the state transition equation of the time-inhomogeneous short-rate process in the jump model, we note that when estimating the jump model we cannot explicitly identify the individual effect of scheduled and unscheduled jumps on the term structure. However, once realized we know both the size of the jump in IORB and if it was scheduled or not from the following FOMC announcements. Assuming no risk-premium on the unscheduled jumps, this allows us to pre-estimate the effect of the unscheduled jumps outside the Kalman filtering algorithm from the empirical frequency and jump sizes. Thus, under both the $P-$ and Q-measure we fix the unscheduled jump intensity at the empirical frequency during our sample $\nu^P = 0.428$ and the unscheduled jump size distributions are likewise fixed at the empirical mean $\mu^P = -0.0075$ and variance $(\sigma^P)^2 = 1.25\text{e}-5$.[10] For the filtering we then update the target rate with its realized unscheduled jump sizes during the unscheduled rate changes in March of 2020. Thus, only considering the scheduled jumps in IORB, we define the state transition equation of the discretized short rate process r_{t_i} with $\Delta t = t_i - t_{i-1} = 1/252$ as

$$r_{t_i} = \begin{cases} r_{t_{i-1}} + \Gamma^{P'} X^j_{t_{i-1}} + \varrho_{t_i} & t_i \in \mathcal{T} \\ r_{t_{i-1}} & t_i \notin \mathcal{T} \end{cases} \tag{4.5.1}$$

where $\varrho_{t_i} \sim \mathcal{N}(0, \omega^2)$. The conditional variance of r_{t_i} is therefore ω^2 if $t_i \in \mathcal{T}$ and zero if $t_i \notin \mathcal{T}$. The zero conditional variance of r_{t_i} on non-FOMC dates due to the offline estimation of unscheduled jumps is essential during estimation since it implies that the policy rate cannot change during the Kalman filtering process, thus enforcing the piecewise constant pattern of the policy rate between FOMC meeting dates. Similarly to the continuous model specification, the remaining state variables in the jump model are simply time-homogeneous Gaussian diffusions and we obtain the transition equation from the discretized dynamics under the physical measure.

The standard Kalman filter also requires an affine measurement equation. From Appendix 4.A we note that the one-month futures rates are already affine in the state variables, whereas we use log transformations and consider futures and overnight yields to obtain affine expressions for the overnight and three-month rates, i.e.,

$$y^{O/N}(t,T) = \frac{1}{T-t} \log\left(1 + (T-t) R^{O/N}(t,T)\right), \tag{4.5.2}$$

$$y^{3m}(t;S,T) = \frac{1}{T-S} \log\left(1 + (T-S) f^{3m}(t;S,T)\right). \tag{4.5.3}$$

Denoting by y_{t_i} the stacked vector of futures and overnight observations for each observation date t_i, the measurement equation can be written as

$$y_{t_i} = A_{t_i} + B_{t_i} X_{t_i} + \epsilon_{t_i}. \tag{4.5.4}$$

[9] See Skov and Skovmand (2021) and Skov and Skovmand (2022) for applications and details on estimating continuous time-homogeneous term structure models on historical SOFR futures data.

[10] Recall from table 4.1 that we observe two unscheduled jumps of -100 and -50 basis points during our sample.

ϵ_{t_i} is a vector of measurement errors, which we assume to be independent for each observed overnight and futures rate. Furthermore, we assume mean zero Gaussian errors with standard deviation σ^{rates} for each observation. The assumption puts a tight requirement for the models to simultaneously fit the entire range of overnight and futures rates.[11] When including data on futures options, the measurement equation becomes non-affine in the state vector. Instead, we apply the extended Kalman filter, computing the required derivatives using small perturbations in the state vector. We also assume a separate standard deviation $\sigma^{options}$ for the option measurement errors.

4.6 Empirical Results

4.6.1 Parameter estimates and state variables

Parameter estimates for both the continuous and jump model specifications are presented in Table 4.2. Focusing on the jump model estimates, we first observe a near zero estimate for the mean of the stochastic mean process θ^{θ}. Jumps in the policy rate are thus expected to mainly occur at the nearest FOMC dates, with the Federal Reserve expected to keep its policy rate fixed in the long run. Furthermore, we find a significant negative correlation between the jump state factors, as indicated by $\rho = -0.94$. A positive shock to the expectation of the nearest FOMC meeting is thus expected to be offset by an almost equivalent decrease in the expectation of future jumps. Finally, while the market price of risk parameter estimates display fairly large standard deviations, we see a sizeable scheduled jump risk premium as implied by $\Gamma_1^P = 0.61$, which is notably lower than the fixed $\Gamma_1^Q = 1$.

Figure 4.2 plots the filtered policy related short-rate factor and SOFR-IORB spread factor for each specification. The figure clearly shows how the continuous short rate specification is not able to reflect the discontinuous path for IORB, whereas the jump specification is fully consistent with such a path. Furthermore, during the recent Fed hiking cycle, in order to compensate for the continuous short-rate path, the spread factor oscillates around jumps to fit the overnight SOFR fixings.

4.6.2 Log-likelihood contributions and FOMC dates

The continuous and jump models are not nested models, hindering the use of standard likelihood ratio tests. However, simply comparing the maximized log-likelihoods for each model in Table 4.2, we note that the jump specification produces a significantly higher overall log-likelihood value, suggesting a better fit to the observed data. In order to further study the cause of the difference in log-likelihood values, consider

[11] Skov and Skovmand (2021) allow for individual variances of each futures observation. This additional flexibility of the measurement errors makes it harder to identify if the models are misspecified.

Jump		Continuous	
Parameter	Estimate	Parameter	Estimate
κ^r	1.6988 (0.3072)	ρ_0	0.0033 (0.0013)
κ^θ	1.7046 (0.3047)	K_{11}	1.8398 (2.9764)
κ^s	0.0442 (0.0330)	K_{21}	2.1303 (0.6243)
θ^θ	-0.0003 (0.0000)	K_{22}	0.3574 (0.0180)
θ^s	0.1056 (0.0777)	K_{31}	-2.3387 (2.3426)
σ^ξ	0.0070 (0.0002)	K_{32}	-1.9901 (1.6970)
σ^θ	0.0088 (0.0026)	K_{33}	1.8505 (2.9684)
σ^s	0.0112 (0.0002)	κ^s	200.903 (3.7261)
ρ	-0.9447 (0.0138)	θ^s	-0.0001 (0.0000)
ω	0.0013 (0.0000)	σ_{31}	-0.0025 (0.0013)
λ^ξ	0.4895 (0.8824)	σ_{32}	-0.0006 (0.0010)
λ^θ	0.8414 (0.5654)	σ_{33}	0.0036 (0.0006)
λ^s	-0.4783 (0.4175)	σ^s	0.0298 (0.0003)
Γ_1^P	0.6088 (0.0481)	λ_1	-0.2539 (0.8591)
-	-	λ_2	0.5479 (0.6389)
-	-	λ_3	-0.6841 (0.7330)
-	-	λ^s	-1.4819 (1.1976)
$\sigma^{rates} \times 10^4$	2.74 (0.10)	$\sigma^{rates} \times 10^4$	3.79 (0.07)
Log-likelihood	107,109	Log-likelihood	102,961

Table 4.2: *Full sample parameter estimates for the jump and continuous model specifications. Standard deviations are shown in parenthesis.*

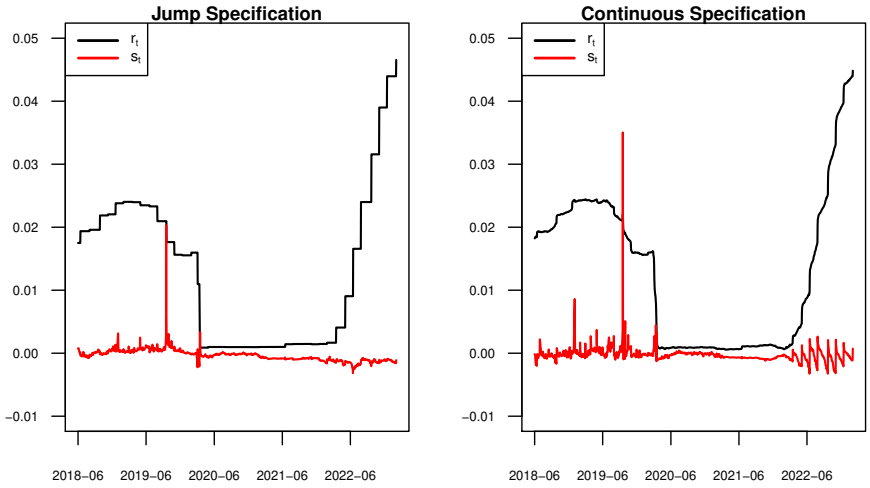

Figure 4.2: *The plots display the filtered r_t and s_t state variables in both the continuous and jump specification.*

the daily log-likelihood contributions based on the optimal parameters. The daily log-likelihood contributions throughout the sample period are plotted in Figure 4.3. During the first two years of the sample we see occasional downward spikes in the

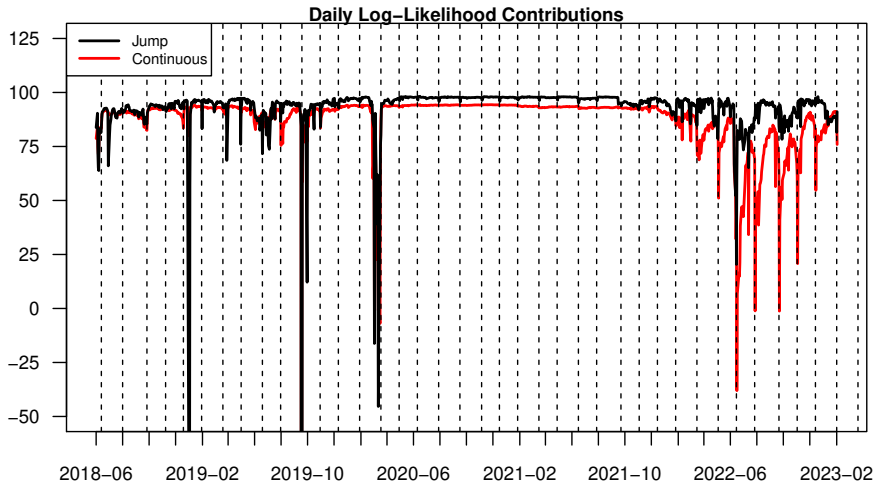

Figure 4.3: *Full sample daily log-likelihood values based on the optimal parameter estimates. The vertical dotted lines marks FOMC meeting dates.*

daily log-likelihood contributions of both models due to overnight spikes in SOFR, most notably during the SOFR surge of September 2019. As noted in Section 4.3, we do not attempt to model spikes in SOFR and the negative spikes in log-likelihood values are thus to be expected. Likewise, the large drop in log-likelihoods following the market stress of the COVID-19 Crisis is no surprise. During the subsequent zero interest rate environment both specifications produce steady log-likelihood contributions with slightly higher values obtained by the jump-model. The largest differences are seen during the most recent period in 2022, following the multiple policy rate hikes by the Fed. Figure 4.4 highlights the log-likelihood values from January 2022 to the end of our sample in February 2023. The plot shows the distinct crashes in the log-likelihood values of the continuous model specification following FOMC meetings, whereas the jump specification correctly captures the scheduled jumps in the overnight rates at FOMC dates and thus displays little to no difference in log-likelihood contributions on these dates. The large deterioration in log-likelihood values clearly reflects the misspecification of the continuous model around scheduled FOMC dates with policy rate changes.

4.6.3 In-sample fit

In order to compare the ability of each of the models to fit the time variation in the cross-section of overnight and futures rates, we compute the fitted overnight and futures rates based on the filtered state variables. The resulting root-mean-square errors (RMSE) are reported in Table 4.3. Based on the full sample RMSEs, we observe an improvement across almost all futures rates when comparing the jump specification to the classical continuous model. Focusing on the overnight rates, the

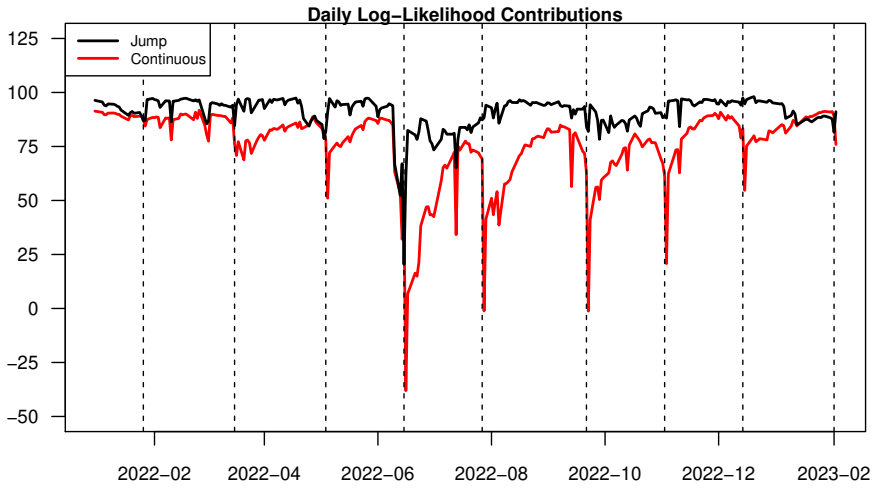

Figure 4.4: *Daily log-likelihood values from January 2022 to the end of our sample based on the optimal parameter estimates. The vertical dotted lines marks FOMC meeting dates.*

continuous model has a surprisingly good fit to overnight SOFR. This is because of the SOFR spread process, s_t, which in the continuous model is estimated with a very strong mean reversion, $\kappa^s = 200.9$, and mean zero such that variations in this process basically only impact the overnight SOFR fixings and enables the model to fit the overnight SOFR fixings even when spikes are present. In the jump model, the SOFR spread accounts for the entire term structure of the spread. Thus, it is not able to fully capture the spikes during the first part of the sample.

We also report RMSEs for subsamples of the full data period. Specifically, we consider the first period of our sample from June 1, 2018 to the end of 2022, and the final part of the sample from January 1, 2022 to February 2, 2023 separately. Studying the RMSEs of the subsamples, we see that the improvement in the jump specification is mainly driven by a significant improvement in the most recent period from January 2022 to February 2023. During this period the Federal Reserve increased its policy rates multiple times following scheduled FOMC meetings. While there was a degree of uncertainty about the size of the policy rate hikes, the hikes were anticipated thus creating a highly discontinuous expected path for the policy rate and in turn SOFR. The jump specification is perfectly capable of fitting these discontinuities and shows no real deterioration in fit during this period. However, the continuous specification clearly fails to accurately capture the expected short-rate path as seen by the significant increase in RMSEs across all overnight and futures rates.

Model	Sample	O/N Rates		One-Month Futures							Three-Month Futures				
		IORB	SOFR	1st	2nd	3rd	4th	5th	6th	7th	1st	2nd	3rd	4th	5th
Jump	Full	1.0	5.1	2.0	4.0	2.5	2.1	1.8	1.7	1.9	1.5	2.1	2.1	1.7	2.3
	Start	1.0	5.5	2.2	4.2	2.3	1.9	1.7	1.6	1.7	1.4	2.1	2.0	1.2	1.9
	End	0.7	3.3	1.3	3.5	3.1	2.5	2.0	1.9	2.4	1.6	2.0	2.5	2.7	3.4
Continuous	Full	6.6	1.4	3.9	5.8	3.9	3.2	2.6	2.3	2.4	2.6	2.2	2.1	1.8	2.8
	Start	4.4	1.4	2.7	3.8	2.4	1.9	1.5	1.4	1.7	1.5	1.9	1.9	1.1	1.8
	End	11.1	1.2	6.6	9.7	6.8	5.8	4.6	4.1	3.7	4.8	3.1	2.9	3.0	4.9
Jump	Full	-	-	1.8	1.9	2.1	2.0	1.7	1.2	1.4	0.9	1.2	1.8	1.6	1.6
	Start	-	-	1.7	1.7	1.9	1.8	1.6	1.1	1.2	0.9	1.0	1.6	1.1	1.0
	End	-	-	2.2	2.5	2.4	2.4	1.8	1.4	1.9	0.9	1.7	2.3	2.6	2.7
Continuous	Full	-	-	1.6	2.9	3.3	3.0	2.5	1.7	1.5	1.0	1.2	1.5	1.3	1.4
	Start	-	-	0.9	1.6	1.9	1.7	1.5	1.1	1.0	0.8	0.9	1.3	0.9	0.8
	End	-	-	2.8	5.2	5.8	5.4	4.3	3.1	2.6	1.6	1.8	2.0	2.2	2.6
Jump	Full	-	-	-	-	-	-	-	-	-	0.9	1.5	1.2	1.4	01.0
	Start	-	-	-	-	-	-	-	-	-	0.7	1.3	1.1	1.0	0.6
	End	-	-	-	-	-	-	-	-	-	1.4	2.2	1.6	2.2	1.8
Continuous	Full	-	-	-	-	-	-	-	-	-	0.4	0.7	1.0	0.9	0.5
	Start	-	-	-	-	-	-	-	-	-	0.4	0.6	0.9	0.8	0.4
	End	-	-	-	-	-	-	-	-	-	0.5	1.0	1.2	1.3	0.8

Table 4.3: *Comparative RMSEs for the jump and continuous models. "Start" refers to the subsample covering the first period of our sample from June 1, 2018 to the end of 2022, and "End" refers to the final part of the sample from January 1, 2022 to February 2, 2023.*

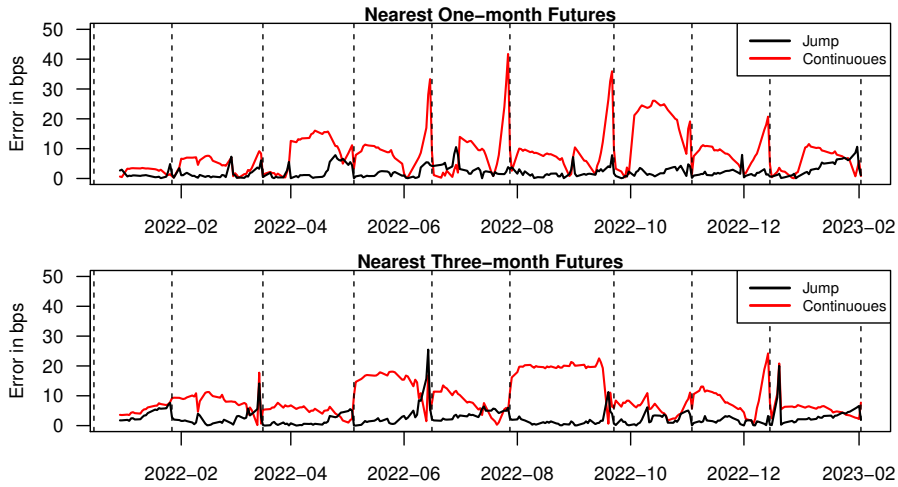

Figure 4.5: *Absolute fitting errors for the nearest futures contracts during the recent Fed hiking cycle. The futures rates are adjusted to only reflect the implied futures rate for the remaining reference period of the contract. The vertical lines mark scheduled FOMC dates.*

Table 4.3 suggests better fits for the nearest one- and three-month futures contracts compared to the second nearest contract. This is somewhat misleading and a result of the fixing in arrears of the futures rate, which means that the nearest futures contract has already accumulated a part of its underlying overnight SOFR fixings. Therefore, when a large part of these fixings have already accumulated, even a highly misspecified model will provide a decent fit to the futures rate. To account for this, we adjust for the rate that has already accumulated and re-calculate the RMSEs based on just the part of the futures rate that has not yet fixed.[12] Focusing on the last period of the sample starting from January 1, 2022, we find that the RMSE for the nearest one-month futures in the continuous model is 11.2 bps compared to 3.0 bps for the jump model. Similarly, for the three-month contract the RMSE is 11.0 and 3.8 bps for the continuous and jump model, respectively. Figure 4.5 plots the absolute errors between the observed and model-implied futures rates for the nearest contracts while adjusting for the part of the contract, which has already accumulated. The graphs clearly show the better fit of the jump model, especially for the one-month contract around FOMC meetings.

Backwell and Hayes (2022) find that unscheduled jumps are necessary when fitting

[12]Specifically we adjust the observed and modeled rates by removing the accumulated fixings and rescaling the resulting rate for the remaining period to reflect an annual rate. E.g. for the nearest one-month contract with $S < t < T$ we obtain

$$f^{1m}_{adjusted}(t;S,T) = \frac{T-S}{T-t}\left(f^{1m}(t;S,T) - \frac{1}{T-S}\sum_{i=1}^{N_t}\frac{1}{360}R^s_{t_i}\right)$$

where $S \leq t_1, ..., t_{N_t} \leq t$.

the term structure (up to one year) of SONIA. However, in their model the state variables impact the jump distribution for the next meeting only, and all scheduled jumps in the short rate after the upcoming meeting have expectation zero. This implies, that in their model futures contracts starting to accumulate after the next scheduled meeting are determined solely, by unscheduled jumps. Their model setup thus necessitates a more rich model structure for the arrival intensity of unscheduled jumps in order to get a realistic representation of the futures curve. Furthermore, the need to have a significant unscheduled jump component is likely exacerbated by the relatively low frequency of scheduled jumps in the UK. Backwell and Hayes (2022) consider the quarterly meetings of the Bank of England's Monetary Policy Committee (MPC) as opposed to the eight annual meetings of the FOMC. In contrast, our results thus suggest that a pure jump specification of the short rate can fit the term structure without including stochastic intensity or a state dependent jump size distribution of the unscheduled jumps (possibly because unscheduled jumps appear quite rarely). This does not imply that unscheduled jumps are not part of the US overnight rate dynamic, as clearly seen from the recent COVID-19 crisis. However, the impact of the unscheduled and scheduled jumps on the term structure cannot be separately identified from futures contracts and the scheduled FOMC meetings are sufficiently frequent to allow for the scheduled jumps to capture the term structure of SOFR futures rates.

Unsurprisingly, and as seen by the RMSEs, correctly modeling the discontinuities becomes increasingly important the shorter the tenor of the considered rate due to the averaging of the overnight fixings present in longer tenors. Next, we therefore investigate the ability of each model to fit subsets of the daily observed rates. We start by removing the overnight rates from the sample, leaving only the one-month and three-month futures rates in the estimation. Subsequently, we also remove the one-month futures contracts, such that only the three-month futures contracts remain. After removing the overnight rates from the sample, we observe close to identical fits in the three-month futures rates between the models. However, the jump specification still significantly outperforms the continuous model in fitting the one-month futures rate, particularly during the end of the sample. This becomes increasingly important if one estimates a model based on Federal Funds futures, since these contracts only exist with a one-month reference period. It suggests that even when the overnight fixings are not of concern, accurately modeling the stochastic discontinuities of the underlying overnight rate can significantly improve the fit of a model. Lastly, when our sample consists of only three-month SOFR futures rates we see a notable decrease in the RMSEs of the continuous specification, which then outperforms our jump specification. The tenor structure of this subsample is effectively similar to a sample of the Eurodollar futures that three-month SOFR futures are replacing, except for the nearest three-month SOFR futures contract, which due to the accumulation

during the contract period differs from the nearest Eurodollar futures contract.[13] Therefore, when the fixings are based on sufficiently long tenors, as is the case with contracts referencing LIBOR or three-month SOFR futures contracts, a continuous specification seems able to fit the term structure even if the underlying overnight rates are highly discontinuous.

4.6.4 Model implied term rates and CME term SOFR

As a part of the transition to SOFR, the ARRC expressed the need for a forward-looking term SOFR rate once sufficiently liquid derivative markets referencing SOFR to support such a rate had developed.[14,15] In May 2021, the ARRC chose CME as the administrator of term SOFR.[16] CME Term SOFR for tenors of 1, 3, and 6 month was accepted by the ARRC on July 29, 2021 and later on May 21, 2022 the 12 month tenor was also endorsed.[17] With over three trillion USD in loans as of February 2023, a model should be able to produce forward-looking SOFR term rates consistent with those published by the CME.[18] Using the historical record of CME Term SOFR rates since the approval by the ARRC as an out of sample benchmark, we evaluate the ability of each model to produce SOFR term rates consistent with those published by the CME. In order to accurately compare the model-implied term rates we follow the conventions used by CME when calculating Term SOFR. CME Term SOFR Rates are published on all overnight SOFR publishing dates at 5:00 am and based on CME SOFR futures rates from the previous trading day. The tenor starts on the second business day (included) after the publication day calculated using the Following business day convention. Next, the term is calculated for the relevant tenor using the Modified Following convention with an Actual/360 day count convention. The rates are based on the five and twelve nearest one- and three-month futures, respectively.[19] Thus, denoting by t the calculation date, S the start date

[13]This is not to say that the underlying rates are the same: The accumulated overnight rate underlying three-month SOFR futures is quite distinct from the LIBOR term rate underlying Eurodollar futures. For a discussion of this issue, see Backwell et al. (2019).

[14]See https://www.sec.gov/spotlight/fixed-income-advisory-committee/arrc-faqs-041519.pdf

[15]Despite the name, Term SOFR does not reflect actual term lending. Rather, it is derived from the futures market. We refer to Backwell et al. (2019), Skov and Skovmand (2022), and Filipović and Trolle (2013) for a discussion on term rates.

[16]See https://www.newyorkfed.org/medialibrary/Microsites/arrc/files/2021/20210521-ARRC-Press-Release-Term-Rate-RFP.pdf

[17]See https://www.newyorkfed.org/medialibrary/Microsites/arrc/files/2021/ARRC_Press_Release_Term_SOFR.pdf and https://www.newyorkfed.org/medialibrary/Microsites/arrc/files/2022/ARRC_CME_12-Month_SOFR_Term_Rate.pdf]

[18]Updated numbers on the use of Term SOFR is available at https://www.cmegroup.com/market-data/cme-group-benchmark-administration/term-sofr.html

[19]Full documentation on the calculation of CME Term SOFR is available at https://www.cmegroup.com/market-data/files/cme-term-sofr-reference-rates-benchmark-methodology.pdf

Model	Tenor			
	One-Month	Three-Month	Six-Month	Twelve-Month
Jump	3.1	2.0	2.0	2.7
Continuous	9.3	3.7	2.2	2.4

Table 4.4: *Out of sample CME Term SOFR RMSEs.*

and T the end date of the tenor, we calculate the model-implied term SOFR as

$$R^s_{Term}(t;S,T) = \frac{360}{T-S}\left(\frac{p^s(t,S)}{p^s(t,T)} - 1\right). \tag{4.6.1}$$

where $p^s(t,T)$ is the SOFR zero coupon bond calculated as $\psi(0,t,T)$ in Appendix 4.A. There are, however, still multiple reasons for the term rates to differ. First, the CME methodology computes futures rates from forward rates and thus ignores the futures convexity correction (see Skov and Skovmand (2021)). Second, CME term SOFR rates are based on discrete compounding whereas we use a continuously compounded approximation. Finally, CME Term SOFR uses aggregated futures prices between 7:00am and 2:00pm CT, while we estimate the models using end-of-day prices. Table 4.4 reports the RMSEs between the model-implied and observed CME Term SOFR rates. As with the futures rates, we note a substatial improvement (relative to the continuous model) in the fit of the one-month term rate. Already at the three-month tenor the improvement decreases notably, while the errors become similar in size at the six- and twelve-month tenors. The agreement between the jump model and the CME term rates is no surprise, as the calculation of CME Term SOFR is based on a step-function for the SOFR forward rates, which are allowed to jump on FOMC meeting dates as in Heitfield and Park (2019). The results further emphasize the need to include scheduled jumps to accurately capture the dynamics of the short end of the SOFR curve if CME Term SOFR continues to gain popularity as a forward-looking term rate benchmark.

4.6.5 Overnight policy rate forecasts

In this section, we investigate the ability of each model specification to forecast future values of the IORB. In order to obtain real time estimates of the model-forecasted IORB fixings, we perform rolling re-estimations starting from January 3, 2022 to the end of our data period in February 2023. Each estimation is therefore based on at least three and a half years of daily data from June 2018 to January 2022.[20] In the

[20]While the focus of our study is on SOFR and SOFR futures, similar models estimated on EFFR and Federal Funds futures data would allow for much longer data samples. Also, the EFFR-IORB spread is less volatile compared to the SOFR-IORB spread, which might further improve on the accuracy of the forecasted IORB.

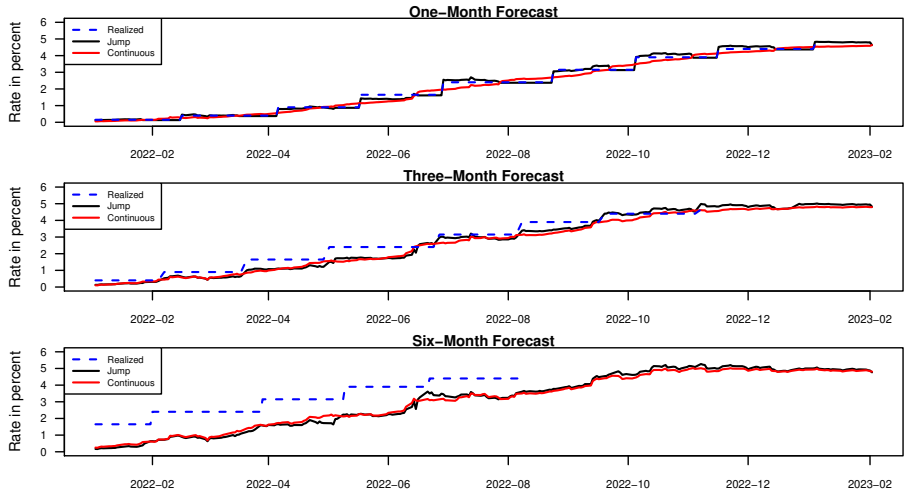

Figure 4.6: *The figure compares the one-, three-, and six-month IORB forecasts for both the continuous and jump specification. The plot displays the time t forecasts based on rolling re-estimations as well as the future realized value of the IORB.*

jump specification, we calculate the forecasted IORB value under the P-measure as

$$\begin{aligned}\mathbb{E}_t^P[r_u] &= r_t + \sum_{j=\eta(t)}^{\eta(u)-1} \mathbb{E}_t^P\left[J_{\tau_j}^D\right] + \mathbb{E}_t^P\left[\sum_{i=N_t^P}^{N_u^P-1} Z_i\right] \\ &= r_t + \sum_{j=\eta(t)}^{\eta(u)-1} \left(\gamma^P + \Gamma^{P'}\mathbb{E}_t^P\left[X_{\tau_j-}^j\right]\right) + (u-t)\nu^P\mu^P \qquad (4.6.2)\end{aligned}$$

with each $\mathbb{E}_t^P\left[X_{\tau_j-}^j\right]$ computed as in Eq. (4.A.15), but under the P-dynamics.

In Figure 4.6, we plot the IORB forecasts against the actual subsequent realization of the policy rate. Focusing on the one-month IORB forecast, we note that this results in at most one FOMC meeting during the forecasting period. The forecasted IORB value for IORB in the jump specification is therefore still highly discontinuous with the forecasted IORB values jumping whenever a new FOMC meeting enters the forecasting period. When we observe an FOMC meeting during the forecasting period the forecasted IORB changes as the market expectations about the future FOMC decision changes, however, when there is no FOMC meeting during the forecasting period, the only change in the forecasted IORB is due to the very slight changes in the filtered r_t value because of the rolling re-estimations. Also, with no FOMC meetings during the forecasting period the only difference between the current and forecasted value of IORB is due to the impact of the constant intensity, unscheduled jumps. These features of the jump specification result in very different short-term policy forecasts compared to the one-month IORB forecasts in the continuous model, which continuously change during the rolling re-estimations. Next, for the three-month

Model	One-Month		Three-Month		Six-Month	
	Mean	RMSE	Mean	RMSE	Mean	RMSE
Jump	1.2	11.4	-28.0	40.0	-136.0	138.9
Continuous	-6.6	21.4	-35.5	45.1	-130.0	132.5
Random Walk	-34.0	47.4	-114.3	122.6	-242.3	247.1

Table 4.5: *IORB Forecast errors summarized as mean and and root-mean-squared errors. All values are in basis points.*

and six-month forecasts we observe that as the forecasting period increases and multiple scheduled FOMC meetings become present during the forecasting period the forecasted policy rate of the jump specification becomes increasingly diffusive, resembling the continuous specification.

Table 4.5 lists summary statistics for the IORB forecast errors for both model specifications. As a reference we also include the static forecasts implied by a random walk model. Comparing the one-month forecast errors, we note that the jump specification greatly outperforms the continuous specification. At a three-month term, however, the relative increase in forecast performance is less evident, while at a six-month term the performance of both models significantly deteriorates, with the continuous version performing slightly better. The sizeable negative three- and six-month mean forecast errors reported are of course a result of the large and frequent policy rate hikes by the Fed during 2022, as also indicated by the even greater negative mean forecasting errors of the random walk model. The results clearly reflect the difficulty in obtaining accurate policy rate estimates beyond the very short term. However, in the short term the forecasting performance can be significantly improved by accurately incorporating the scheduled jumps following FOMC meetings.

4.6.6 Including SOFR futures options data

In this section, we extend the data sample by including data on three-month SOFR futures options. As noted in Section 4.5, these contracts have only recently started to trade and our study is thus preliminary. Furthermore, neither of the considered models include stochastic volatility and accurately capturing the option dynamics cannot be expected.[21] Instead, the main purpose is to study the impact of scheduled jumps on implied volatilities.

Table 4.6 reports the RMSEs for the implied volatilities. These indicate a substantially better fit by the continuous model specification. Due to the expiration of the option before the three-month accumulation period, the three-month SOFR

[21] An immediate way to include stochastic volatility in the jump model would be to allow for state dependence in the the variance of the normally distributed scheduled jumps. However, we note that a part of the volatility also arises from the volatility of the processes determining the mean of the jump size distribution.

Model	Three-Month Option			
	1st	2nd	3rd	4th
Jump	60.5	47.2	33.7	20.1
Continuous	16.7	28.8	30.2	24.3

Table 4.6: *Black implied volatility fitting errors summarized as root-mean-squared errors. All values are in basis points.*

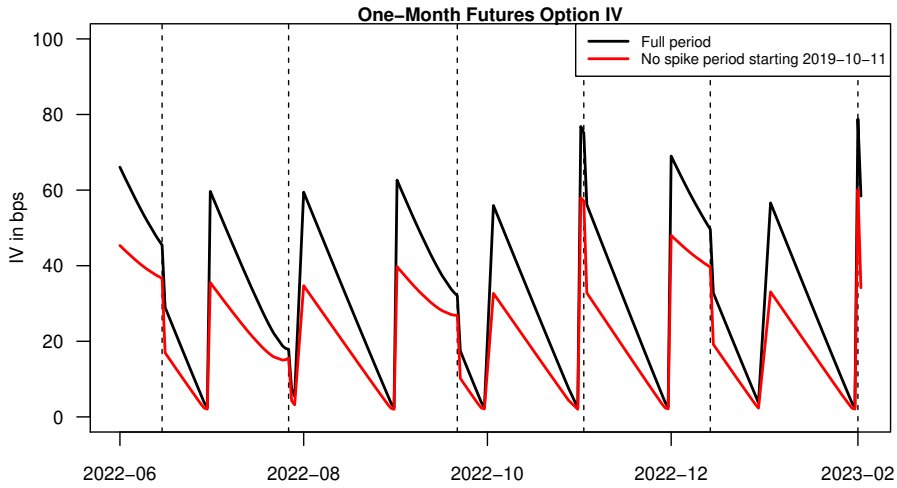

Figure 4.7: *Nearest one-month at-the-money futures call option Black implied volatily from the jump model considering both a full sample estimation and a reducued sample period starting after spikes in overnight SOFR disappeared. The vertical lines mark scheduled FOMC dates.*

futures option greatly resembles the Eurodollar futures option it is supposed to replace. Thus, it is an option on a forward-looking three-month rate, the dynamics of which the continuous specification is able to capture. The results are consistent with those in Section 4.6.3, showing that the continuous specification performs well when a sample of only three-month futures contracts are considered. Furthermore, the additional Brownian motion allows for a more flexible volatility specification in the continuous model. However, based on our previous analysis, one may not expect the continuous model to be able to accurately model the one-month SOFR futures option. This is particularly true for the nearest contract since, as noted in Section 4.4, the one-month option expire at the end of the accumulation period. The constant volatility continuous model results in a linear decay in implied volatility during the accumulation period. As shown in Figure 4.7, the jump model, even without stochastic volatility, produces kinks in implied volatility around FOMC dates. Also, implied volatilities are dependent on the existence and timing of an FOMC meeting during the futures reference month. The validity of this behaviour can of course only be verified if these contracts start to trade in the market. The graph based on the

estimation on the full data set suggests that the majority of the volatility is not due to the scheduled jumps, but rather the unscheduled jumps and the SOFR-IORB spread process. However, this result is largely due to the spikes observed at the beginning of the sample, which in the estimation result in substantial volatility for the spread process. Consequently, the contribution of scheduled jumps (i.e., FOMC meeting dates) to the time evolution of implied volatility of the one-month options is much more evident when the initial part of the sample is excluded from the model estimation. Arguably, this is a better reflection of market reality going forward, as policy action by the Fed seems to have prevented the recurrence of SOFR spikes in recent years.

4.7 Conclusion

The ongoing benchmark transition from LIBOR to Risk-Free Rates has made the overnight rate the main building block in fixed income products. Studying the changes in SOFR in relation to US policy rates, we argue that the primary policy rate affecting changes in the level of SOFR is the IORB. Inspired by this, we develop a dynamic term structure model, which is able to jointly model IORB, SOFR and SOFR futures rates. Comparing our model to a standard time-homogeneous continuous affine term structure model, we find that accounting for scheduled jumps, identified by the FOMC meeting calendar, is necessary to accurately capture shorter-term interest rate dynamics. However, modeling the scheduled jumps becomes less important as the term of the rate is increased. In particular, when only three-month futures rates are considered, the diffusive dynamics of the continuous model are able to describe the time-variation in the cross-section of futures rates.

As the SOFR futures options market matures, an immediate addition for future research would be to extend our framework with stochastic volatility. This would be of particular interest if options on one-month SOFR futures start to trade more actively, as their shorter tenor and expiration date at the end of the underlying futures contract month lead a model incorporating scheduled jumps to predict a behaviour that is quite distinct from the behaviour predicted by a more traditional interest rate term structure model.

4.A Affine Pricing of Futures with Scheduled Jumps

Pricing in the standard continuous affine setup is well-known and we refer to Bikbov and Chernov (2005) or Feldhütter, Trolle, and Schneider (2008) for pricing of Eurodollar futures and futures options and Skov and Skovmand (2022) for a treatment using SOFR futures. When computing the time t futures rates in the jump setup we

will consider the auxiliary unscheduled jump process $\hat{J}_s^P$ for $s \geq t$ defined by

$$d\hat{J}_s^P = dJ_s^P, \quad \hat{J}_t^P = 0. \tag{4.A.1}$$

4.A.1 Overnight rates

We calculate the model implied overnight IORB as the simple rate

$$R(t, t+d) = \frac{1}{d}\left(\frac{1}{p(t, t+d)} - 1\right) \tag{4.A.2}$$

with $d = \frac{1}{360}$ the day count fraction and $p(t, t+d) = \mathbb{E}_t^Q\left[e^{-\int_t^{t+d} r(s)ds}\right]$, which we calculate as

$$p(t, t+d) = e^{-dr_t}\mathbb{E}_t^Q\left[e^{-\int_t^{t+d}\sum_{j=\eta(t)}^{\eta(u-)-1} J_{\tau_j}^D + \hat{J}_u^P du}\right]. \tag{4.A.3}$$

When computing the overnight rate, we assume that at the time of observation any scheduled jumps either have already occurred and thus are included in r_t or are scheduled at least one day ahead and therefore do not impact the overnight rate.[22] Focusing on the unscheduled jumps and recalling that $\hat{J}_t^P = 0$ we calculate $\mathbb{E}_t^Q\left[e^{-\int_t^{t+d}\hat{J}_u^P du}\right] = e^{\alpha^J(d)}$ where $\alpha^J(\tau)$ solves the ODE

$$\frac{\partial \alpha^J(\tau)}{\partial \tau} = \nu^P\left(e^{-\mu^P\tau + \frac{(\sigma^P\tau)^2}{2}} - 1\right), \quad \alpha^J(0) = 0. \tag{4.A.4}$$

Similarly, the SOFR fixings are defined as

$$R^s(t, t+d) = \frac{1}{d}\left(\frac{1}{p^s(t, t+d)} - 1\right) \tag{4.A.5}$$

where $p^s(t, t+d)$ includes the SOFR-IORB spread process. From the independence of the spread process and unscheduled jumps we have (again assuming that the scheduled jumps do not affect the overnight tenor)

$$p^s(t, t+d) = \mathbb{E}_t^Q\left[e^{-\int_t^{t+d} r_u + s_u du}\right] = e^{-dr_t}\mathbb{E}_t^Q\left[e^{-\int_t^{t+d}\hat{J}_u^P du}\right]\mathbb{E}_t^Q\left[e^{-\int_t^{t+d} s_u du}\right]. \tag{4.A.6}$$

It only remains to compute the contribution from the spread process, which is given by $\mathbb{E}_t^Q\left[e^{-\int_t^{t+d} s_u du}\right] = e^{\alpha^s(d) + \beta(d)s_t}$ where $\alpha^s(\tau)$ and $\beta^s(\tau)$ are as in the Vasicek model

$$\beta^s(\tau) = \frac{e^{-\kappa^s\tau} - 1}{\kappa^s} \tag{4.A.7}$$

$$\alpha^s(\tau) = -\theta^s\tau + \frac{(\sigma^s)^2\tau}{2(\kappa^s)^2} + \left(\frac{\theta^s}{\kappa^s} - \frac{(\sigma^s)^2}{(\kappa^s)^3}\right)(1 - e^{-\kappa^s\tau}) + \frac{(\sigma^s)^2(1 - e^{-2\kappa^s\tau})}{4(\kappa^s)^3}. \tag{4.A.8}$$

such that

$$p^s(t, t+d) = e^{-dr_t}e^{\alpha^J(d) + \alpha^s(d) + \beta(d)s_t} \tag{4.A.9}$$

[22] In reality this is always the case, since announced changes to the policy rate are effective at a one-day lag.

4.A.2 Three-month futures

We consider the continuously compounded approximation of the discrete compounding in Eq. (4.4.3)

$$f^{3m}(t;S,T) = \mathbb{E}_t^Q\left[\frac{1}{T-S}\left(e^{\int_S^T r_u^s du} - 1\right)\right]. \tag{4.A.10}$$

By the independence of the scheduled jumps we can write

$$\mathbb{E}_t^Q\left[e^{\int_S^T r_u^s du}\right] = e^{(T-S)r_t}\mathbb{E}_t^Q\left[e^{\int_S^T \sum_{j=\eta(t)}^{\eta(u-)-1} J_{\tau_j}^D du}\right]\mathbb{E}_t^Q\left[e^{\int_S^T \hat{\jmath}_u^P + s_u du}\right] \tag{4.A.11}$$

For the scheduled jumps we note that the integral can be rewritten as

$$\int_S^T \sum_{j=\eta(t)}^{\eta(u-)-1} J_{\tau_j}^D du = \sum_{j=\eta(t)}^{\eta(T-)-1} \min(T-S, T-\tau_j) J_{\tau_j}^D. \tag{4.A.12}$$

Repeated use of iterated expectations then yields

$$\begin{aligned}
&\mathbb{E}_t^Q\left[e^{\sum_{j=\eta(t)}^{\eta(T-)-1}\min(T-S,T-\tau_j)J_{\tau_j}^D}\right]\\
&= \mathbb{E}_t^Q\left[e^{\sum_{j=\eta(t)}^{\eta(T-)-2}\min(T-S,T-\tau_j)J_{\tau_j}^D}\mathbb{E}^Q_{\tau_{\eta(T-)-1}-}\left[e^{\min(T-S,T-\tau_{\eta(T-)-1})J^D_{\tau_{\eta(T-)-1}}}\right]\right]\\
&= \mathbb{E}_t^Q\left[e^{\sum_{j=\eta(t)}^{\eta(T-)-2}\min(T-S,T-\tau_j)J_{\tau_j}^D}e^{\min(T-S,T-\tau_{\eta(T-)-1})(\gamma+\Gamma' X^j_{\tau_{\eta(T-)-1}-})+\frac{\min(T-S,T-\tau_{\eta(T-)-1})^2}{2}\omega^2}\right]\\
&= \mathbb{E}_t^Q\Big[e^{\sum_{j=\eta(t)}^{\eta(T-)-3}\min(T-S,T-\tau_j)J_{\tau_j}^D}\\
&\times \mathbb{E}^Q_{\tau_{\eta(T-)-2}-}\left[e^{\min(T-S,T-\tau_{n-1})J^D_{\tau_{\eta(T-)-2}}}e^{\min(T-S,T-\tau_{\eta(T-)-1})(\gamma+\Gamma' X^j_{\tau_{\eta(T-)-1}-})+\frac{\min(T-S,T-\tau_{\eta(T-)-1})^2}{2}\omega^2}\right]\Big]\\
&= \mathbb{E}_t^Q\Big[e^{\sum_{j=\eta(t)}^{\eta(T-)-3}\min(T-S,T-\tau_j)J_{\tau_j}^D}e^{\min(T-S,T-\tau_{\eta(T-)-2})(\gamma+\Gamma' X^j_{\tau_{\eta(T-)-2}-})+\frac{\min(T-S,T-\tau_{\eta(T-)-2})^2}{2}\omega^2}\\
&\times \mathbb{E}^Q_{\tau_{\eta(T-)-2}-}\left[e^{\min(T-S,T-\tau_{\eta(T-)-1})(\gamma+\Gamma' X^j_{\tau_n-})+\frac{\min(T-S,T-\tau_{\eta(T-)-1})^2}{2}\omega^2}\right]\Big]\\
&= \mathbb{E}_t^Q\Big[e^{\min(T-S,T-\tau_{\eta(t)})(\gamma+\Gamma' X^j_{\tau_{\eta(t)}-})+\frac{\min(T-S,T-\tau_{\eta(t)})^2}{2}\omega^2}\\
&\times \mathbb{E}^Q_{\tau_{\eta(t)}-}\Big[e^{\min(T-S,T-\tau_{\eta(t)+1})(\gamma+\Gamma' X^j_{\tau_{\eta(t)+1}-})+\frac{\min(T-S,T-\tau_{\eta(t)+1})^2}{2}\omega^2}\cdots\\
&\times \mathbb{E}^Q_{\tau_{\eta(T-)-2}-}\left[e^{\min(T-S,T-\tau_{\eta(T-)-1})(\gamma+\Gamma' X^j_{\tau_{\eta(T-)-1}-})+\frac{\min(T-S,T-\tau_{\eta(T-)-1})^2}{2}\omega^2}\right]\cdots\Big]\Big]\\
&= e^{\alpha^j(t;S,T)+\beta^j(t;S,T)' X_t^j}
\end{aligned} \tag{4.A.13}$$

Since X_t^j is Gaussian we have an analytical solution for the Laplace transform and can simply iterate through the expectations using the actual FOMC dates to get $\alpha^j(t;S,T)$ and $\beta^j(t;S,T)$ with no need to assume an approximate equidistant grid as in Piazzesi (2005). The Gaussian conditional Laplace transform is

$$\mathbb{E}_t^Q\left[e^{a+b' X_u^j}\right] = e^a e^{b'\mathbb{E}_t^Q[X_u^j]+\frac{1}{2}b'\mathbb{V}_t^Q[X_u^j]b} \tag{4.A.14}$$

with mean

$$\mathbb{E}_t^Q\left[X_u^j\right] = \left(I - e^{-K^j(u-t)}\right)\theta^j + e^{-K^j(u-t)}X_t^j, \tag{4.A.15}$$

and variance

$$\mathbb{V}_t^Q\left[X_u^j\right] = \int_t^u e^{-K^j(\nu-t)}\Sigma^j\Sigma^{j'}\left(e^{-K^j(\nu-t)}\right)' d\nu. \tag{4.A.16}$$

We calculate the variance using the analytical solution in Fisher and Gilles (1996). The unscheduled jumps and stochastic SOFR spread contribution can be calculated using the tower property and standard methods on affine jump diffusions from Duffie, Pan, and Singleton (2000) as

$$\mathbb{E}_t^Q\left[e^{\int_S^T \hat{J}_u^P + s_u du}\right] = \mathbb{E}_t^Q\left[\mathbb{E}_S^Q\left[e^{\int_S^T \hat{J}_u^P + s_u du}\right]\right] = \mathbb{E}_t^Q\left[e^{\alpha^{AJD}(T-S)+\beta^{AJD}(T-S)s(S)+(T-S)\hat{J}^P(S)}\right]$$

where $\beta^{AJD}(\tau)$ and $\alpha^{AJD}(\tau)$ solve the ODEs

$$\frac{\partial\beta^{AJD}(\tau)}{\partial\tau} = -\kappa^s\beta^{AJD}(\tau) + 1, \quad \beta^{AJD}(0) = 0, \tag{4.A.17}$$

$$\frac{\partial\alpha^{AJD}(\tau)}{\partial\tau} = \kappa^s\theta^s\beta^{AJD}(\tau) + \frac{1}{2}\left(\sigma^s\beta^{AJD}(\tau)\right)^2 + \nu^P\left(e^{\mu^P\tau+\frac{(\sigma^P\tau)^2}{2}} - 1\right), \quad \alpha^{AJD}(0) = 0. \tag{4.A.18}$$

Next, we calculate

$$\mathbb{E}_t^Q\left[e^{\alpha^{AJD}(T-S)+\beta^{AJD}(T-S)s(S)+(T-S)\hat{J}^P(S)}\right] = e^{\tilde{\alpha}^{AJD}(S-t)+\tilde{\beta}^{AJD}(S-t)s_t} \tag{4.A.19}$$

where $\tilde{\beta}^{AJD}(\tau)$ and $\tilde{\alpha}^{AJD}(\tau)$ solve the ODEs

$$\frac{\partial\tilde{\beta}^{AJD}(\tau)}{\partial\tau} = -\kappa^s\tilde{\beta}^{AJD}(\tau), \tag{4.A.20}$$

$$\frac{\partial\tilde{\alpha}^{AJD}(\tau)}{\partial\tau} = \kappa^s\theta^s\tilde{\beta}^{AJD}(\tau) + \frac{1}{2}\left(\sigma^s\tilde{\beta}^{AJD}(\tau)\right)^2 + \nu^P\left(e^{\mu^P(T-S)+\frac{(\sigma^P(T-S))^2}{2}} - 1\right) \tag{4.A.21}$$

with initial conditions $\tilde{\beta}^{AJD}(0) = \beta^{AJD}(T-S)$ and $\tilde{\alpha}^{AJD}(0) = \alpha^{AJD}(T-S)$.

4.A.3 One-month futures

Again, we consider the common continuous approximation of the sum in Eq. (4.4.2)

$$f^{1m}(t;S,T) = \frac{1}{T-S}\mathbb{E}_t^Q\left[\int_S^T r_u^s du\right]. \tag{4.A.22}$$

We treat the scheduled jumps, unscheduled jumps, and stochastic spread separately

$$\begin{aligned}\mathbb{E}_t^Q\left[\int_S^T r_u^s du\right] = (T-S)r_t &+ \mathbb{E}_t^Q\left[\int_S^T \sum_{j=\eta(t)}^{\eta(u-)-1} J_{\tau_j}^D du\right] \\ &+ \mathbb{E}_t^Q\left[\int_S^T \hat{J}_u^P du\right] + \mathbb{E}_t^Q\left[\int_S^T s_u du\right].\end{aligned}$$

Applying Eq. (4.A.12) and using iterated expectations we get

$$\begin{aligned}
\mathbb{E}_t^Q\left[\int_S^T \sum_{j=\eta(t)}^{\eta(u-)-1} J_{\tau_j}^D du\right] &= \mathbb{E}_t^Q\left[\sum_{j=\eta(t)}^{\eta(T-)-1} \min(T-S, T-\tau_j) J_{\tau_j}^D\right] \\
&= \mathbb{E}_t^Q\left[\sum_{j=\eta(t)}^{\eta(T-)-1} \min(T-S, T-\tau_j) \mathbb{E}_{\tau_j-}^Q\left[J_{\tau_j}^D\right]\right] \\
&= \mathbb{E}_t^Q\left[\sum_{j=\eta(t)}^{\eta(T-)-1} \min(T-S, T-\tau_j)\left(\gamma + (\Gamma)' X^j(\tau_{j-})\right)\right] \\
&= \sum_{j=\eta(t)}^{\eta(T-)-1} \min(T-S, T-\tau_j)(\gamma + (\Gamma)' \mathbb{E}_t^Q\left[X^j(\tau_{j-})\right]).
\end{aligned} \tag{4.A.23}$$

Thus we only need to calculate mean of the underlying state variables given by (4.A.15). Since the unscheduled jumps are modeled as a compound Poisson process we get

$$\int_S^T \mathbb{E}_t^Q\left[\hat{J}_u^P\right] du = \frac{1}{2}(T-S)^2 \nu^P \mu^P. \tag{4.A.24}$$

And lastly the continuous spread is calculated as

$$\int_S^T \mathbb{E}_t^Q\left[s_u\right] du = (T-S)\theta^s + \frac{e^{-\kappa^s(S-t)} - e^{-\kappa^s(T-t)}}{\kappa^s}(s_t - \theta^s). \tag{4.A.25}$$

4.A.4 Three-month SOFR futures options

Having adjusted our options data for the American feature, we consider the time t value of a European call option on a three-month SOFR futures with reference quarter from time S to T. The option expires at time u with $u < S$. Specifically, for three-month quarterly SOFR futures options traded on the CME the option expires on the last Friday before the Wednesday when the reference quarter of the contract begins. Let $k = 100 - K$ then

$$\begin{aligned}
\pi^{3m}(t;u,S,T) &= E_t^Q\left[e^{-\int_t^u r_z^s dz}\left(F^{3m}(u;S,T) - K\right)^+\right] \\
&\approx E_t^Q\left[e^{-\int_t^u r_z^s dz}\left(k - 100 f^{3m}(u;S,T)\right)^+\right] \\
&= E_t^Q\left[e^{-\int_t^u r_z^s dz}\left(k - 100\left(\frac{1}{T-S}\mathbb{E}_u^Q\left[e^{\int_S^T r_z^s dz}\right] - \frac{1}{T-S}\right)\right)^+\right].
\end{aligned} \tag{4.A.26}$$

Where the approximation is from the continuously compounded approximation of the futures rate. Let $\alpha^{3m}(u;S,T) = \alpha^j(u;S,T) + \tilde{\alpha}^{AJD}(S-u)$ and $\beta^{3m}(u;S,T) =$

$(T-S, \beta^j(u;S,T), \tilde{\beta}^{AJD}(S-u))'$ then we can write (4.A.26) as

$$\begin{aligned}
&\frac{100}{T-S} e^{\alpha^{3m}(u;S,T)} E_t^Q \left[e^{-\int_t^u r_z^s dz} \left(\hat{k} - e^{\beta^{3m}(u;S,T)' X_u} \right) 1_{\left(\beta^{3m}(u;S,T)' X_u < \log(\hat{k})\right)} \right] \\
&= \frac{100}{T-S} e^{\alpha^{3m}(u;S,T)} \left(\hat{k} G_{0,\beta^{3m}(u;S,T)}(\log(\hat{k}) - G_{\beta^{3m}(u;S,T),\beta^{3m}(u;S,T)}(\log(\hat{k}) \right)
\end{aligned} \tag{4.A.27}$$

with $\hat{k} = e^{-\alpha^{3m}(u;S,T)} \left(\frac{k(T-S)}{100} + 1 \right)$ and

$$G_{a,b}(y) = \mathbb{E}_t^Q \left[e^{-\int_t^u r_z^s dz} e^{a' X_u} 1_{(b' X_u < y)} \right]. \tag{4.A.28}$$

We calculate $G_{a,b}(y)$ using its Fourier transform

$$\begin{aligned}
\hat{G}_{a,b}(y) &= \int_{\mathbb{R}} e^{iwy} dG_{a,b}(y) \\
&= \mathbb{E}_t^Q \left[e^{-\int_t^u r_z^s dz} e^{(a+iwb)' X_u} \right] = \psi(a+iwb, t, u).
\end{aligned} \tag{4.A.29}$$

Let $a = (a^r, a^j, a^{AJD})'$ and $b = (b^r, b^j, b^{AJD})'$ be the coefficients referring to the short-rate, scheduled jump factors and spread factor, respectively. We then calculate the transform as

$$\begin{aligned}
\psi(a+iwb,t,u) &= \mathbb{E}_t^Q \left[e^{-\int_t^u r_z^s dz} e^{(a+iwb)' X_u} \right] \\
&= \mathbb{E}_t^Q \Big[e^{-(u-t) r_t - \int_t^u \sum_{j=\eta(t)}^{\eta(z-)-1} J_{\tau_j}^D dz - \int_t^u \hat{J}_z^P + s_z dz} \\
&\quad \times e^{(a^r + iwb^r) r_u + (a^j + iwb^j)' X_u^j + (a^{AJD} + iwb^{AJD}) s_u} \Big] \\
&= e^{(a^r + iwb^r - (u-t)) r_t} \mathbb{E}_t^Q \left[e^{\sum_{j=\eta(t)}^{\eta(u-)-1} (a^r + iwb^r - (u-\tau_j)) J_{\tau_j}^D} e^{(a^j + iwb^j)' X_u^j} \right] \qquad (4.A.30) \\
&\quad \times \mathbb{E}_t^Q \left[e^{-\int_t^u s_z + \hat{J}_z^P dz} e^{(a^{AJD} + iwb^{AJD}) s_u + (a^r + iwb^r) \hat{J}_u^P} \right]. \qquad (4.A.31)
\end{aligned}$$

The scheduled jumps in (4.A.30) can be calculated by repeated use of iterated expectations using a similar approach to (4.A.13)

$$\begin{aligned}
&\mathbb{E}_t^Q \left[e^{\sum_{j=\eta(t)}^{\eta(u-)-1} (a^r + iwb^r - (u-\tau_j)) J_{\tau_j}^D} e^{(a^j + iwb^j)' X_u^j} \right] \\
&= \mathbb{E}_t^Q \Big[e^{(a^r + iwb^r - (u - \tau_{\eta(t)}))(\gamma + \Gamma' X^j_{\tau_{\eta(t)}-}) + \frac{(a^r + iwb^r - (u-\tau_{\eta(t)}))^2}{2} \omega^2} \\
&\times \mathbb{E}_{\tau_{\eta(t)}-}^Q \Big[e^{(a^r + iwb^r - (u - \tau_{\eta(t)+1}))(\gamma + \Gamma' X^j_{\tau_{\eta(t)+1}-}) + \frac{(a^r + iwb^r - (u-\tau_{\eta(t)+1}))^2}{2} \omega^2} \dots \\
&\times \mathbb{E}_{\tau_{\eta(T-)-2}-}^Q \Big[e^{(a^r + iwb^r - (u - \tau_{\eta(T-)-1}))(\gamma + \Gamma' X^j_{\tau_{\eta(T-)-1}-}) + \frac{(a^r + iwb^r - (u-\tau_{\eta(T-)-1}))^2}{2} \omega^2} \\
&\times \mathbb{E}_{\tau_{\eta(T-)-1}-}^Q \left[e^{(a^j + iwb^j)' X_u^j} \right] \Big] \dots \Big] \Big]
\end{aligned} \tag{4.A.32}$$

The term in Eq. (4.A.31) is a standard time-homogeneous affine jump diffusion, which we calculate as

$$\mathbb{E}_t^Q\left[e^{-\int_t^u s_z+\hat{J}_z^P dz}e^{(a^s+iwb^s)s_u+(a^r+iwb^r)\hat{J}_u^P}\right]=e^{\alpha^\psi(u-t)+\beta^\psi(u-t)s_t} \tag{4.A.33}$$

where $\alpha^\psi(\tau))$ and $\beta^\psi(\tau)$ solve the ODEs

$$\frac{\partial\beta^\psi(\tau)}{\partial\tau}=-\kappa^s\beta^\psi(\tau)-1, \tag{4.A.34}$$

$$\frac{\partial\alpha^\psi(\tau)}{\partial\tau}=\kappa^s\theta^s\beta^\psi(\tau)+\frac{1}{2}\left(\sigma^s\beta^\psi(\tau)\right)^2+\nu^P\left(e^{\mu^P(a^r+iwb^r-\tau)+\frac{(\sigma^P(a^r+iwb^r-\tau))^2}{2}}-1\right) \tag{4.A.35}$$

with initial conditions $\alpha^\psi(0)=0$ and $\beta^\psi(0)=a^{AJD}+iwb^{AJD}$. From the the Fourier inversion theorem we then obtain

$$G_{a,b}(y)=\frac{\psi(a,t,u)}{2}-\frac{1}{\pi}\int_0^\infty\frac{\psi(a+iwb,t,u)e^{-iwy}}{w}dw. \tag{4.A.36}$$

During estimation we truncate the integral at 5000 and evaluate it with Gauss–Legendre quadrature using 50 points of the integral. We note that due to the time-inhomogeneity we get different $\alpha^{3m}(u,S,T)$ and $\beta^{3m}(u,S,T)$ for each futures contract that the options are referencing. However, we only consider options referencing the quarterly three-month SOFR futures contracts with fixed accumulations periods. This results in a manageable set of initial conditions for our estimation. Note that this is very different from something like a caplet where the accumulation period would change for each observation date and thus require new initial values for each observation date in the sample.

4.A.5 One-month SOFR futures options

We again disregard the American feature of the one-month futures option and consider the time t value of a European call option on a one-month SOFR futures with reference month from time S to T. The one-month option expires at the end of the accrual period of the underlying futures contract, i.e. at time T

$$\begin{aligned}\pi^{1m}(t;S,T)&=E_t^Q\left[e^{-\int_t^T r_z^s dz}\left(F^{1m}(T;S,T)-K\right)^+\right]\\&\approx E_t^Q\left[e^{-\int_t^T r_z^s dz}\left(100(1-f^{1m}(T;S,T))-K\right)^+\right]\\&=\frac{100}{T-S}E_t^Q\left[e^{-\int_t^T r_z^s dz}\left(k-\int_S^T r_z^s dz\right)^+\right]\\&=\frac{100}{T-S}p^s(t,T)E_t^{Q_T}\left[\left(k-\int_S^T r_z^s dz\right)^+\right].\end{aligned} \tag{4.A.37}$$

Where $k = \frac{T-S}{100}(100 - K)$ and Q_T denotes the T-forward measure defined by the $p^s(t,T)$ bond numeraire. The expectation in (4.A.37) can then be calculated using Theorem 4 in Filipović, Larsson, and Trolle (2017) as

$$E_t^{Q_T}\left[\left(k - \int_S^T r_z^s dz\right)^+\right] = \frac{1}{\pi}\int_0^\infty \text{Re}\left(\frac{\hat{q}(h+iw)}{(h+iw)^2}\right) dw \tag{4.A.38}$$

with $\hat{q}(x) = E_t^{Q_T}\left[e^{x\left(k - \int_S^T r_z^s dz\right)}\right]$ where $x \in \mathbb{C}$ and $h > 0$ such that $\hat{q}(h) < \infty$. in order to compute $\hat{q}(x)$ we first change back to the risk-neutral measure

$$\hat{q}(x) = E_t^{Q_T}\left[e^{x\left(k - \int_S^T r_z^s dz\right)}\right] = \frac{1}{p^s(t,T)} E_t^Q\left[e^{-\int_t^T r_z^s dz} e^{x\left(k - \int_S^T r_z^s dz\right)}\right] \tag{4.A.39}$$

Note that the $p^s(t,T)$ in the denominator cancels out when inserted in (4.A.37). Focusing on the nearest futures option with $t \geq S$ we include the accumulated part of the rate in the modified strike as $\hat{k} = k - \int_S^t r_z^s dz$ such that

$$\begin{aligned}\hat{q}(x) &= \frac{e^{x\hat{k}}}{p^s(t,T)} E_t^Q\left[e^{-(1+x)\int_t^T r_z^s dz}\right] \\ &= e^{-(T-t)(1+x)r_t}\mathbb{E}_t^Q\left[e^{\sum_{j=\eta(t)}^{\eta(T-)-1} -(u-\tau_j)(1+x)J_{\tau_j}^D}\right]\mathbb{E}_t^Q\left[e^{-(1+x)\int_t^T s_z + \hat{J}_z^P dz}\right].\end{aligned} \tag{4.A.40}$$

Again, we calculate the first expectation as in (4.A.13)

$$\begin{aligned}&\mathbb{E}_t^Q\left[e^{\sum_{j=\eta(t)}^{\eta(T-)-1} -(u-\tau_j)(1+x)J_{\tau_j}^D}\right] \\ &= \mathbb{E}_t^Q\Big[e^{-(u-\tau_{\eta(t)})(1+x)(\gamma+\Gamma' X_{\tau_{\eta(t)}-}^j) + \frac{((u-\tau_{\eta(t)})(1+x))^2}{2}\omega^2} \\ &\times \mathbb{E}_{\tau_{\eta(t)}-}^Q\Big[e^{-(u-\tau_{\eta(t)+1})(1+x)(\gamma+\Gamma' X_{\tau_{\eta(t)+1}-}^j) + \frac{((u-\tau_{\eta(t)+1})(1+x))^2}{2}\omega^2}\cdots \\ &\times \mathbb{E}_{\tau_{\eta(T-)-2}-}^Q\Big[e^{-(u-\tau_{\eta(T-)-1})(1+x)(\gamma+\Gamma' X_{\tau_{\eta(T-)-1}-}^j) + \frac{((u-\tau_{\eta(T-)-1})(1+x))^2}{2}\omega^2}\Big]\cdots\Big]\Big]\end{aligned} \tag{4.A.41}$$

The second expectation is given by

$$\mathbb{E}_t^Q\left[e^{-(1+x)\int_t^T s_z + \hat{J}_z^P dz}\right] = e^{\alpha^q(T-t) + \beta^q(T-t)s_t} \tag{4.A.42}$$

where $\alpha^q(\tau))$ and $\beta^q(\tau)$ solve the ODEs

$$\frac{\partial \beta^q(\tau)}{\partial \tau} = -\kappa^s \beta^q(\tau) - (1+x), \tag{4.A.43}$$

$$\frac{\partial \alpha^q(\tau)}{\partial \tau} = \kappa^s\theta^s\beta^q(\tau) + \frac{1}{2}\left(\sigma^s\beta^q(\tau)\right)^2 + \nu^P\left(e^{\mu^P(-(1+x)\tau) + \frac{(\sigma^P(-(1+x)\tau))^2}{2}} - 1\right) \tag{4.A.44}$$

with initial conditions $\alpha^q(0) = \beta^q(0) = 0$. For longer dated options with $t < S$, $\hat{q}(x)$ can be computed using iterated expectations

$$\hat{q}(x) = \frac{e^{xk}}{p^s(t,T)} E_t^Q \left[e^{-\int_t^S r_z^s dz} E_S^Q \left[e^{x\left(-(1+x)\int_S^T r_z^s dz\right)} \right] \right]. \tag{4.A.45}$$

Bibliography

Alfeus, Mesias, Martino Grasselli, and Erik Schlögl (2020). A consistent stochastic model of the term structure of interest rates for multiple tenors. *Journal of Economic Dynamics and Control* **114**(103861).

Allen, Franklin, Elena Carletti, and Douglas Gale (2009). Interbank market liquidity and central bank intervention. *Journal of Monetary Economics* **56**(5), pp. 639–652.

Alternative Reference Rate Committee (2018). *Second report*. URL: `https://www.newyorkfed.org/medialibrary/Microsites/arrc/files/2018/ARRC-Second-report`.

Alternative Reference Rate Committee (2019). *Users Guide to SOFR*. URL: `https://www.newyorkfed.org/medialibrary/Microsites/arrc/files/2019/Users_Guide_to_SOFR.pdf`.

Alternative Reference Rate Committee (2020). *Paced Transition Plan for SOFR*. URL: `https://www.newyorkfed.org/medialibrary/microsites/arrc/files/paced-timeline-plan.pdf`.

Anbil, Sriya, Alyssa G Anderson, and Zeynep Senyuz (2020). What Happened in Money Markets in September 2019? *FEDS Notes* (2020-02), p. 27.

Andersen, Leif BG and Dominique RA Bang (2020). Spike Modeling for Interest Rate Derivatives with an Application to SOFR Caplets. *Available at SSRN 3700446*.

Andrew Bailey (2017). *The future of LIBOR*. URL: `https://www.fca.org.uk/news/speeches/the-future-of-libor`.

Backwell, Alex and Joshua Hayes (2022). Expected and unexpected jumps in the overnight rate: consistent management of the Libor transition. *Journal of Banking & Finance*, p. 106669.

Backwell, Alex, Andrea Macrina, Erik Schlögl, and David Skovmand (2019). Term Rates, Multicurve Term Structures and Overnight Rate Benchmarks: A Roll-Over Risk Approach. *Available at SSRN 3399680*.

Bartholomew, Helen (2021). Pick a rate: pitfalls and prizes in the post-Libor world. *Available at Risk.Net*.

Berndt, Antje, Darrell Duffie, and Yichao Zhu (2020). Across-the-Curve Credit Spread Indices.

Bikbov, Ruslan and Mikhail Chernov (2005). Term structure and volatility: Lessons from the Eurodollar futures and options. *Columbia Business School, Columbia University*.

Black, Fischer (1995). Interest rates as options. *the Journal of Finance* **50**(5), pp. 1371–1376.

Boyarchenko, Nina, Anna M Costello, and Or Shachar (2019). The Long and Short of It: The Post-Crisis Corporate CDS Market. *FRB of New York Staff Report* (879).

Brace, Alan, Karol Gellert, and Erik Schlögl (2022). SOFR Term Structure Dynamics-Discontinuous Short Rates and Stochastic Volatility Forward Rates. *Available at SSRN 4270811*.

Broadie, Mark, Mikhail Chernov, and Michael Johannes (2007). Model specification and risk premia: Evidence from futures options. *The Journal of Finance* **62**(3), pp. 1453–1490.

Brunnermeier, Markus K and Lasse Heje Pedersen (2009). Market liquidity and funding liquidity. *The review of financial studies* **22**(6), pp. 2201–2238.

Christensen, Jens H. E., Jose A Lopez, and Glenn D. Rudebusch (2015). Analytical Formulas for the Second Moment in Affine Models with Stochastic Volatility. URL: `https://cepr.org/sites/default/files/events/1854_Analytical_second_moments_affine_models_Fisher_and_Gilles_1996.pdf`.

Christensen, Jens HE, Francis X Diebold, and Glenn D Rudebusch (2011). The affine arbitrage-free class of Nelson–Siegel term structure models. *Journal of Econometrics* **164**(1), pp. 4–20.

Christensen, Jens HE, Jose A Lopez, and Glenn D Rudebusch (2013). How Efficient is the Kalman Filter at Estimating Affine Term Structure Models? *Manuscript, Federal Reserve Bank of San Francisco*.

Christensen, Jens HE, Jose A Lopez, and Glenn D Rudebusch (2014). Do central bank liquidity facilities affect interbank lending rates? *Journal of Business & Economic Statistics* **32**(1), pp. 136–151.

Christensen, Jens HE and Glenn D Rudebusch (2016). *Modeling yields at the zero lower bound: Are shadow rates the solution?* Emerald Group Publishing Limited.

Collin-Dufresne, Pierre and Bruno Solnik (2001). On the term structure of default premia in the swap and LIBOR markets. *The Journal of Finance* **56**(3), pp. 1095–1115.

Copeland, Adam, Darrell Duffie, and Yilin Yang (2021). *Reserves were not so ample after all*. Tech. rep. National Bureau of Economic Research.

Dai, Qiang and Kenneth J Singleton (2000). Specification analysis of affine term structure models. *The journal of finance* **55**(5), pp. 1943–1978.

Diebold, Francis X and Canlin Li (2006). Forecasting the term structure of government bond yields. *Journal of econometrics* **130**(2), pp. 337–364.

Duan, Jin-Chuan and Jean-Guy Simonato (1999). Estimating and testing exponential-affine term structure models by Kalman filter. *Review of quantitative finance and accounting* **13**(2), pp. 111–135.

Dubecq, Simon, Alain Monfort, Jean-Paul Renne, and Guillaume Roussellet (2016). Credit and liquidity in interbank rates: A quadratic approach. *Journal of Banking & Finance* **68**, pp. 29–46.

Duffee, Gregory R (2002). Term premia and interest rate forecasts in affine models. *The Journal of Finance* **57**(1), pp. 405–443.

Duffie, Darrell and Rui Kan (1996). A yield-factor model of interest rates. *Mathematical finance* **6**(4), pp. 379–406.

Duffie, Darrell, Jun Pan, and Kenneth Singleton (2000). Transform analysis and asset pricing for affine jump-diffusions. *Econometrica* **68**(6), pp. 1343–1376.

Feldhütter, Peter and David Lando (2008). Decomposing swap spreads. *Journal of Financial Economics* **88**(2), pp. 375–405.

Feldhütter, Peter, Anders B Trolle, and Paul Schneider (2008). "Jumps in Interest Rates and Pricing of Jump Risk–Evidence from the Eurodollar Market". In: *EFA 2008 Athens Meetings Paper*.

Filipović, Damir, Martin Larsson, and Anders B Trolle (2017). Linear-rational term structure models. *The Journal of Finance* **72**(2), pp. 655–704.

Filipović, Damir and Anders B Trolle (2013). The term structure of interbank risk. *Journal of Financial Economics* **109**(3), pp. 707–733.

Fisher, Mark and Christian Gilles (1996). Term premia in exponential-affine models of the term structure. *Manuscript, Board of Governors of the Federal Reserve System*.

Flesaker, Bjorn (1993). Testing the Heath-Jarrow-Morton/Ho-Lee model of interest rate contingent claims pricing. *Journal of Financial and Quantitative Analysis*, pp. 483–495.

Fontana, Claudio, Zorana Grbac, Sandrine Gümbel, and Thorsten Schmidt (2020). Term structure modelling for multiple curves with stochastic discontinuities. *Finance and Stochastics*, pp. 1–47.

Fontana, Claudio, Zorana Grbac, and Thorsten Schmidt (2022). Term structure modelling with overnight rates beyond stochastic continuity. *arXiv preprint arXiv:2202.00929*.

Gallitschke, Janek, Stefanie Seifried, and Frank Thomas Seifried (2017). Interbank interest rates: Funding liquidity risk and XIBOR basis spreads. *Journal of Banking & Finance* **78**, pp. 142–152.

Gellert, Karol and Erik Schlögl (2021). Short Rate Dynamics: A Fed Funds and SOFR perspective. *arXiv preprint arXiv:2101.04308*.

Gorton, Gary, Andrew Metrick, and Lei Xie (2021). The flight from maturity. *Journal of Financial Intermediation* **47**, p. 100872.

Grbac, Zorana and Wolfgang J Runggaldier (2015). *Interest rate modeling: post-crisis challenges and approaches*. Springer.

Heitfield, Erik and Yang-Ho Park (2019). Inferring term rates from SOFR futures prices. *Available at SSRN 3352598*.

Henrard, Marc (2018). Overnight futures: Convexity adjustment. *Available at SSRN 3134346*.

Henrard, Marc Pierre (2019). LIBOR fallback and quantitative finance. *Risks* **7**(3), p. 88.

Hu, Grace Xing, Jun Pan, and Jiang Wang (2021). Tri-party repo pricing. *Journal of Financial and Quantitative Analysis* **56**(1), pp. 337–371.

Hunt, Philip and Joanne Kennedy (2004). *Financial derivatives in theory and practice*. John Wiley & Sons.

Junge, Benjamin and Anders B Trolle (2015). Liquidity risk in credit default swap markets. *Swiss Finance Institute Research Paper* (13-65).

Keller-Ressel, Martin, Thorsten Schmidt, and Robert Wardenga (2019). Affine processes beyond stochastic continuity. *Annals of Applied Probability* **29**(6), pp. 3387–3437.

Kim, Don H and Jonathan H Wright (2014). *Jumps in bond yields at known times*. Tech. rep. National Bureau of Economic Research.

King, Thomas B, Kurt F Lewis, et al. (2020). Credit Risk, Liquidity, and Lies. *International Journal of Central Banking* **16**(5), pp. 219–267.

Klingler, Sven and Olav Syrstad (2021). Life after LIBOR. *Journal of Financial Economics* **141**(2), pp. 783–801.

Kuttner, Kenneth N (2001). Monetary policy surprises and interest rates: Evidence from the Fed funds futures market. *Journal of monetary economics* **47**(3), pp. 523–544.

Lando, David (2009). *Credit risk modeling: theory and applications*. Princeton University Press.

Liu, Jun, Francis A Longstaff, and Ravit E Mandell (2006). The market price of risk in interest rate swaps: The roles of default and liquidity risks. *The Journal of Business* **79**(5), pp. 2337–2359.

Lou, Wujiang (2021). SOFR term rates from treasury repo pricing. *The Journal of Derivatives*.

Lyashenko, Andrei and Fabio Mercurio (2019). Looking forward to backward-looking rates: A modeling framework for term rates replacing LIBOR. *Available at SSRN 3330240*.

Macrina, Andrea and David Skovmand (2020). Rational savings account models for backward-looking interest rate benchmarks. *Risks* **8**(1), p. 23.

Mercurio, Fabio (2018). A simple multi-curve model for pricing sofr futures and other derivatives. *Available at SSRN 3225872*.

Michaud, François-Louis and Christian Upper (2008). What drives interbank rates? Evidence from the Libor panel. *BIS Quarterly Review, March*.

Piazzesi, Monika (2005). Bond yields and the Federal Reserve. *Journal of Political Economy* **113**(2), pp. 311–344.

Piazzesi, Monika and Eric T Swanson (2008). Futures prices as risk-adjusted forecasts of monetary policy. *Journal of Monetary Economics* **55**(4), pp. 677–691.

Priebsch, Marcel (2013). Computing arbitrage-free yields in multi-factor Gaussian shadow-rate term structure models.

Risk.net (2020). URL: `https://www.risk.net/derivatives/7657771/term-sofr-rate-still-possible-this-year-benchmark-firms-say`.

Risk.net (2021). URL: `https://www.risk.net/derivatives/7845596/sofr-alternatives-remain-on-track-despite-regulatory-warnings`.

Rosen, Jonathan (2019). Averaged Overnight Rate Futures: Convexity Adjustment. *Available at SSRN 3350745*.

Rutkowski, Marek and Matthew Bickersteth (2021). Pricing and Hedging of SOFR Derivatives under Differential Funding Costs and Collateralization. *Available at SSRN 3995735*.

Schlögl, Erik, Jacob Bjerre Skov, and David Skovmand (2023). Term Structure Modeling of SOFR: Evaluating the Importance of Scheduled Jumps.

Schrimpf, Andreas and Vladyslav Sushko (2019). Beyond LIBOR: a primer on the new benchmark rates. *BIS Quarterly Review March*.

Schwarz, Krista (2019). Mind the gap: Disentangling credit and liquidity in risk spreads. *Review of Finance* **23**(3), pp. 557–597.

Skov, Jacob Bjerre and David Skovmand (2021). Dynamic Term Structure Models for SOFR Futures. *Journal of Futures Markets* **41**, pp. 1520–1544.

Skov, Jacob Bjerre and David Skovmand (2022). Decomposing LIBOR in Transition: Evidence from the Futures Markets. *Available at SSRN 4011937*.

Smith, Josephine (2010). The term structure of money market spreads during the financial crisis. *Preprint*.

Vasicek, Oldrich (1977). An equilibrium characterization of the term structure. *Journal of financial economics* **5**(2), pp. 177–188.

[dataset] Heitfield, Erik and Yang-Ho Park (2021). *The Fed Indicative SOFR Term Rate*. URL: `https://www.federalreserve.gov/econres/notes/feds-notes/indicative-forward-looking-sofr-term-rates-20190419.htm`.

[dataset] Refinitiv Eikon (2021). *Futures Data*. URL: `https://www.refinitiv.com/`.

[dataset] The Federal Reserve (2021). *Historical SOFR and EFFR*. URL: `https://www.newyorkfed.org/markets/reference-rates/effr#historical-search`.